Ingenieurfakultät Bau Geo Umwelt

Lehrstuhl für Hydrogeologie

Assessing denitrification in groundwater using environmental isotopes, oxygen reduction rates and Monte Carlo simulations

LISA MARIA WILD

Vollständiger Abdruck von der Ingenieurfakultät Bau Geo Umwelt der Technischen Universität München zur Erlangung des akademischen Grades eines

Doktor der Naturwissenschaften (Dr. rer. nat.)

genehmigten Dissertation.

Vorsitzender:	apl. Prof. Dr. sc. nat. habil. Hans Albert Gilg
Prüfer der Dissertation:	
1.	Prof. Dr. rer. nat. Florian Einsiedl
2.	apl. Prof. Dr. agr. Karl Auerswald
3.	Prof. Dr. rer. nat. Gunnar Nützmann (emeritiert), HU Berlin

Diese Dissertation wurde am 21.10.2019 bei der Technischen Universität München eingereicht und durch die Ingenieurfakultät Bau Geo Umwelt am 21.01.2020 angenommen.

Water is the driving force of all nature

— Leonardo da Vinci

ABSTRACT

Intense farming is commonly associated with the excessive use of manure or fertilizers and the subsequent long-term deterioration of the groundwater quality in many aquifers worldwide. In these agriculturally impacted groundwater systems, nitrate (NO_3^-) is often one of the main pollutants. Availability and reactivity of electron donors control the prevalent redox conditions in aquifers and past nitrate contamination of groundwater may be ameliorated if denitrification occurs.

The study area is located in southern Germany and the catchment area is underlain by agricultural land with intensive hog farming. Using aqueous geochemistry data and the stable isotope composition of dissolved nitrate ($\delta^{15}N$ & $\delta^{18}O$), we found that nitrate concentrations above the WHO drinking water guideline were caused predominantly by manure and to a lesser extent by synthetic fertilizer applications. We also assessed that denitrification was not a significant nitrate removal process in the studied porous groundwater system that consists of a deep aquifer, a main aquifer (MA) and several smaller perched aquifers (PA). Moreover, we applied environmental isotopes (δ^2H & $\delta^{18}O$, $^3H/^3He$, ^{14}C) linked with a lumped parameter approach to determine apparent mean transit times (MTT) of groundwater that ranged from < 5 years to > 100 years. Furthermore, we identified low reduction rates of dissolved oxygen (O_2) of 0.015 1/year for first-order kinetics. By extrapolating the O_2 reduction rates beyond the apparent MTT ranges of sampled groundwater, denitrification lag times (time prior to commencement of denitrification) of approximately 114 years were determined. This suggests that it will take many decades to considerably reduce nitrate concentrations in the porous aquifer via denitrification, even if future nitrate inputs were significantly reduced.

Stable isotopes of dissolved nitrate ($\delta^{15}N$ and $\delta^{18}O$) are widely used to determine sources of nitrate contamination and denitrification processes in groundwater but are often difficult to interpret. To explain $\delta^{15}N$ observations in the two top aquifers (PA and MA), Monte Carlo simulations were carried out. For evaluating potential contributions, frequency distributions of $\delta^{15}N$ were simulated deriving from (I) the mixing of different nitrate sources, related to land use, as input to groundwater, combined with (II) transport of nitrate in groundwater and (III) microbial denitrification. Simulation results indicate a source-driven isotopic shift to heavier $\delta^{15}N$ values of nitrate in groundwater. In the study area, this may be explained by land use changes towards a more intensified agriculture releasing high amounts of manure. Therefore, denitrification processes are unlikely for the MA, as reasonable simulation curve fits for such a scenario were obtained predominantly for unrealistic portions of nitrate sources and related land use. Microbial denitrification may only play a role in the PA, with simulated $\delta^{15}N$ distributions close to the observations. These results are also in agreement with the interpretation of $\delta^{15}N$ and $\delta^{18}O$ values of dissolved nitrate originating from the perched aquifer. The applied approach can be used to qualitatively and quantitatively evaluate the influence of different potential contributions, which might mask

each other due to overlapping $\delta^{15}N$ ranges, and it can support the estimation of nitrate input related to land use.

ZUSAMMENFASSUNG

Eine zu intensive landwirtschaftliche Bewirtschaftung ist oft mit einer Überdüngung und verstärkter Ausbringung von Gülle verbunden. Dies führt weltweit zu einer langfristigen Verschlechterung der Grundwasserqualität in landwirtschaftlich genutzten Einzugsgebieten, die oft mit einem signifikanten Anstieg der Nitratkonzentrationen einhergeht. Das Selbstreinigungspotential von Grundwasserleitern wird insbesondere durch die Verfügbarkeit und Reaktionsfreudigkeit der Elektronendonoren im Aquifer kontrolliert. Die Nitratbelastung kann daher bei geeigneten Redoxbedingungen durch Denitrifikationsprozesse im Grundwasserleiter signifikant verringert werden.

Das in dieser Studie untersuchte Gebiet befindet sich in Süddeutschland und ist stark von landwirtschaftlich genutzten Flächen und der Schweinemast geprägt. Unter Verwendung von wasserchemischen Daten und der stabilen Isotopen im gelösten Nitrat ($\delta^{15}N$ & $\delta^{18}O$), haben wir zum einen festgestellt, dass im untersuchten Grundwasserleiter das aus der Gülle stammende Nitrat und zu einem geringeren Anteil Mineraldünger als Nitratquelle für die Nitratkonzentrationen oberhalb des von der Weltgesundheitsorganisation festgelegtem Grenzwertes verantwortlich sind. Zum anderen haben wir in dem porösen Grundwassersystem, welches aus einem Tiefenaquifer, dem Hauptaquifer und zahlreichen schwebenden Grundwasserstockwerken besteht, über die Isotopensignatur im Nitrat gezeigt, dass vermutlich kein wesentlicher mikrobieller Abbau von Nitrat im Hauptaquifer zu beobachten ist.

Um die Verzögerungszeit für eine einsetzende Denitrifikation im untersuchten Aquifer zu bestimmen, wurden zunächst mit Hilfe der Umweltisotope $\delta^{2}H$ & $\delta^{18}O$, $^{3}H/^{3}He$, ^{14}C, verknüpft mit einem einfachen 'Lumped Parameter'-Modell mittlere Grundwasserverweilzeiten von < 5 bis > 100 Jahren für den Aquifer ermittelt. Unter Annahme einer Reaktion 1. Ordnung konnten somit geringe Sauerstoffreduktionsraten von 0,015 1/Jahr für den Aquifer abgeschätzt werden. In Verbindung mit den modellierten mittleren Verweilzeiten ergaben sich somit Denitrifikationszeitverzögerungen von etwa 114 Jahren für den Grundwasserleiter. Die Ergebnisse deuten darauf hin, dass es in dem porösen Aquifer viele Jahrzehnte dauern wird, bis die Nitratkonzentrationen mittels Denitrifikation signifikant zurückgehen, selbst wenn in dem Einzugsgebiet der Stickstoffeintrag zeitnah beträchtlich reduziert werden würde.

Die Isotopensignaturen im gelösten Nitrats ($\delta^{15}N$ und $\delta^{18}O$) werden zwar weitreichend angewendet, um die Quellen der Nitratkontamination und Denitrifikationsprozesse im Grundwasser zu ermitteln, sind aber oft schwierig und nicht immer eindeutig zu interpretieren. Für zwei Grundwasserleiter im Arbeitsgebiet, den Hauptaquifer und die schwebenden Grundwasserleiter wurden deshalb zusätzlich Monte-Carlo-Simulationen durchgeführt, um die Interpretation der Isotopendaten für das gelöste Nitrat weiter zu stützen. Dafür haben wir verschiedene Szenarien (Mischung, Transport und reaktiver Transport) simuliert, um die im Grundwasser beobachteten $\delta^{15}N$ Werte des Nitrats zu erklären.

Der beobachtete Isotopenshift im $\delta^{15}N$ des gelösten Nitrats im Grundwasserleiter des Untersuchungsgebietes zu schwereren Isotopen wird auf Grund der Ergebnisse der Monte-Carlo-Simulationen ebenfalls hauptsächlich auf die Veränderung der Landnutzung, hin zu einer in den letzten Jahrzehnten zunehmenden Gülleausbringung (> $\delta^{15}N$ Werte), und nicht mit denitrifizierenden Prozessen im Aquifer erklärt. Gute Kurvenanpassungen bei Simulationsszenarien, die die Denitrifikation berücksichtigen, konnten nur für Verhältnisse von Nitratquellen und Landnutzung bestimmt werden, die für das Untersuchungsgebiet unrealistisch erscheinen. Mikrobielle Denitrifikation ist nur für die schwebenden Grundwasserstockwerke zu vermuten, da hier im Gegensatz zum Hauptaquifer die simulierten $\delta^{15}N$-Verteilungen unter Berücksichtigung einer ablaufenden Denitrifikation gut mit den beobachteten Verteilungen übereinstimmten. Die Ergebnisse zeigen, dass Monte-Carlo-Simulationen ein geeignetes Werkzeug darstellen, um die verschiedenen potentiellen Anteile von Nitratquellen mit unterschiedlicher Isotopensignatur im Grundwasser, qualitativ und quantitativ zu bewerten. Außerdem kann die Methode dazu beitragen, die Ermittlung von Stickstoffeinträgen in Relation zur Landnutzung zu unterstützen.

PUBLICATIONS

Some text, figures and tables have appeared previously in the following publications:

- **Decadal delays in groundwater recovery from nitrate contamination caused by low O_2 reduction rates**

  Lisa M. Wild, Bernhard Mayer and Florian Einsiedl

  Water Resources Research (2018), 54(12), p.9996–10012,
  DOI: 10.1029/2018WR023396

- **Monte Carlo simulations as a decision support to interpret δ^{15}N values of nitrate in groundwater**

  Lisa M. Wild, Arno Rein and Florian Einsiedl

  accepted in *Groundwater* (August, 2019),
  DOI: 10.1111/gwat.12936

ACKNOWLEDGEMENTS

We must find time to stop and thank the people who make a difference in our lives.

— John F. Kennedy

First of all, I would like to thank my supervisor Prof. Florian Einsiedl for giving me the possibility to conduct this research and supporting me in every step of it. Thank you for always checking up on my progress and giving the right amount of pressure.

Furthermore, I would like to thank my mentor Prof. Dr. Gunnar Nutzmann for his advice and taking over my mentorship at short notice, but also for his participation as an examiner. For the participation as an examiner, I would also like to thank Prof. Dr. Karl Auerswald.

I am also very grateful for the good time at the Chair of Hydrogeology, TU Munich. A big thanks to the whole team of the chair, but also to the project team of the Bavarian Environment Agency. Special thanks goes to Susanne Thiemann for her great support in the laboratory and Ruth Müller for all her efforts in the field. I would also like to thank Michael Wrobel for his consistent support and the realization of the Hohenthann project.

Moreover, a big thank you goes to my co-authors Bernhard Mayer and Arno Rein, who have contributed very much to improve the manuscripts. Thanks for your insightful input and expert knowledge.

Thank you also to my family and friends, who always give me advice and support my plans and actions. I especially would like to thank my parents for giving me the possibility to pursue my career path and my sister and brother in law for their support and proof reading. Last, but not least, I'd like to thank my husband for his patience, support and his continuous efforts to improve my work-life balance.

CONTENTS

ABBREVIATIONS

AMS	Accelerated mass spectrometer
Anammox	Anaerobic ammonium oxidation
ANME	Anaerobic methanotrophic
BMM	Binary mixing model
CH_4	Methane
DM	Dispersion model
DIC	Dissolved inorganic carbon
DOC	Dissolved organic carbon
DNRA	Dissimilatory nitrate reduction to ammonium
EC	Electrical Conductivity
E_h	Redox potential
Fe^{2+}	Iron (II)
Fe^{3+}	Iron (III)
FeS_2	Pyrite
FFL	Fluviatile Freshwater Layers
GWM	Groundwater monitoring station
^3He	Helium
^3H	Tritium
LFL	Limnic Freshwater Layers
LMWL	Local meteoric water line
LPM	Lumped parameter model
MAE	Mean absolute error
MA	Main aquifer
MF	Mineral fertilizer
MTT	Mean transit time
N_2	Nitrogen gas
NH_4^+	Ammonium

NH_3	Ammonia
NO_3^-	Nitrate
NO_2^-	Nitrite
NGS	Northern Gravel Series
O_2	Oxygen
UFM	Upper Freshwater Molasse
UFMy	Younger Upper Freshwater Molasse
R^2	Coefficient of determination
P	Precipitation
PA	Perched aquifer
PDF	Probability density function
Sc.	Scenario
T	Temperature
TOC	Total organic carbon
TTS	Tracer time series
V-SMOW	Vienna-Standard mean ocean water
WFD	Water framework directive

1 INTRODUCTION

With the discovery of the Haber-Bosch process in 1913, it was possible to artificially fix atmospheric nitrogen (N_2) to ammonia (NH_3) and produce synthetic fertilizer. Around that time the human population started to grow exponentially and although there were many factors involved, the securing of the food production was a crucial one (Galloway and Cowling, 2002). The Haber-Bosch process was a great breakthrough in the early 20th century but is also responsible for some of the major ecological challenges in the 21st century, such as eutrophication and nitrate contamination of groundwater and surface water. As groundwater is one of the main drinking water resources in Europe, and worldwide 2 billion people are dependent on it, nitrate pollution of groundwater is a large concern (Kemper, 2004).

Nitrate (NO_3^-) itself is not toxic to the human body, however its reduced metabolite nitrite (NO_2^-) can oxidize hemoglobin (Fe^{2+}) to methemoglobin (Fe^{3+}) in red blood cells (Knobeloch et al., 2000). As iron (III) (Fe^{3+}) is not able to bind oxygen, the essential oxygen supply to human organs, in particular the brain, is reduced, which may lead to cyanosis symptoms. This illness is named methemoglobinemia, better known as the blue baby syndrome as it affects in particular infants under the age of 3 months. Next to the unusual blue-gray to lavender skin color, some clinical symptoms include irritability, diarrhea, vomiting and lethargy. If methemoglobin levels are larger than 50% of the red blood cells counts per mL and not adequately treated, methemoglobinemia can be fatal for infants (ibid.).

Regarding carcinogenicity and gastric cancer, nitrate itself has not been shown to be carcinogenic, but nitrite reacts with nitrosatable compounds and forms N-nitroso compounds. As these compounds have been shown to be carcinogenic in cell cultures, animal experiments and humans, it has been suggested to be carcinogenic (WHO, 2007). Based on the harmful character of nitrite, nitrate concentrations in the drinking water are limited to 50 mg/L in Europe (WHO, 2004).

1.1 NITRATE AS A CONTAMINANT IN GROUNDWATER

Elevated nitrate concentrations above drinking water limits can be observed worldwide in groundwater (Wick et al., 2012). Especially the influence of intensive livestock farming on drinking water quality has become a major concern in the last decades (Hansen et al., 2011; Hooda et al., 2000). In rural areas with agricultural influence, an aquifer may be impacted by fertilizers (synthetic and manure) and/or effluents from septic tanks. Nitrate sources can be determined by isotope methods as shown in many case studies (Aravena et al., 1993; Mayer et al., 2002; Widory et al., 2005). But even though sources can be identified, nitrate contamination persists in Europe and elsewhere. Therefore, the European Water Framework Directive (WFD) 2000/60/EC was introduced in 2000 to not further deteriorate and consequently improve the chemical water status of the European water bodies by 2015 (Teodosiu et al., 2018). According

to the status report 2012 of the European Environmental Agency (EEA), approximately 25% of all aquifers across Europe are in a poor chemical status, for which mainly nitrate contamination is responsible (Werner and O'Doherty, 2012). Furthermore, 33% of all analyzed groundwater bodies are affected by diffuse pollution from agriculture and contrary to expectations and major efforts to reduce nitrate inputs into aquifers through changes in land use, land management and other measures (Suchy et al., 2018), some EU countries including Germany have not met the objectives of the European Water Framework Directive by 2015 (European Commission, 2000, 2015; Voulvoulis et al., 2017). A lack of timely response to such measures in the level of nitrate contamination in groundwater has puzzled stakeholders and has prompted the EU to delay its aspiration for 'good qualitative status' for all EU water bodies by more than a decade, from 2015 to 2027 (European Commission, 2012).

1.2 THE NITROGEN CYCLE IN GROUNDWATER

In the environment, nitrogen occurs in various oxidation states ranging from −3 (NH_3 and NH_4^+) to +5 (NO_3^-). Nitrogen gas can be naturally fixed from the atmosphere with the energy of lightning. Moreover, soil bacteria are able to fix N_2 asymbiotically while symbiotically heterotrophs such as *Rhizobia* are much more productive and may bind up to 300 kg N/ha/year. A symbiotic relationship may be formed with roots of bean plants or other legumes. In aquatic environments, cyanobacteria are mainly responsible for nitrogen fixation and bind up to 1600 kg N/ha/year in rice paddy (Ibanez et al., 2007).

$$R - NH_2 \rightarrow NH_3 + H_2O \rightarrow NH_4^+ + OH^- \tag{1}$$

The fixed organic nitrogen is mainly found in the reduced amino form and is converted to ammonia (NH_3) and then ammonium (NH_4^+) with the typical reaction as shown in equation 1.

1.2.1 *Aerobic processes*

The nitrogen cycle includes several transformation processes as shown in Figure 1. Each of them is defined by redox conditions and other factors such as microbial activity and nutrient availability (Clark, 2015). One of the main processes regulating the nitrate input into groundwater is the nitrification. In this process, ammonia (NH_3) and ammonium (NH_4^+) are oxidized to nitrite (NO_2^-) and then to nitrate (NO_3^-) as shown in equation 2 and 3 respectively. Nitrification is mainly performed by chemolithotrophic bacteria, whereby NH_4^+ is oxidized to NO_2^- by *Nitrosomonas* and *Nitrobacter* oxidizes NO_2^- to NO_3^- (Prosser, 1989). However, recent studies have discovered that two species of *Nitrospira* are able to completely oxidize NH_4^+ to NO_3^- (van Kessel et al., 2015).

$$2NH_4^+ + 3O_2 \rightarrow 2NO_2^- + 2H_2O + 4H^+ \tag{2}$$

$$2NO_2^- + O_2 \rightarrow 2NO_3^- \tag{3}$$

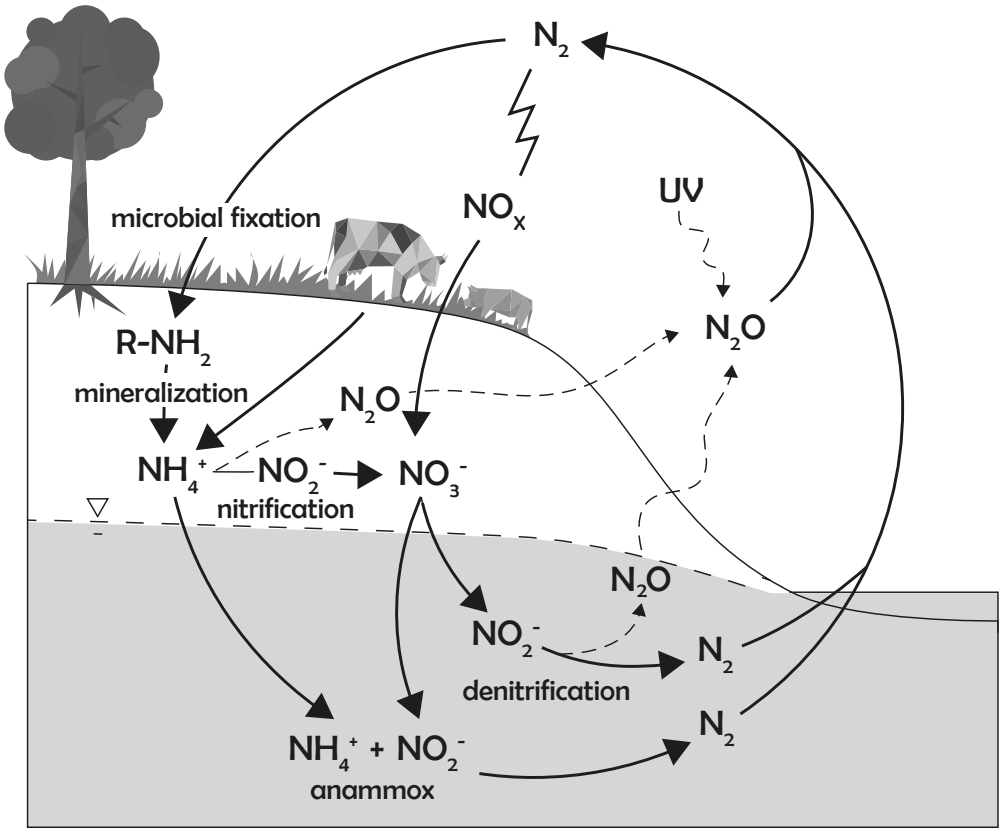

Figure 1: The nitrogen cycle displaying the principal reactions in the environment, based on Clark (2015)

The nitrification process is strictly aerobic and nitrate is the most thermodynamically stable aqueous species of nitrogen in oxic environments. Moreover, nitrification plays a large role in the transport of nitrogen in the unsaturated and saturated zone. NH_4^+ as positively charged ion tends to be bound by negatively charged clay particles, whereas nitrate as a negatively charged ion tends to show only little sorption and does not precipitate as mineral phase in oxic groundwater systems (Hamdi et al., 2013; Ibanez et al., 2007). Therefore, nitrate transport is assumed to be conservative in oxic environments. However, nitrate may be photolysed by natural sunlight producing hydroxyl radicals, which are strong oxidizers (Ibanez et al., 2007).

1.2.2 *Anaerobic processes*

In contrast, one of the dominant processes to reduce nitrate in aqueous anoxic environments is denitrification. Around ten years ago, nitrate reduction via denitrification was thought to be the only process that eliminates nitrogen from a system (Appelo and Postma, 2005). The process reduces nitrate via nitrite, nitric oxide, nitrous oxide, and eventually to nitrogen gas (Burt et al., 1999; Ibanez et al., 2007; Korom, 1992). This pathway is found in bacteria, fungi and archaea (Zumft, 1997).

$$2NO_3^- + 12H^+ + 10e^- \rightarrow N_2 + 6H_2O \tag{4}$$

Equation 4 shows the half reaction of the nitrate reduction. The dominant electron donor in most aquatic systems is organic carbon, however, inorganic electron donors,

such as pyrite (FeS_2), have also been shown to be effective in aquatic systems (Boettcher et al., 1990; Böhlke et al., 2002; Kölle et al., 1985; Postma et al., 1991).

Redox reactions follow a systematic order, which is defined by the free Gibbs-Energy ($\Delta G°$). An organic or inorganic electron donor, thus, favors an acceptor holding the highest free energy available. Dissolved O_2 (−501 kJ) is first consumed, subsequently nitrate (−476 kJ), then manganese(IV) (−340 kJ) and subsequently iron(III) (−116 kJ) is reduced, followed by bacterial sulfate reduction (−102 kJ) and finally methanogenesis occurs with −93 kJ (Rivett et al., 2008). Consequently, O_2 must be first depleted before nitrate and other electron acceptors are able to react with the available electron donors such as Dissolved Organic Carbon (DOC), FeS_2, and Fe(II) in the groundwater system. Once the environment becomes anoxic, facultative anaerobes start to use nitrate (nearly the same energy yield) as electron acceptors and as the environment becomes more anoxic, obligate anaerobes take over. The transition from O_2 reduction to denitrification has been determined to commence at O_2 concentrations of <60 µmol/L in aquifers (Böhlke et al., 2002; Tesoriero and Puckett, 2011). Other case studies, however, indicate O_2 threshold values for the denitrification commencement of as low as 0.3 µmol/L (Calderer et al., 2010; Starr and Gillham, 1993; Vogel et al., 1981).
In laboratory studies, the availability of dissolved O_2 was found to be an important factor for the efficiency of denitrification processes and it has been suggested that nitrate reduction was not most efficient under strictly anaerobic conditions (Payne, 1983; Tiedje, 1988). For instance, it has been reported that the enzymes involved in the different steps of denitrification, such as nitrate (NaR), nitrite (NiR) and N_2O (N_2OR) reductase require different O_2 threshold concentrations (Bonin et al., 1989; Davies et al., 1989; Hochstein et al., 1984; Körner and Zumft, 1989; Robertson and Kuenen, 1984). Therefore, O_2 represents an important factor limiting the commencement of denitrification in groundwater, and the term 'denitrification lag time' refers to the period required to reduce O_2 concentrations in groundwater to levels low enough so that denitrification can occur. Although some studies have focused on denitrification with the role of O_2 concentrations on nitrate turnover, the determination of O_2 reduction rates that allow the estimation of potential nitrate reduction processes has received only little attention (Böhlke and Denver, 1995; Einsiedl et al., 2009; Katz et al., 2004; Stoewer et al., 2015; Tesoriero and Puckett, 2011; Tesoriero et al., 2000).

Denitrifying bacteria gain their energy from the oxidation of organic (heterotrophism) or inorganic species (autotrophism). Heterotrophic bacteria (*Pseudomonas denitrificans*) use complex organic substances (e. g. methanol, ethanol, methane etc.) as its electron donor. Autotrophic bacteria, such as *Thiobacillus denitrificans*, *Ferrobacillus*, use inorganic compounds, such as reduced iron (Fe^{2+}) or sulfur (e. g.in FeS_2) (Archna et al., 2012; Boettcher et al., 1990; Clark, 2015; Knöller et al., 2005).

$$10Fe^{2+} + 2NO_3^- + 14H_2O \rightarrow 10FeOOH + N_2 + 18H^+ \quad (5)$$

$$6Fe^{2+} + 2NO_3^- + 2H_2O \rightarrow 2Fe_3O_4 + N_2 + 4H^+ \quad (6)$$

Equation 5 and 6 show generic stoichiometric equations of the reduction of nitrate by Fe^{2+}, where the produced Fe^{3+} precipitates as oxyhydroxide or oxide minerals. Moni-

toring shows that Fe^{2+} bearing groundwater holds little to no nitrate, which approves abiotic and biotic autotroph denitrification by ferrous iron (Fe^{2+}) (Korom, 1992).

$$5FeS_2 + 14NO_3^- + 4H^+ \rightarrow 7N_2 + 10SO_4^{2-} + 5Fe^{2+} + 2H_2O \quad (7)$$

Iron sulfide or pyrite (FeS_2) has been demonstrated to be an effective electron donor in carbon-limited aquifers and the reaction of equation 7 is mediated by various heterotroph and autotroph bacteria (Rivett et al., 2008). The oxidation of pyrite has also been suggested in several studies and evidence has been found using $\delta^{34}S$ isotopes (Boettcher et al., 1990; Pauwels et al., 2000; Schwientek et al., 2008). However, the distinction between autotroph and heterotroph denitrification is essential for the understanding of geochemical processes, it is always important to consider both and not only one or the other as they often co-occur (Korom, 1992). The availability of electron donors such as DOC, FeS_2 and Fe^{2+} may be among other factors potentially limiting denitrification (Einsiedl et al., 2007; Schwientek et al., 2008; R. L. Smith et al., 2016).

An anaerobic process that is sometimes underestimated in groundwater and only recently discovered, is the anaerobic ammonium oxidation (anammox). As shown in equation 8, NH_4^+ can be oxidized by nitrite to N_2 and H_2O (Mulder et al., 1995). The anammox process with $\Delta G° = -360$ kJ/mol represents a thermodynamically more favorable reaction than heterotrophic denitrification with $\Delta G° = -252.47$ kJ/mol (Jetten, 2001).

$$NO_2^- + NH_4^+ \rightarrow N_2 + 2H_2O \quad (8)$$

In anaerobic aquatic systems with both NH_4^+ and NO_2^- present, NH_4^+ may serve as the electron donor for the reduction of NO_2^- to N_2 gas. This may be the case in wastewater, anoxic marine environments or contaminated groundwater. The NO_2^- used in this reaction may be produced by partial denitrification of NO_3^-. Jetten (ibid.) concluded that the growth rate of the bacterial community is very slow with 11 days, but the anammox process has been suggested to be of great importance in waste water treatment systems, especially in combination with the partial nitrification process (SHARON®) that allows high conversion rates of NH_4^+ and NO_2^- (Jetten, 2001; Van Dongen et al., 2001). In marine systems, the anammox process has been widely investigated and reported in literature (Hu et al., 2011). In groundwater systems anammox has often been underestimated, however, recent studies have found evidence of its great importance to the system and relevant N loss (Clark et al., 2008; Granger and Wankel, 2016; Hu et al., 2011; Schubert et al., 2006). Moreover, anammox may also favor the changing interfaces of anoxic and oxic conditions in terrestrial environments (Hu et al., 2011).

Another process that reduces NO_3^- is the dissimilatory nitrate reduction to ammonium (DNRA). DNRA is performed by obligate anaerobes and believed to be limited by nitrate (e^--acceptor) and carbon (e^--donor) concentrations (Tiedje, 1988). This assumption can be explained by the electron requirements of the two redox reactions. As shown in equation 4, the denitrification reaction only needs 5 e^- to reduce one nitrate

molecule to half a molecule of N_2 , whereas the DNRA reaction requires 8 e^- for the reduction of one nitrate to NH_4^+, as displayed in Equation 9.

$$NO_3^- + 10H^+ + 8e^- \rightarrow NH_4^+ + 3H_2O \tag{9}$$

A recently discovered process has shed some light on the poorly understood atmospheric methane (CH_4) budget. CH_4 is one of the strongest greenhouse gases and atmospheric CH_4 concentrations have been rising since the 1750s, leading to an increasing need to understand the dissimilation of CH_4. Major anthropogenic sources of CH_4 are agriculture and fossil fuel exploitation with a contribution of about 230 Tg CH_4 yr^{-1}, a minor source is waste treatment (landfills, manure and sewage) and biomass burning (Montzka et al., 2011). Major natural sources include wetlands (150-180 Tg CH_4 yr^{-1}, 22%) and rice fields (12%) (Augenbraun et al., 2010). In freshwater habitats, methane can be used as the carbon source (e^--donor) for the aerobic methane oxidation but also for the recently (2006) discovered anaerobic methane oxidation coupled to denitrification. Raghoebarsing et al. (2006) have been the first describing the nitrite dependent anaerobic methane oxidation (n-damo) with the reaction, displayed in equation 10.

$$3CH_4 + 8NO_2^- + 8H^+ + 8e^- \rightarrow 3CO_2 + 4N_2 + 10H_2O \tag{10}$$

Ettwig et al. (2010) discovered a new 'intra-aerobic' pathway of nitrite reduction, whereby *M. oxyfera* bypasses the denitrification intermediate nitrous oxide with converting two nitric oxide molecules to N_2 and oxygen that was then used to oxidize CH_4. Moreover, it was established that the bacteria *Candidatus Methylomirabilis oxyfera* belonging to the phylum NC10 performs the nitrite-dependent anaerobic methane oxidation (n-damo) and clearly prefers nitrite over nitrate (Ettwig et al., 2009; Ettwig et al., 2010, 2008). Ettwig et al. (2008) also found that the NC10 bacterium are dominant after 16 months of cultivation and an archaeal partner, such as anaerobic methanotrophic (ANME)-I, -II or -III, are not necessarily required for n-damo with nitrite as the electron acceptor. However, the role of the Archaea in the initial enrichment is still uncertain and it was observed that the Archaea oxidized CH_4 not only in syntrophy with denitrifying bacteria but also without a partner, which was supported by archaeal lipids that were depleted in $\delta^{13}C$ (−67‰) compared to the provided CH_4 (−27‰) (ibid.). Another study by Rasigraf et al. (2012) showed microbial oxidation for n-damo by measuring $\delta^{13}C$ and δ^2H, finding enrichment factors ϵ of −29.2±2.6‰ for $^{13}CH_4$ and −227.6±13.5‰ for ^2H, calculated with the Rayleigh equation. A preferential environment for the n-damo would be rich in nitrite/nitrate and methane, low in organic matter and sulphate to reduce competition to classical denitrifiers and sulphate reducing denitrification (Nordi and Thamdrup, 2014). Other studies by Bjerg et al. (1995) and R. L. Smith et al. (1991) found evidence of the anaerobic methane oxidation coupled to denitrification in connection to a methane plume of a landfill. Other benchmarking studies have revealed evidence of anaerobic methane oxidation coupled to denitrification in the sediment of freshwater lakes, such as Lake Lugano and Lake Constance, Switzerland (Deutzmann and Schink, 2011; Lehmann et al., 2004). In freshwater lakes, the close proximity of oxygen and nitrate reducing environments can mask n-damo as aerobic methane oxidation. To investigate this, Deutzmann et al.

(2014) analysed the denitrifying methanotrophs in vertical sediment cores of Lake Constance to conclude that n-damo can be a major CH_4 sink, if nitrate is present in the anaerobic zones.

1.3 ENVIRONMENTAL ISOTOPES

Environmental isotopes are a powerful tool to determine denitrification potential, nitrate sources and electron donors for the denitrification process (Einsiedl and Mayer, 2006; Koh et al., 2010; Sebilo et al., 2006; Stoewer et al., 2015; Wassenaar, 1995; Wunderlich et al., 2012). Moreover, environmental isotopes, such as δ^2H/ $\delta^{18}O$, $^3H/^3He$ and ^{14}C may be applied to model mean groundwater transit times (Maloszewski and Zuber, 1982; Sültenfuß, 1998; Sültenfuß et al., 2011).

1.3.1 *Sources and processes affecting stable isotopes of nitrate*

Nitrogen shows an abundance of 0.003% in the earth (97.76% in rocks) and 2.01% in the atmosphere. It has two stable isotopes: ^{14}N and ^{15}N, whereby 99.64% of atmospheric nitrogen consists of ^{14}N and only 0.36% of ^{15}N. Oxygen has three stable isotopes including ^{16}O with an abundance of 99.76%, ^{17}O with 0.04% and ^{18}O with 0.2% (Clark, 2015; Kendall and McDonnell, 1998b). To enhance measurement quality and interlaboratory results, the measured ratios of heavy (^{15}N) to light (^{14}N) isotopes in samples are compared to a standard ratio (e. g. AIR for ^{15}N:^{14}N , which is the reference of N_2 in atmospheric air or Vienna Standard Mean Ocean Water (VSMOW) for ^{18}O:^{16}O) as shown in equation 11 and 12, respectively (Böhlke and Coplen, 1995; Kendall and McDonnell, 1998b).

$$\delta^{15}N_{AIR}[‰] = \frac{(^{15}N/^{14}N)_{Sample}}{(^{15}N/^{14}N)_{AIR}} - 1 \tag{11}$$

$$\delta^{18}O_{VSMOW}[‰] = \frac{(^{18}O/^{16}O)_{Sample}}{(^{18}O/^{16}O)_{VSMOW}} - 1 \tag{12}$$

The δ notation was introduced to compare the standardized ratios of isotopes. With this method, even small variations in isotope ratios may be determined to identify biogeochemical processes. If chemical and physical processes are completed, the resulting $\delta^{15}N$ values are equal in the substrate and product. However, if the processes are incomplete, fractionation of isotopes occurs and $\delta^{15}N$ values differ in substrate and product (Ryabenko, 2013).

Two fractionation processes were found to be influencing the isotopic composition: the equilibrium and kinetic fractionation. The equilibrium fractionation is reversible and driven by energy changes of molecules. It is based on the understanding that in equilibrium isotopically lighter species are bound less strongly compared to heavier species (Bigeleisen, 1965). The factor $\alpha_{eq.}$ for equilibrium exchange reaction of $A \leftrightarrow B$ is shown in equation 13.

$$\alpha_{eq.} = \frac{R_A}{R_B} \tag{13}$$

where R is $^{15}N/^{14}N$

Kinetic fractionation is irreversible and defined by the bonding strength of the reacting molecules. In low temperature environments, kinetic fractionation effects are more important than the equilibrium fractionation effects as these decrease with temperature (Kendall and McDonnell, 1998b; Ryabenko, 2013). Kinetic fractionation factors may vary strongly depending on reaction rates, product and reactant concentrations, conditions etc. Kinetic fractionation is based on the understanding that heavier isotopes (more neutrons) react slower than lighter isotopes (less neutrons), which leads to an enrichment of heavier isotopes in the remaining substrate. Consequently, the products that are formed in the system/substrate, are isotopically lighter and depleted in heavier isotopes. Therefore, ^{15}N and ^{18}O will be enriched in the remaining nitrate, if denitrification takes place. The kinetic fractionation factor is commonly described by the rate constants for the molecules of light and heavy isotopes as displayed in equation 14.

$$\alpha_{kin.} = \frac{^{14}k}{^{15}k} \tag{14}$$

where ^{14}k and ^{15}k are the rate constants for the light and heavy isotopes.

The fractionation factor may also be expressed with the enrichment ϵ that describes the isotopic enrichment of the product relative to the substrate in ‰ as shown in equation 15.

$$\epsilon = (\alpha - 1) \times 1000 \tag{15}$$

The kinetic fractionation process can also be described with the Rayleigh equation (equation 16), where the isotope ratio (R) is a function of the initial ratio (R_0), the remaining fraction of the reservoir (f), which can also be described as C_t/C_0, and the fractionation factor α (Clark and Fritz, 1997).

$$R = R_0 \times \frac{c_t}{c_0}^{(\alpha-1)} = R_0 \times f^{(\alpha-1)} \tag{16}$$

where R is $^{15}N/^{14}N$

Fractionation of ^{15}N varies significantly depending on the process. The N fixing process, which includes mainly bacterial fixation but also lighting induced fixation, shows only little ^{15}N fractionation and small fractionations are mainly ascribed to bacterial strains, nutrient supply and soil moisture (Bergersen et al., 2009; Ledgard, 1989; Shearer et al., 1986). Commonly $\delta^{15}N$ values are in general slightly lower than 0‰ for bacterial fixation of N_2 by nitrogenase. Fractionation factors range from −3 to +1‰ (Fogel and Cifuentes, 1993).

N_2 fixation is sometimes viewed as a specific type of assimilation, however, the majority of literature considers only the incorporation or uptake of NH_4^+, NO_3^-,

NO_2^- into organisms as assimilation. NO_3^- and NO_2^- reductases initially reduce all oxidized forms of N to NH_4^+, which is then assimilated into organic matter (Kendall and McDonnell, 1998b). As anticipated, molecules including the lighter isotopes ^{14}N are preferred over the heavier isotopes ^{15}N for incorporation. Hübner (1986) found that measured values for fractionation of microorganisms in soils ranged from −1.5 to +1‰ averaging at −0.52‰. Similar ranges are found for fractionations by vascular plants (Mariotti et al., 1980). N uptake by plants, however, produces only negligible fractionation. In field studies it has been observed that NH_4^+ is preferred over NO_3^- for assimilation in microbial-detrital pools (Currie and Nadelhoffer, 1999; Davidson et al., 2007). In field and laboratory studies, fractionations ranging from −27 to 0‰ have been found for NH_4^+ and NO_3^- assimilation by algae in aquatic environments (Fogel and Cifuentes, 1993).

Mineralization, which is sometimes also called ammonification, is the production of NH_4^+ from soil organic matter and produces only small fractionations of ±1‰ (Kendall and McDonnell, 1998b). In literature a wide range of fractionation values can be found for mineralization. However, in these studies mineralization often includes the whole process of mineralized N being converted to NO_3^-, which is in fact not correct and large fractionations are produced by nitrification and not by the transformation of organic N to NH_4^+. Nitrification includes several transformation steps and intermediates, reacting from NH_4^+ to NH_2OH, to NO_2^- and finally to NO_3^-. In several laboratory and field studies, it was suggested that in the microbial nitrification processes two thirds of the oxygen atoms in the newly formed nitrate are derived from water and one third from the dissolved atmospheric O_2 (Amberger and Schmidt, 1987; Böhlke et al., 1997; Durka et al., 1994; Hollocher, 1984; Kendall and McDonnell, 1998b; Wassenaar, 1995). The theoretically expected $\delta^{18}O_{nitrate}$ derived from nitrification may therefore be calculated (Stumpp et al., 2009). Voerkelius (1990) found in laboratory studies similar $\delta^{18}O$ values for nitrate that was formed by nitrification between −2 and +2‰ using $\delta^{18}O$ values for water of −10‰ and a $\delta^{18}O_{O_2}$ value of 23.5±0.3‰ (Kroopnick and Craig, 1972). However, recent studies have shown that the O-exchange between $\delta^{18}O$ from water, molecular O_2 and NO_2^-, and isotope fractionation can have a significant impact on the $\delta^{18}O_{\ nitrate}$ (Buchwald et al., 2012; Casciotti et al., 2010; Fang et al., 2012; Snider et al., 2010). Therefore, $\delta^{18}O$ values of nitrate from microbial nitrification can vary widely depending on soil types, pH and C content (Amberger and Schmidt, 1987; Einsiedl and Mayer, 2006; Mayer et al., 2001; Voerkelius, 1990).

The fractionation of soil NH_4^+ may be influenced by nitrification, dilution of atmospheric NH_4^+ and sorption processes in soil-water interaction (Buzek et al., 1997). The overall isotope fractionation for nitrification shows enrichment factors $\epsilon(NO_2^-\text{-}NH_4^+)\approx$ −12 to −29‰ (Kendall and McDonnell, 1998b). The enrichment of ^{15}N depends strongly on the rate determining step. The oxidation of NO_2^- to NO_3^- is generally rapid and not rate determining in natural systems, but the comparably slow oxidation of NH_4^+ to NO_2^- by *Nitrosomonas* is suggested to cause most of the fractionation. Therefore, the rate determining step of NH_4^+ to NO_2^- enriches the ^{15}N in NH_4^+ and depletes the ^{14}N in NO_2^-. However, Casciotti (2009) found an inverse kinetic isotope effect from NO_2^- to NO_3^- with −12.8‰. Due to this inverse isotope effect, the $\delta^{15}N$ (and $\delta^{18}O$) values of NO_2^- are lower than these of NO_3^-. Moreover, the fractionation

depends also on the size of substrate pools and may be negligible in N-limited systems.

Another process that may significantly influence the $\delta^{15}N$ values, is volatilization, which is the common term for the loss of NH_3 from near-surface soils leaving higher $\delta^{15}N$ values in the residual NH_4^+. The fractionation of volatilization consists for one of the equilibrium fractionation of NH_4^+ and NH_3 in solution, and also between aqueous and gaseous NH_3. Moreover, the kinetic fractionation causes a depletion of ^{15}N in the diffused NH_3 and an isotopic enrichment in the remaining NH_4^+.
In addition, patterns of decreasing nitrate concentrations coupled to exponential increase of $\delta^{15}N$ and $\delta^{18}O$ in the residual nitrate along a groundwater flow path have been shown to be an effective indicator of denitrification in aquifers (Boettcher et al., 1990; Böhlke et al., 2002; Knöller et al., 2011; Koh et al., 2010; Mariotti et al., 1988; Schwientek et al., 2008; Sebilo et al., 2006; Wassenaar, 1995). Studies have identified enrichment factors for heterotrophic denitrification ranging from −40 to −5‰ (Fukada et al., 2003; Kendall and McDonnell, 1998b; R. L. Smith et al., 1991). Torrentó et al. (2010) investigated autotrophic denitrification by *Thiobacillus denitrificans* under controlled conditions and found isotopic enrichment factors ϵN and ϵO ranging from −13.5‰ to −15.0‰ and from −19.0‰ to −22.9‰, respectively.

In marine aquatic environments such as the Arabian Sea, denitrification was often seen as the main N loss process in the oxygen minimum zone (B. B. Ward et al., 2009). However, investigating $^{15}NO_2^-$ showed that there is a direct link between DNRA and anammox, which was often mistaken as ^{15}N enrichment for denitrification (Jensen et al., 2011). Anammox and DNRA may also occur in freshwater environments (Böhlke et al., 2006; Brunner et al., 2013; Clark et al., 2008; R. L. Smith et al., 2015), but $\delta^{15}N$ studies in these habitats are limited compared to those in marine environments (Hu et al., 2011). Brunner et al. (2013) found that $^{15}NH_4^+$ gets depleted in the remaining pool with isotopic effects of +23.5 to +29.1‰. Moreover, isotope effects during the reduction of NO_2^- to N_2 and NO_3^- include 1) an inverse kinetic isotope effect during the oxidation of NO_2^- to NO_3^- (−31.1±3.9‰), 2) normal kinetic isotope fractionation during the reduction of NO_2^- to N_2 (+16.0±4.5‰) and 3) an equilibrium N isotope effect between NO_3^- and NO_2^- (−60.5±1.0‰). The latter is stimulated by environmental stress, which may superimpose the N isotope exchange effects over the kinetic N isotope fractionation. Granger and Wankel (2016) summarizes enrichment factors of the different processes and studies.

Moreover, the stable isotope composition of nitrate has been successfully used to determine sources of nitrate in contaminated groundwater (Aravena et al., 1993; Böhlke, 2002; Böhlke et al., 2002; Choi et al., 2007; Kendall and McDonnell, 1998b; Mayer et al., 2002). Common nitrate sources in catchments with intensive anthropogenic N inputs are synthetic fertilizers, manure, waste waters and septic systems among others (Kendall and McDonnell, 1998b). $\delta^{15}N$ and $\delta^{18}O$ ranges from these sources have been collected and are displayed in Figure 2. Nitrate sources may then be identified by plotting measured $\delta^{15}N$ and $\delta^{18}O$ values on the 2-dimensional plot.

However, isotope fractionation during denitrification may have a significant influence on the $\delta^{15}N$ and $\delta^{18}O$ values. Groundwater that has been influenced by denitrification may show data points along a straight line with empirical $\delta^{15}N$:$\delta^{18}O$ trajectories of

0.5 to 0.8 in freshwater systems, relating to its initial nitrate source (Amberger and Schmidt, 1987; Casciotti et al., 2002). In addition, there have been ambiguities and difficulties interpreting $\delta^{15}N$ and $\delta^{18}O$ values of nitrate in groundwater systems. For instance, the mixing of different unreacted nitrate sources such as manure (elevated $\delta^{15}N > 7‰$, low $\delta^{18}O \leqslant 5‰$) with unreacted nitrate deriving from precipitation (low $\delta^{15}N \approx 0‰$, elevated $\delta^{18}O \approx 60‰$) (Kendall and McDonnell, 1998b) can be misleadingly interpreted as microbial denitrification (Pauwels et al., 2000; Xue et al., 2009). Therefore, the identification of denitrification via a characteristic slope in a 2D isotope plot ($\delta^{18}O$ versus $\delta^{15}N$) may often fall short for groundwater systems impacted by a mixture of different nitrate sources. Moreover, during denitrification, $\delta^{18}O$ originating from ambient water may be incorporated into dissolved nitrate by back reactions of NO_2^- to NO_3^- and can overprint the expected enrichment of ^{18}O in the remaining nitrate as reported in literature (Granger and Wankel, 2016; Wunderlich et al., 2013). This also implies that there is no typical slope as a robust diagnostic tool for the characterization of denitrification under environmental conditions as often suggested in literature (e. g. by Amberger and Schmidt (1987) and Boettcher et al. (1990)). Therefore, a combination of aqueous (geo)chemical and isotopic techniques may be an effective approach to determine O_2 threshold concentrations for denitrification and the extent to which nitrate reduction occurs in aquifers.

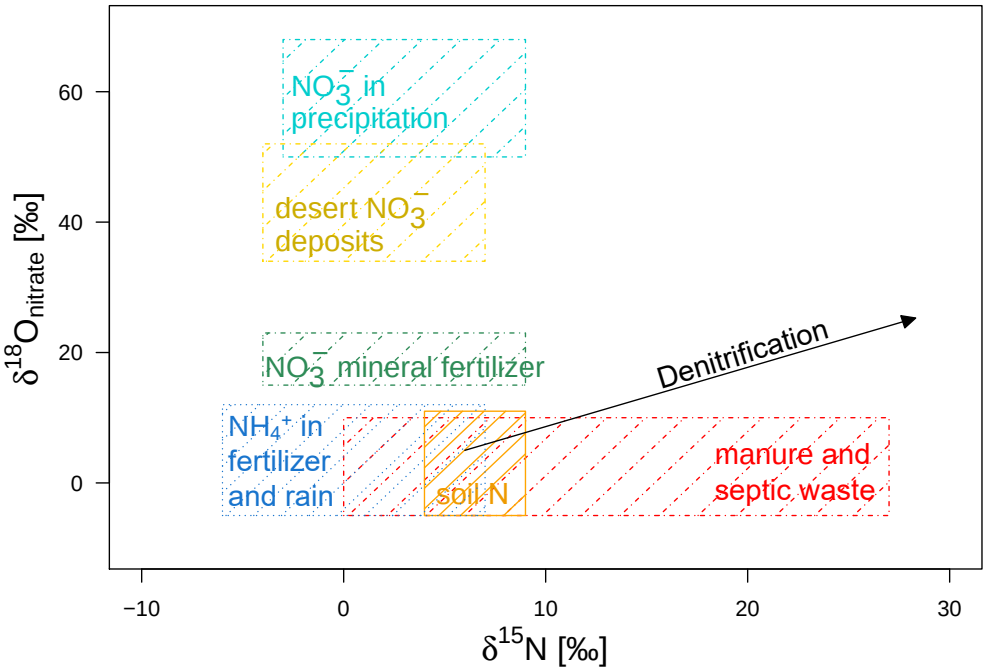

Figure 2: 2-dimensional isotope plot of $\delta^{18}O$ and $\delta^{15}N$ for a determination of nitrate sources, based on Kendall and McDonnell (1998b)

As nitrate shows no or only little sorption effects on the aquifer matrix and does not precipitate as mineral phase under oxic redox conditions, transport of nitrate in groundwater is assumed conservative (Hamdi et al., 2013; Harper, 1924; Singh and Kanehiro, 1969). In such oxic aquifers, the residence time of nitrate in groundwater may vary from less than one year to several decades or even centuries depending on the apparent mean transit time (MTT) of groundwater (Koh et al., 2010; Sebilo et al., 2013; Wassenaar et al., 2006). Fogg et al. (1999) for instance, estimated the vulnerability of groundwater to nitrate contamination by modeling its transport in both the vadose

zone and the aquifer to produce travel time maps of the Salinas Valley, California, USA that may indicate nitrate vulnerable zones. Furthermore, apparent groundwater MTTs have been successfully determined combining environmental isotope measurements and the use of transport models (Böhlke, 2002; Einsiedl and Mayer, 2006; Maloszewski and Zuber, 1982).
By combining O_2 concentrations and modeled MTTs, it appears possible to estimate O_2 reduction rates and the time frames required to reduce O_2 in an aquifer to levels where denitrification can commence (denitrification lag time) so that nitrate removal from groundwater can be accelerated dependent on the availability of electron donors in the system.

1.3.2 *Sulfur isotope ratios ($\delta^{34}S$) of sulfate*

Sulfur has four stable isotopes (^{32}S, ^{33}S, ^{34}S and ^{36}S) and one radioactive naturally occurring isotope ^{35}S with a half-life of 87.5 days (Cooper et al., 1991). ^{32}S and ^{34}S are the most abundant with 95.02 and 4.21%, respectively, and therefore mass spectrometry is usually restricted to these two isotopes. The $\delta^{34}S$ notation is defined in equation 17. The historic international standard is the Canon Diablo troilite (V-CDT). However, the International Atomic Energy Agency was prompted to define the IAEA-S1 standard due to small isotopic discrepancies in the V-CDT. The IAEA-S1 standard has a $\delta^{34}S$ value of −0.30‰ (Kendall and McDonnell, 1998b).

$$\delta^{34}S[‰] = \frac{(^{34}S/^{32}S)_{Sample}}{(^{34}S/^{32}S)_{standard}} - 1 \tag{17}$$

The analysis of $\delta^{34}S$ represents an additional tool to identify sources of sulfate and pyrite oxidation in groundwater (Bottrell et al., 2000; Einsiedl and Mayer, 2005; Knöller et al., 2005; Moncaster et al., 2000; Pauwels et al., 2000; Schwientek et al., 2008). Sulfur may originate from four different sources, which include atmospheric deposition, S containing fertilizers, contaminated surface waters, and S bearing minerals in the aquifer material. $\delta^{34}S$ values in atmospheric sulfur range widely from 0.5 to 19.4‰, sampled worldwide in aerosol and precipitation (Kendall and McDonnell, 1998b; Mayer et al., 1995; Newman et al., 1991). $\delta^{34}S$ values of S containing fertilizers range from 0 to +7‰ (Mizota and Sasaki, 1996). The oxidation of pyrite may be identified by negative $\delta^{34}S$ values and there is no or only minor S isotope fractionation expected (Balci et al., 2007; Krouse and Grinenko, 1991).

1.3.3 *Stable isotopes of δ^2H and $\delta^{18}O$*

The stable isotopes of water (δ^2H and $\delta^{18}O$) in precipitation and the hydrologic cycle have been excessively studied and are an indispensable tool for environmental scientists (Jouzel et al., 1997; Lee and Fung, 2007; Maloszewski et al., 1992; Rodhe et al., 1996; Stumpp et al., 2014). Temperature and the proportion of residual water vapor in precipitation are the two main factors that influence the isotopic composition of water. As a result of these factors, several effects including the continental, altitude, latitude and amount effect, control the δ^2H and $\delta^{18}O$ composition in precipitation (Kendall and McDonnell, 1998b). Craig (1961) first described the co-variance of δ^2H and $\delta^{18}O$ in all meteoric water with the $\delta^2H = 8 \cdot \delta^{18}O + 10$. This relationship has

been named the global meteoric water line (GMWL) and is often applied for the comparison of stable isotopic data, but local isotopic data may vary with different meteoric conditions, which requested the term local meteoric water line (LMWL).

Long-term data series of stable isotopes in spring water and shallow groundwater, allow the assessment of MTTs that are younger than 4-5 years. To determine the MTT of groundwater, the stable isotopes $\delta^{18}O$ und $\delta^{2}H$ need to be monitored over at least a year (Trcek and Zojer, 2010). When seasonal variations are observed, a transit time of less than 4-5 years can be assumed and the measured data are fitted to theoretical output concentrations by using an advective-dispersive model, which allows a prediction of the groundwater transit times and α_L, the dispersivity (m) in the spring/shallow groundwater catchment (Maloszewski and Zuber, 1982). Furthermore, $\delta^{18}O$ and $\delta^{2}H$ can differentiate water infiltrated in the Holocene (last 11.700 years of the Earth's history) from water infiltrated in the Pleistocene (11,700 to 2,588,000 years) (Geyh, 2000).

1.3.4 $^{3}H/^{3}He$

Groundwater MTTs of 5 to slightly more than 100 years can be determined by measuring and modeling the natural occurring radioactive isotope Tritium (^{3}H). Natural ^{3}H-concentrations of up to 5 TU (Tritium units) are produced by cosmic ray neutrons colliding with nitrogen in the upper atmosphere and producing ^{15}N, which decays into common ^{12}C and ^{3}H as displayed in equation 18.

$$^{14}N + n \rightarrow ^{15}N \rightarrow ^{12}C + ^{3}H \tag{18}$$

Anthropogenic ^{3}H concentrations, which were emitted into the atmosphere during hydrogen bomb tests in the 1950s and 60s, reached a maximum in 1963 with up to 10,000 TU in the northern hemisphere where bombing took place (Mazor, 2004). In 1963, an international treaty stopped the bomb testing and since then concentrations have been decreasing steadily with a half-life of 12.3 years. Nowadays, concentrations have declined to pre-bombing concentrations i. e. natural concentrations. ^{3}H decays to the light and rare isotope ^{3}He, which occurs with a $^{3}He/^{4}He$ -ratio of 1.38×10^{-6} in the atmosphere (Clarke et al., 1976; Lucas and Unterweger, 2012). Helium in comparison, is present with 5.24 ppm in the atmosphere (Glückauf and Paneth, 1946). If two ^{3}H concentrations with a time difference of several decades (>25 years) have been measured in groundwater and the ^{3}H input function is well known, a reasonable and certain determination of groundwater residence time can be calculated (Kendall and McDonnell, 1998a).

However, if modeling of ^{3}H time series demonstrates ambiguous results, it may be combined with the decay product ^{3}He, which allows a more exact and reliable determination of the groundwater MTT. If there is no ^{3}H data from the past available, a piston flow age can be calculated with the $^{3}H/^{3}He$ method; however, a piston flow age may not be very accurate. The time parameter of the $^{3}H/^{3}He$-age can be assessed with equation 19 with the decay constant λ = 0.05626 s^{-1} (Sültenfuß and Massmann, 2004).

$$\tau = \frac{1}{\lambda} \times (1 + \frac{^{3}He_{tri}}{^{3}H}) \tag{19}$$

As Neon (Ne) is naturally not present in the aquifer, the excess air component may be calculated by means of measuring the Ne concentration and therefore determine potential degassing of the water (Sültenfuß et al., 2011; Sültenfuß and Massmann, 2004).

1.3.5 ^{14}C

^{14}C, also known as radiocarbon, is the radioactive isotope of carbon and has a half-life of 5730 years. ^{14}C is naturally produced in the atmosphere by cosmic ray interactions. The natural abundance is $\approx$1 atom ^{14}C per 10^{12} atoms ^{12}C. Anthropogenic ^{14}C may be produced by nuclear reactors and weapon testing. Next to ^{14}C, there are two stable isotopes of carbon that may also be used as tracers in earth science: ^{12}C with an abundance of 98.89% and ^{13}C with 1.11%. The isotopic ratio of ^{13}C to ^{12}C are often applied in ecological and atmospheric studies (Bender, 1971; Ciais et al., 1995; B. N. Smith and Epstein, 1971). ^{14}C in dissolved inorganic carbon (DIC) is often applied to determine groundwater MTTs of more than 1000 years to up to several 10,000 years (Aravena et al., 1995; Campana and Simpson, 1984; Castro et al., 2000).

1.4 MODELING OF GROUNDWATER MEAN TRANSIT TIMES USING ENVIRONMENTAL ISOTOPES

To evaluate and characterize a groundwater system, it is of great importance to determine the groundwater MTT. Knowing the apparent MTT of groundwater linked with reactive redox parameters, such as O_2 concentrations, allows us to estimate the self-purification potential of other redox sensitive parameter like nitrate. Generally, it is stated that the longer the MTT, the better is the self-purification potential (Merkel and Planer-Friedrich, 2008). If geochemical or redox conditions are, however, not suitable, there might be no self-purification despite long MTTs. Still, the assessement of MTTs may give information on how long the contaminants remain in the aquifer, if there is no reduction taking place. Therefore, a key scientific question is the residence time of nitrate in groundwater that is determined by transport processes and redox reactions that occur along groundwater flow paths. An accelerated removal of dissolved nitrate from aquifers at time scales faster than the apparent MTT of groundwater can only occur through the redox processes denitrification and anammox. To evaluate and predict groundwater MTT using environmental isotopes (e. g. δ^2H/ $\delta^{18}O$, $^3H/^3He$ and ^{14}C), a lumped parameter model (LPM) is often applied (Maloszewski and Zuber, 1982; Zuber, 1986). The simplest approach is the piston-flow model as shown in equation 20 and describes the transport of water without any mixing, such as in a pipe. Therefore, it is assumed that all transport pathways have the same length.

$$g(\tau) = \delta(\tau - T^*) \tag{20}$$

Where τ is the integration of the transit time distribution, T^* the transit time of the tracer and in favorable conditions equal to the mean age of water (T), and δ is the Dirac delta function

The exponential model (equation 21) includes also a lateral flow, but additionally different flow lengths and an exponential distribution of MTTs are assumed. Consequently, the tracer moves on different flow paths and flow lengths, but no mixing is taking

place.

$$g(\tau) = \frac{1}{T^*} \times e^{-\frac{\tau}{T^*}} \tag{21}$$

In the dispersion model (DM) as shown in equation 22, mixing along the different flow paths is assumed.

$$g(\tau) = \frac{1}{\sqrt{4\pi P_D^* \tau/T^*}} \times \frac{1}{\tau} \times exp[-\frac{(1-\tau/T^*)^2}{4P_D^* \tau/T^*}] \tag{22}$$

Where P_D^* is the apparent dispersion parameter (inverse of the Peclet number)

These three models can be described by the black-box model in theory using an input concentration converted to an output with a function (Maloszewski and Zuber, 1982; Zuber, 1986). Maloszewski and Zuber (1982) have established that the exponential piston-flow model (exponential distribution of transit times combined with a piston -flow model) and the dispersion model give the best results for groundwater MTTs. However, the dispersion model has also been widely used to model groundwater MTTs for conditions with limited mixing (dispersion) (Schwientek et al., 2008; Visser et al., 2013).

1.5 PROBABILISTIC MODELING OF $\delta^{15}N_{NITRATE}$ DISTRIBUTIONS IN GROUNDWATER

Transport modeling often applies numerical solutions to include heterogeneities (Cirpka and Helmig, 1999). However, in many study areas calibration may be difficult due to a low spatial resolution of known aquifer properties and details about geology. Otherwise, numerical modeling requires a stochastic framework for uncertainty analysis (Simmons et al., 1995). Literature also shows that if an extended data set for a groundwater system is missing, it makes sense to use simple lumped-parameter models (Maloszewski and Zuber, 1982, 1996), which also use a statistical characterization of the variability of groundwater ages, notwithstanding the many other sources of uncertainty. Isotope mixing models implementing a Bayesian framework are widely used in ecological food web studies (Bond and Diamond, 2011; Dennard et al., 2009; Ikeda et al., 2010; McClellan et al., 2010; Nosrati et al., 2018, 2014; E. J. Ward et al., 2010). These Bayesian mixing models include for instance the SIAR (Stable Isotope Analysis in R) using the Markov chain Monte Carlo method with an overall residual error term (Parnell et al., 2013, 2010) or the MixSIR (Moore and Semmens, 2008), applying sample importance resampling.

Recently, these models were applied to determine the quantitative contribution of different nitrate sources to nitrate contamination of groundwater and surface water (El Gaouzi et al., 2013; Korth et al., 2014; Xu et al., 2016; Zhang et al., 2015). In a hydrological context, similar models using the generalized likelihood uncertainty estimation (GLUE) methodology that also includes Markov Chain Monte Carlo methods, have been developed to better understand complex environmental systems (Beven and Freer, 2001). Nevertheless, Bayesian models, such as SIAR, were rarely applied for

describing microbial denitrification processes in published case studies to date (Li et al., 2019; Xia et al., 2017; Yue et al., 2015). Next to Bayesian models, Monte Carlos simulations are simpler and can also be used to model such processes coupled with statistical tools. Similar to Bayesian models, an advantage of Monte Carlo simulations is their inherent ability to characterize uncertainties and to provide probabilistic risk estimates of certain scenarios (Sadegh and Vrugt, 2014). However, a best fit is highly dependent of the given data series and may also implicate uncertainties. To further advance isotope interpretation methods, Monte Carlo simulations can play an important role, especially for data from study sites with a complex hydrogeology and an input of different nitrate sources. Probability density functions (PDFs) can be assigned to each parameter reflecting uncertainty, and parameter sensitivity. Therefore, results can be evaluated in terms of probabilities, rather than deterministic values.

1.6 AIMS AND OBJECTIVES

As nitrate contamination in surface and groundwater has become a widespread problem in Europe and elsewhere, stakeholders and decision makers are prompted to find feasible and applicable tools to determine nitrate sources and the denitrification potential of the catchment area. In the past, the stable isotope composition of nitrate has been successfully used to determine sources of nitrate causing a deterioration of groundwater quality in catchments with intensive anthropogenic N inputs from synthetic fertilizers, manure, waste waters and septic systems among others (Aravena et al., 1993; Böhlke, 2002; Böhlke et al., 2002; Choi et al., 2007; Kendall and McDonnell, 1998b; Mayer et al., 2002). In addition, patterns of decreasing nitrate concentrations coupled with enrichment of ^{15}N and ^{18}O in the remaining nitrate along a groundwater flow path have been shown to be an effective indicator of denitrification in aquifers (Boettcher et al., 1990; Böhlke et al., 2002; Knöller et al., 2011; Koh et al., 2010; Mariotti et al., 1988; Schwientek et al., 2008; Sebilo et al., 2006; Wassenaar, 1995).

We hypothesize that the determination of O_2 reduction rates linked with stable nitrogen isotopes are critical to assess the vulnerability of groundwater systems to redox sensitive parameters such as nitrate. To assess O_2 threshold concentrations for denitrification and the extent to which nitrate reduction occurs in aquifers, a combination of aqueous (geo)chemical and stable isotope techniques may be an effective approach. If (geo)chemical information is combined with knowledge of apparent groundwater MTTs, it appears possible to estimate O_2 reduction rates and the time frames required to reduce O_2 in an aquifer to levels where denitrification can commence (denitrification lag time) so that nitrate removal from groundwater can be accelerated dependent on the availability of electron donors in the system. By combining information from O_2 concentration measurements, environmental isotope data, chemical parameters and calculated apparent MTTs of groundwater, we explore whether low O_2 reduction rates represent a limiting factor that delays recovery of nitrate-contaminated porous aquifers over time scales of years or even decades.
To achieve this goal, we investigated a nitrate-contaminated aquifer in an area with intensive hog farming in south-eastern Germany with the objective to determine O_2 reduction rates and to use the stable isotope composition of dissolved nitrate ($\delta^{15}N$ & $\delta^{18}O$) to evaluate nitrate sources and the extent to which denitrification has occurred in groundwater. For that, we also determined the apparent MTT of the groundwater using environmental isotopes (δ^2H & $\delta^{18}O$, $^3H/^3He$, ^{14}C) linked with a lumped parameter modelling approach. By comparing O_2 reduction rates with apparent MTTs of groundwater, we estimated the denitrification lag time in the investigated aquifer.

Moreover, in recent literature (i. e. Pauwels et al. (2000) and Xue et al. (2009)) ambiguities and difficulties interpreting $\delta^{15}N$ and $\delta^{18}O$ values of nitrate in groundwater systems emerged. Hydrodynamic processes in the groundwater systems, such as mixing and transport, may influence the initial $\delta^{15}N$ and $\delta^{18}O$ values. This may lead to a misinterpretation of isotope signatures and denitrification potential. Therefore, we hypothesize that Monte Carlo simulations have the potential to further assess and understand the processes influencing $\delta^{15}N$ distributions in a groundwater system with a complex hydrogeological structure and can support decision makers in the assessment of nitrate isotope data. In order to simulate $\delta^{15}N$-value distributions in groundwater

arising from specific potential contributions, we proceeded stepwise by including 1) the land use and related input (agricultural versus non-agricultural land use and mixing of the nitrate sources manure, mineral fertilizer and precipitation), 2) hydrodynamic processes (advection and dispersion) in groundwater, and finally 3) possible microbial denitrification. Such contributions may explain δ^{15}N-values observed in groundwater in more detail and may support the interpretation of isotope data, which have been analyzed in different simulation scenarios.

2

MATERIAL AND METHODS

2.1 STUDY SITE, GEOLOGY AND HYDROGEOLOGY

The study was conducted in an 270 km^2 agricultural area near Hohenthann located 90 km north-east of Munich (Bavaria, Germany) within the Bavarian Tertiary Molasse-Hills. 65% of the area is agriculturally used with maize as the predominant crop and intensive hog farming, whereas the remaining 35% are forested and urban areas as displayed in Figure 3a. The central village Hohenthann has a population of around 4,000 inhabitants and the hog farms in its surroundings house 65,000 pigs (Lill, 2013). According to a farmer's survey, manure and mineral fertilizer were applied in equal amounts to the fields. The area receives annual rainfall of around 800mm (Kainzmaier et al., 2007). The mean annual air temperature is 7.5 to 8.0°C.

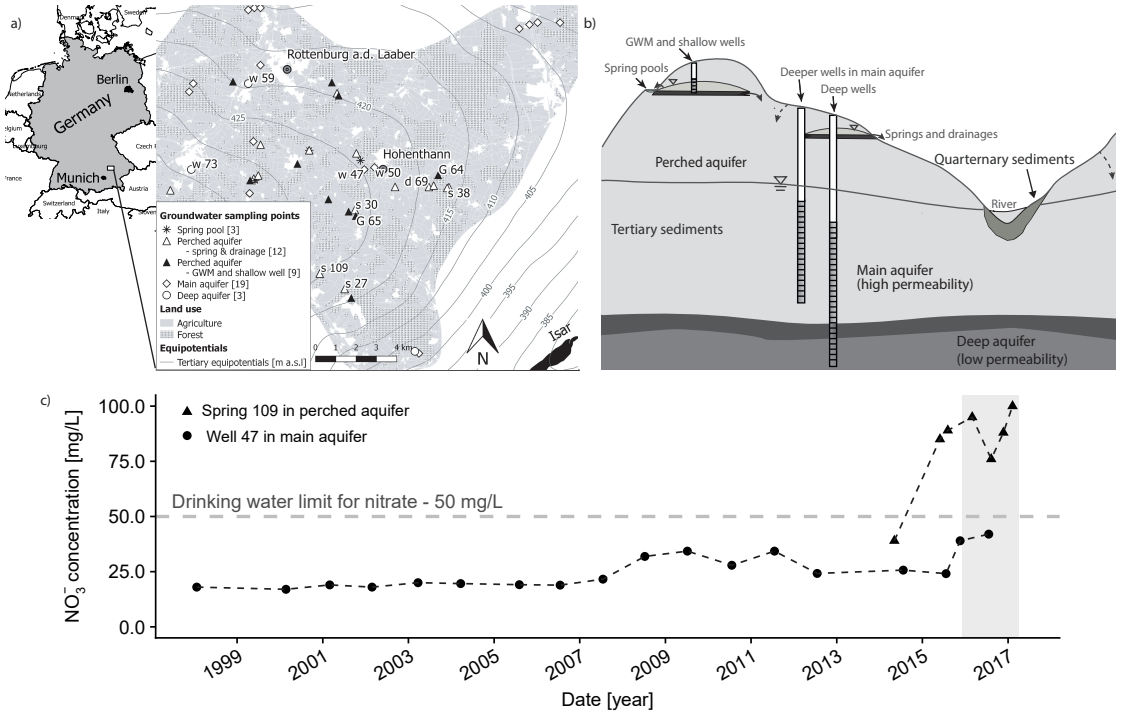

Figure 3: a) Location of sampling sites (d = drainage, s = spring, G = GWM, w = well), b) Schematic cross-section of the hydrogeology and c) Trend of nitrate concentrations with time for spring 109 and well 47; shaded area shows sampling period

Since there are no major rivers and large creeks, surface runoff of N compounds is assumed to be very limited. Hence, most of the agricultural nitrate may reach the hydrosphere mainly via groundwater recharge through sandy to silty soils at quite variable recharge rates due to the heterogeneity of the materials in the water-unsaturated zone. As the landscape is compiled of rolling hills, the depth

to the saturated zone is quite variable and ranges between 0.4 and 53 mbgl with a median of 16.6 mbgl. There are hardly any wetlands and riparian zones that could facilitate denitrification or anammox during nitrate infiltration into the aquifer. Within the catchment, a hydrological divide runs east-west demarcating a boundary where groundwater flows to the north-west or south-west, towards the rivers Danube (not shown in Figure 3a) and Isar. From the hydrogeological point of view, the groundwater is hydraulically connected to the surface water and could discharge to both rivers. Consequently, the discharge of groundwater with elevated nitrate concentrations into surface water could result in a significant decrease of surface water quality.

The study area is underlain by various aquifers in heterogeneous clastic sediments of the South-German Molasse basin as displayed in a schematic cross-section in Figure 3b. A perched aquifer (PA) at depths above 45 mbgl is formed by locally occurring clay layers with coarser sand and gravel above with groundwater being partly discharged to springs. The main aquifer (MA) from 45 to 150 m depth is composed of the Younger Upper Freshwater Molasse (UFMy), the Northern Gravel Series (NGS) and the Fluviatile Freshwater Layers (FFL) of the Upper Freshwater Molasse (UFM). The facies is described as sandy, gravelly to silty, with K_f-values of 10^{-6} to 10^{-4} m/s (Kainzmaier et al., 2007). A deep aquifer in 150 to 200 m depth in the Limnic Freshwater Layers (LFL) belongs to a sequence of fine clastic sediments and is located underneath the UFM and the MA. The facies includes purple colored sandy clays and marl together with light brown micaceous fine to medium-grained sand. The LFL belong to the Upper Brackish Molasse (late Ottnangian/early Kapatian) and the hydraulic conductivities are lower with K_f-values between 8×10^{-7} and 5×10^{-5}m/s (Doppler et al., 2005; Kainzmaier et al., 2007).

The groundwater recharge for the PA ranges between 54 and 89 mm/a, whereas the recharge for the MA is much less with around 16 mm/a (Kainzmaier et al., 2007). For the deep aquifer, no recharge rates have been determined. Nitrate concentrations are generally high in groundwater of the study area and displayed often increasing trends throughout the last two decades. For instance, nitrate concentrations in groundwater from well 47 completed in the MA increased from 18 mg/L (0.29 mmol/L) in 1998 to 44 mg/L (0.71 mmol/L) in 2016, while a spring (#109) draining groundwater from the PA had nitrate concentrations increasing from 39 mg/L (0.63 mmol/L) in 2014 to 100 mg/L (1.61 mmol/L) in 2017 as displayed in Figure 3c.

2.2 SAMPLING

Sampling was conducted within a project campaign of the Bavarian Environmental Agency between December 2015 and March 2017, with the main sampling of deep wells conducted in the summer of 2016. During the sampling campaign three spring pools, which are springs draining into small surface water ponds (n=3), twelve springs and tile drainages (n=12), and nine (n=9) shallow groundwater monitoring (GWM) and domestic wells, all yielding groundwater from the PA were sampled. In addition, 22 deep groundwater wells (n=22) were sampled once, of which 19 wells are screened in the MA (n=19) and three in the deep aquifer (n=3). One electrically cooled precipitation collector was sampled every month. All sampling points are displayed

in Figure 3a.

The field parameters electrochemical conductivity (EC), pH, redox potential (E_h), temperature (T) and the dissolved O_2 concentration were determined in the field for groundwater from wells after either exchanging at least 1.5 $\times$ the volume of the standing water in the wells or after physico-chemical parameters had stabilized while measuring them continuously using a flow cell. For springs and drainages, these parameters were measured directly in the outflow or in a beaker. Samples for major and minor anions (filtered, unacidified) and cations (filtered and acidified) were obtained from all sampling points and analyzed in the laboratory for concentrations. To determine the sources of dissolved nitrate and to assess whether denitrification had occurred, samples for nitrogen (N) and oxygen (O) isotope analyses were obtained from all deep groundwater wells and the spring-fed pond once, while such samples were collected every three months for seepage waters of the agriculturally used fields and the forested areas from twelve drainages and springs and from the nine GWM and shallow domestic wells.

To characterize the apparent MTT of groundwater, samples for the determination of the isotopic composition of water (δ^2H & $\delta^{18}O$) were collected monthly from four selected springs and the four GWM completed in the PA and the precipitation collector. Every 3 months samples were obtained from the shallow domestic wells in the PA and once in summer 2016 from 19 deeper wells (> 45 mbgl) that were screened in the MA. From these wells, samples were also obtained for the analysis of ^3H / ^3He. Three deep wells completed and screened in the deep aquifer (134.5 to 185 mbgl) were sampled for the same parameters as all other wells plus an additional sample for ^{14}C was obtained.

2.3 STANDARD PARAMETERS AND MAJOR IONS

The physico-chemical parameters EC, pH, E_h, T and the dissolved O_2 concentration were measured in the field using a flow cell for groundwater from all wells. To determine these parameters, a WTW Multi 3420 and a Multi 3430 were used. The EC was measured with a WTW TetraCon® electrode, the pH with a WTW SenTix® 940 electrode, the O_2 with a WTW FDO® 925 electrode and the (E_h) with a WTW SenTix® ORP 900 electrode.

Major ions in the water (Na^+, NH_4^+, K^+, Mg^{2+}, Ca^{2+}, F^-, Cl^-, NO_2^-, Br^-, NO_3^-, PO_4^{3-}, SO_4^{2-}) were analyzed with a Sykam ion chromatograph (SYKAM Chromatographie Vertriebs GmbH, Fürstenfeldbruck, Germany). Anion concentrations were determined with a Dionex IonPac AS22 analytical column (4 x 250 mm), which was used isocratically with 4.5 mmol/L sodium carbonate and 1.4 mmol/L sodium hydrogen carbonate as eluents. Column flow was 1.2 mL/min. Cation concentrations were determined on a Dionex IonPac CS 12A analytical column (4 x 250 mm) (Thermo Fischer Scientific, Germering, Germany) with an eluent containing 20 mmol/L methane sulfonic acid. Column flow was 1 mL/min. Concentrations of major cations and anions have an analytical error of less than 3%.

DOC concentrations were determined with a Analytik Jena TOC analyzer Multi N/C® 3100/ 2100 (Analytik Jena AG, Jena, Germany) with an analytical error of approx-

imately ±15% at a DOC concentration of ≈ 0.08 mM. The detection limit of DOC was 16.7 µmol/L, however, 11.8 µmol/L is the calculated lower concentration c_L, where all measured data below the detection limit (d) of 16.7 µmol/L is displayed as $c_L = d/\sqrt{2} = 11.78$ µmol/L.

2.4 NITRATE ISOTOPES ($\delta^{15}N$ & $\delta^{18}O$)

For N and O isotope ratio analysis of nitrate, NO_3^- was extracted from groundwater samples using the methodology of Silva et al. (2000). From the formed anhydrous $AgNO_3$, 300 µg were transferred into a tin cup for nitrogen isotope analysis and 1000 µg into a high purity silver cup for analysis of the O isotope ratios of NO_3^-. Samples were thermally decomposed in an elemental analyser and the resulting N_2 was analyzed by isotope ratio mass spectrometry (IRMS) in a continuous flow mode. To determine O isotope ratios of NO_3^-, CO was generated through pyrolysis using a High Temperature Conversion Elemental Analyzer (TC/EA) reactor (1350°C) coupled to a delta plus XL IRMS in continuous flow mode (Einsiedl and Mayer, 2006). Nitrogen and oxygen isotope ratios of nitrate are expressed in the standard δ (delta) notation in per mill (‰) as calculated in equation 23 with respect to the international standards nitrogen (N_2) in atmospheric air (AIR) for $\delta^{15}N$ and Standard Mean Ocean Water (VSMOW) for $\delta^{18}O$. The uncertainty of the method is ± 0.5‰ for both $\delta^{15}N$ and $\delta^{18}O$.

2.5 SULFUR ISOTOPE RATIOS ($\delta^{34}S$) OF SULFATE

To analyse S isotope ratios in SO_4^{2-}, sample volumes of 1 L were acidified to pH ⩽3 and $BaCl_2$ (10%) was added to precipitate $BaSO_4$, which was then filtered and dried. Isotope analysis was performed by IRMS after complete conversion of $BaSO_4$ to SO_2 via high temperature combustion (1000°C) with V_2O_5 in an elemental analyzer.

2.6 THE ISOTOPIC COMPOSITION OF WATER (δ^2H & $\delta^{18}O$)

To determine the isotopic composition of water (δ^2H and $\delta^{18}O$) the samples were filtered with a 0.22 µm filter and filled into a 2 mL-Vial in the field. Hydrogen and oxygen isotope ratios of water were measured with a 'Triple-Liquid Water Isotope Analyzer (T-LWIA)', which is a infra-red spectrometer for isotopic ratios from the company Los Gatos Research. The analytical precision is ±0.15‰ for $\delta^{18}O$ and ±1‰ for δ^2H. Hydrogen and oxygen isotope ratios are expressed in the internationally accepted δ notation shown in equation 23 with respect to the standard V-SMOW (Vienna-Standard Mean Ocean Water).

$$\delta[‰] = \frac{R_{Sample} - R_{Standard}}{R_{Standard}} \tag{23}$$

where R stands for $^2H/^1H$, $^{15}N/^{14}N$ or $^{18}O/^{16}O$ of samples and references, respectively

2.7 TRITIUM AND HELIUM ($^3H/^3He$)

Samples for tritium analyses were collected in duplicates in 1 L plastic bottles. Samples for helium isotopes and neon (Ne) analyses were collected in duplicates in copper tubes

following the sampling protocol of the Institute of Environmental Physics, Bremen University (http://www.noblegas.uni-bremen.de/documents/sampling_hints.pdf). He and Ne were extracted from the water and separated from other gases using a cryo system at 25 K and 14 K. ^{4}He, ^{20}Ne and ^{22}Ne analyses were conducted with a quadrupole mass spectrometer (Balzer QMG112A), helium isotopes were measured with a high-resolution sector field mass spectrometer (MAP 215-50) and tritium was analyzed with the ^{3}He-ingrowth method (Massmann et al., 2007; Sültenfuß et al., 2009). Ne was analyzed to identify potential atmospheric contamination excess air in ^{3}He samples. If there is excess air in the sample, which may be determined by Δ^{4}He being smaller than ΔNe, fractionation might have taken place and the sample was discarded. The measurement error for ^{3}H is less than 0.01 TU and the error for ^{3}He is determined by the uncertainty of air excess and the infiltration temperature and is estimated to 2% at an equilibrium concentration (Sültenfuß, 1998; Sültenfuß and Massmann, 2004).

2.8 CARBON-14 (^{14}C)

For each of the three deep wells, 2 × 1L of groundwater was collected in plastic bottles for carbon-14 analysis (^{14}C) on dissolved inorganic carbon (DIC). The samples were analyzed in an Acceleration Mass Spectrometer (AMS) at the GADAM Centre in the Silesian University of Technology, Gliwice, Poland following the protocol of Piotrowska (2013).

2.9 MODELING OF MEAN TRANSIT TIMES

Apparent MTT of groundwater were modeled with a lumped-parameter model that is characterized by the transit time distribution function of tracer particles transported between the input (recharge area) and the output (well or a spring). For the interpretation of environmental isotope data (δ^{2}H & δ^{18}O,^{3}H, ^{3}He, ^{14}C), we used the dispersion model as shown in equation 22 (Einsiedl et al., 2009; Kreft and Zuber, 1978; Maloszewski and Zuber, 1982, 1996; Małoszewski and Zuber, 1985) and as modeling software the Excel workbook TraceLPM (Jurgens et al., 2012; Visser et al., 2013).

If theoretical output concentrations could not be fitted to the isotope concentrations measured in groundwater with a simple dispersion model it was assumed that groundwater mixing between old ^{3}H free (old fraction) and young groundwater due to well screens across multiple aquifer units in a well had occurred. For finding a model fit for groundwater that is characterized by an old tritium-free and young ^{3}H containing water component a Binary Mixing Model (BMM) was used. Here the BMM is defined by two dispersion models for the first and second water component (Jurgens et al., 2012). To estimate the apparent groundwater ages of data points that were modeled with a Binary Mixing Model, the second water component was assumed ^{3}H-free and therefore 500 years was set as the MTT and a P_D^* of 0.1 was chosen. However, if there was no good model fit or no realistic MTT and P_D^* for the first component found, the P_D^* of the second water component was changed slightly to obtain less error.

In the dispersion model, the two parameters P_D^* and the MTT are used as fitting parameters and can be found by solving the convolution integral along with the used lumped parameter approach (Maloszewski and Zuber, 1982). The proximity of the in-

vestigated catchment area to Munich (90 km), allowed using ^{3}H data that were taken from a precipitation station in Munich, Neuherberg (Germany). However, the data set was extended by extrapolation with IAEA data from Vienna, Austria as for the years 01/2007 to 07/2009 when no data from Munich were available. Precipitation data was added from the Germany's National Meteorological Service (DWD) data base for the weather station Munich, Neuherberg. To obtain a realistic input signal, the raw input data was adjusted by equation 24 using the yearly weighted precipitation means of Neuherberg, Munich, Germany and a alpha factor of 0.44 that was calculated by using equation 25, including the precipitation and $\delta^{18}O$ data from 1998 to 2002 from Munich, Neuherberg (Grabczak et al., 1984).

$$c = \frac{\sum_i \alpha_i \, P_i \, c_i}{\sum_i \alpha_i \, P_i} \tag{24}$$

$$\alpha = \frac{|\,(\delta P_W - \delta G)\ \sum_i (P_i)_W\,|}{|\,(\delta G - \delta P_S)\ \sum_i (P_i)_S\,|} \tag{25}$$

where δG stands for the mean $\delta^{18}O$ value of the local groundwater originating from recent precipitation; δP_W and δP_S are the long-term weighted mean $\delta^{18}O$ values for the winter and summer precipitation, respectively.

Theoretical ^{3}H output concentrations that were found with the dispersion model were fitted to the tracer time series of ^{3}H in groundwater. If no ^{3}H timeline was available, a tracer-tracer model calculated the apparent MTT for given measured ^{3}H, ^{3}He concentrations the initial tritium concentration $^{3}H_0$ and ^{14}C. In comparison to the tracer time series (TTS) application of the Tracer-LPM, the tracer-tracer model (TTM) evaluates multiple tracer output concentrations with modeled concentrations against each other at a single sampling event (Jurgens et al., 2012). Further, the theoretical output-concentration of ^{3}He was also fitted to the measured ^{3}He concentrations in groundwater that were collected for the wells in 2016. Model fitting for time-series graphs were carried out using a trial-and-error process for ^{3}H and ^{3}He. For the TTM an automated modeling process was conducted by the program and the goodness of fit was quantitatively described by the model efficiency in % error.

2.10 MONTE CARLO SIMULATIONS

For both aquifer units, the PA and the MA, $\delta^{15}N$ values of dissolved nitrate in groundwater were analyzed during the former survey. In the present study, observations from summer 2016 were selected for the PA, since seasonal variations of $\delta^{15}N$ within the observation period (December 2015 to March 2017) revealed to be low. Thus, considered $\delta^{15}N$ values for both aquifers refer to the same time frame. PDFs were fitted to these measured $\delta^{15}N$ values for the MA and PA, respectively, and $\delta^{15}N$ frequency distributions determined, which were then compared to simulated isotopic distributions. The latter were generated by Monte Carlo simulations considering three scenarios that can be assumed for groundwater systems: 1) only mixing of different nitrate sources with characteristic $\delta^{15}N$ signatures, 2) mixing combined with hydrodynamic processes (nitrate transport in groundwater without biotic or abiotic reactions) and 3) mixing and nitrate transport in groundwater affected by

microbial denitrification. The three scenarios are described in the following, and Table 1 summarizes the considered parameter ranges and PDFs.

Table 1: Considered parameter ranges and PDFs. Data for $\delta^{15}N$ in manure, mineral fertilizer (MF) and precipitation (P) are taken from Kendall & McDonnell (1998), other parameters are defined for the aquifer system of the study area. PA: perched aquifer, MA: main aquifer, x: flow length, MTT: mean transit time of groundwater, ε: isotope enrichment factor, distr.: distribution, min.: minimum, max.: maximum.

Parameter	Min.	Max.	PDF	PDF parameters
δ^{15}**N(manure)**	6‰	24‰	Beta distr.	α = 1.96, β = 2.24 min.: 3.25, max.:24.6
δ^{15}**N(MF)**	−4‰	6‰	Normal distr.	μ = 2.06, σ = 2.00
δ^{15}**N(P)**	−6‰	12‰	Normal distr.	μ = 0.62, σ = 3.47
$\mathbf{P_D}$	0.01	0.3	Normal distr.	μ = 0.15, σ = 0.1 min., max.
x – PA	50 m	100 m	Uniform distr.	min., max.
x – MA	500 m	1000 m	Uniform distr.	min., max.
MTT –PA	1 a	10 a	Uniform distr.	Min., max.
MTT –MA	14 a	122 a	Log logistic distr.	γ = 4.18, β = 18.01, α = 2.60
ε	−25	−10	Uniform distr.	min., max.

2.10.1 *Scenario 1 - Mixing*

Scenario 1 simulates $\delta^{15}N$ distributions for the mixing of different nitrate sources most relevant for the field site, including manure, mineral fertilizer and nitrate derived from precipitation. Typical $\delta^{15}N$ distributions observed for these nitrate sources are reported by Kendall and McDonnell (1998b), as shown in Figure S3 in the Appendix B. These observed distributions were evaluated by the Anderson-Darling test (kurtosis sensitive), Kolmogorov-Smirnov test (sensitive to the mean of the distribution) and Chi-Squared (null hypothesis) test, and resulting p-values were compared in order to find best-fit distributions (obtained distributions are presented below) (Huber-Carol et al., 2008; Pettitt and Stephens, 1977).

Agricultural (portion p_1) or non-agricultural land use ($1-p_1$) was considered, where p_1 can imply either the use of manure (p_2) or mineral fertilizer ($1-p_2$), and $1-p_1$ is associated to nitrate derived from precipitation as the only nitrate source. $\delta^{15}N$ values in groundwater (GW) are thus obtained as:

$$\delta^{15}N_{GW} = p_1 \cdot [p_2 \cdot \delta^{15}N_M + (1-p_2) \cdot \delta^{15}N_{MF}] + (1-p1) \cdot \delta^{15}N_P \quad (26)$$

Monte Carlo simulations applied random sampling of the fitted $\delta^{15}N$ distributions for manure, mineral fertilizer and precipitation ($\delta^{15}N_M$, $\delta^{15}N_{MF}$ and $\delta^{15}N_P$), where

portions p_1 and p_2 were varied in steps of 0.05 (5%) for Scenario (Sc.) 1 and steps of 0.1 (10%) for further use in Sc. 2 and 3.

2.10.2 *Scenario 2 - Hydrodynamic processes*

In **Scenario 2**, it was assumed that nitrate released from the sources to groundwater is subject to hydrodynamic processes, while being transported along certain distances to the observation wells. As outlined in the introduction, a first modeling approach was done using analytical solutions that consider homogeneous conditions for the perched and the MA. Otherwise, multidimensional numerical advection-dispersion models could address a complex geological structure and hydrogeology, but such models need a detailed data set in high spatial resolution, which is not available for this site. Instead, in our study, aquifer heterogeneities were considered by random sampling from the PDFs, which we have defined for the transport parameters of the analytical model (as described below). Our findings from modeling where then carefully compared to study site observations and literature findings. Accordingly, an analytical solution for a 1D transport has been implemented based upon van Genuchten and Alves (1982), considering constant input to groundwater (at x = 0). $\delta^{15}N$ values in groundwater as a function of time t, at location x downstream of the source, was modeled, accordingly, as:

$$\delta^{15}N_{GW,d}(x,t) = \delta^{15}N_{GW} \times B(x,t) \tag{27}$$

with

$$B(x,t) = \frac{1}{2}exp\left[\frac{(v-u)x}{2D}\right] erfc\left[\frac{Rx-ut}{2\sqrt{DRt}}\right] + \frac{1}{2}exp\left[\frac{(v+u)x}{2D}\right] erfc\left[\frac{Rx+ut}{2\sqrt{DRt}}\right] \tag{28}$$

and $u = v\ (1 + 4kD/v^2)^{0.5}$, where $\delta^{15}N_{GW}$ is initial $\delta^{15}N$ in groundwater (input from sources at x = 0, equation 27), v represents the groundwater flow velocity, x the flow length, t time and D the dispersion coefficient. The latter can be defined as $D = \alpha_L\ v_x = P_D\ v\ x$, with longitudinal dispersivity α_L and dispersion parameter P_D. R is the retardation factor, and was set to 1 (no retardation assumed), and k is a first-order rate constant for degradation, set to zero in Sc. 2 (no degradation assumed). PDFs were defined for the Monte Carlos simulations, as described in the following.

From $^3H/^3He$ measurements and modeling results, we found a range of plausible P_D values for the aquifer. To these values a normal distribution could be fitted with mean $\mu = 0.15$ and standard deviation $\sigma = 0.1$, truncated by 0.01 and 0.3 (corresponding to minimum and maximum P_D identified). The groundwater flow velocity v was calculated by dividing flow length x by the MTT. Corresponding to assumed ranges for the field site (average distance between nitrate sources and downstream groundwater wells), uniform distributions with x = 50 to 100 m and x = 500 to 1000 m were considered for the PA and the MA, respectively. Based upon MTT determined from $^3H/^3He$ dating, an uniform distribution with 1 to 10 years was considered for the PA, and a log logistic distribution with location parameter (shift) $\gamma = 4.18$, scale parameter $\beta = 18.01$, shape parameter $\alpha = 2.60$ was fitted for the MA.

2.10.3 *Scenario 3 - Microbial Denitrification*

In **Scenario 3**, hydrodynamic processes including microbial denitrification with isotopic enrichment of ^{15}N in the remaining nitrate were considered. For that, equation 28 was used, where k (as part of coefficient u) was defined as $k = \mu\,(\alpha - 1)$. There, μ [a^{-1}] is a first-order rate constant for microbial degradation of nitrate and α [-] is the isotope fractionation factor (derivation see Section S1 in the SI). The isotope enrichment factor ε is defined as $\varepsilon = (\alpha - 1) \times 1000$, and a range of ε from −25‰ to −10‰ was considered, which has been observed for porous aquifers (Boettcher et al., 1990; Mariotti et al., 1981, 1982). This range was defined as a uniform distribution for the Monte Carlo simulations. For the first-order degradation rate constant μ, generic values of 0.1 and 1 a^{-1} were presumed in order to consider moderate and high microbial degradation in groundwater, exemplarily (based on typical ranges, (Tesoriero and Puckett, 2011)).

Convergence was analyzed for all Monte Carlo simulations, where a relative stability of the calculated moments (average and variance) was reached after 5000 to 6000 trials, depending on the scenario and realization. This is shown qualitatively in Figure S34 in the Supplementary Information for selected cases. We therefore decided to apply a slightly higher number of 10,000 trials for the Monte Carlo simulations, for which we applied the Microsoft Excel-Add-In @Risk (Palisade Decisiontools) as well as R version 3.5.1 (R Core Team 2018) implemented within RStudio 1.0.143 (RStudio, Inc.). Each realization of a scenario yielded random samples for the observation (using the fitted PDFs as described above) and the simulation. Data pairs of 10,000 random samples, each, represented 'the observation' and 'the simulation' for every realization. We aimed at evaluating probabilities of $\delta^{15}N$ values, i. e. how observations could be explained by the processes considered in Sc. 1 to 3. Thus, we set up histograms, in order to determine the frequency distribution of observed and simulated $\delta^{15}N$-values within certain ranges (bins). These bins were limited to −10 to +20‰ with an interval of 0.1‰. On the basis of these frequency distributions, the goodness of the model fit was evaluated by using the mean absolute error (MAE) and the coefficient of determination (R^2). The MAE indicates a mean absolute deviation between observation and modeling, as shown in equation 29.

$$MAE = \frac{1}{N} \sum_{i}^{N} |\zeta_i' - \zeta_i| \tag{29}$$

where N is the number of bins (301 bins ranging from −10 to +20‰ with a constant bin width of 0.1‰), ζ'_i and ζ_i is the observed and modeled frequency, i. e. the number of random samples for observed and modeled $\delta^{15}N$, respectively, in each bin i.

The smaller the MAE, the better is the model fit. In this study, the MAE was preferred over the root mean squared error (RMSE), which is widely used in modeling studies but often inappropriate and misinterpreted as it should only be applied for Gaussian distributions (Chai and Draxler, 2014; Willmott and Matsuura, 2005). As the best fit cannot be reduced to only the lowest MAE, we defined a best-fit range from the lowest MAE to the maximum acceptable MAE for each scenario. Each MAE relates to a specific run and thus to a specific realization of a scenario. The maximum acceptable

MAE is defined as the 5^{th} percentile of MAE (cumulative distribution of MAE for all realizations of a scenario).

3

DECADAL DELAYS IN GROUNDWATER RECOVERY FROM NITRATE CONTAMINATION CAUSED BY LOW O_2 REDUCTION RATES

3.1 RESULTS

As the physico-chemical parameters, the concentrations of major ions and the compositions of stable isotopes of nitrate ($\delta^{15}N$ & $\delta^{18}O$) only varied to a negligible extent during the sampling campaigns, we present only the results of a single sampling event.

3.1.1 *Field Parameters and Distribution of Major Ions*

Groundwater in the study area is of Ca^{2+}-HCO_3^- type as revealed in a Piper plot, shown in Figure S1, Appendix A and there is no evidence of cation exchange between Ca^{2+} and Na^+. The median, maximum and minimum values of major ions and physico-chemical parameters for the three aquifers are summarized in Table 2. Nitrate concentrations varied between a minimum of 0.003 mmol/L (well 73, deep aquifer) and a maximum of 1.37 mmol/L (spring 109, PA). Almost 50% of the drainages, springs, GWM and shallow wells in the PA show nitrate concentrations above the nitrate drinking water maximum allowable concentration of 0.8 mmol/L and about 40% of the deeper wells in the MA are above 0.4 mmol/L.

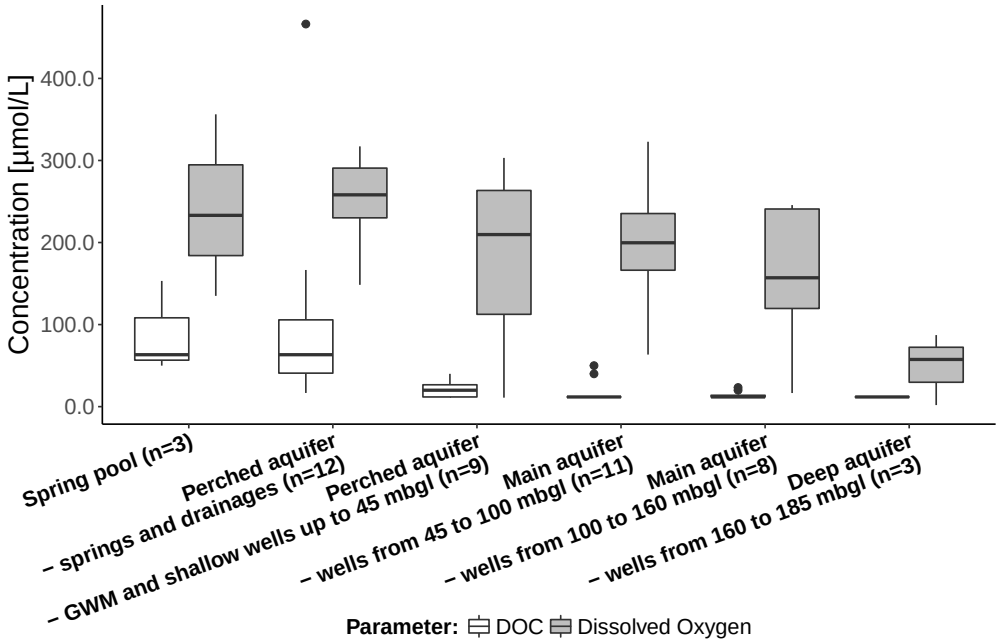

Figure 4: Boxplot of dissolved O_2 and DOC concentrations [µmol/L] in different depths of the aquifer

As shown in Figure 4, O_2 concentrations were highest in the PA with a median of 249.1 µmol/L and decreased slightly in the MA with a median of 198.8 µmol/L, and were lowest in the deep aquifer with a median of 57.5 µmol/L. DOC concentrations decreased rapidly from the spring pools and the springs and drainages in the PA with a median of 33.3 µmol/L to a median of 11.8 µmol/L in the MA and the deep aquifer. Redox potentials ranged between a minimum of −84.4 mV (deep aquifer) to a maximum of +295 mV (MA). Median E_h values ranged from +129 mV in the PA to +198.6 mV in the MA and +162.7 mV in the deep aquifer indicating a lack of reducing conditions in the three aquifers with the exception of groundwater around well 59 in the deep aquifer (−84.4 mV). The pH values in groundwater were near neutral in all measured sampling points ranging from a pH of 6.1 to 8.0 (minimum and maximum measured in the PA).

Table 2: Median, Minimum and Maximum values of the physico-chemical parameters in the different aquifers

Parameter	PA (n=23)			MA (n=19)			Deep aquifer (n=3)		
	Median	Min	Max	Median	Min	Max	Median	Min	Max
O_2 [µmol/L]	249.1	11.0	306.9	198.8	16.6	322.8	57.5	1.9	87.2
O_2 [%]	72.9	3.4	93.7	60.2	5.1	96.5	18.4	0.6	32.2
DOC [µmol/L]	33.3	11.8	466.3	11.8	11.8	50.0	11.8	11.8	11.8
E_h [mV]	129.0	69.4	292.9	198.6	14.3	295.5	162.7	-84.4	182.0
pH [-]	7.2	6.1	8.0	7.4	7.1	7.4	7.3	7.1	7.3
EC [µS/cm] 25°C	675.0	313.0	969.0	590.0	546.0	814.0	582.0	504.0	593.0
Temp. [°C]	10.8	7.3	11.8	10.9	10.0	17.2	13.0	12.9	16.8
HCO_3^- [mmol/l]	4.68	1.13	7.45	5.36	2.86	6.66	6.00	5.70	6.34
SO_4^{2-} [mmol/l]	0.29	0.18	0.57	0.19	0.04	0.42	0.11	0.10	0.19
Cl^- [mmol/l]	0.59	0.16	1.33	0.42	0.11	1.13	0.14	0.03	0.14
F^- [mmol/l]	0.01	0.00	0.02	0.01	0.00	0.01	0.01	0.01	0.01
NO_3^- [mmol/l]	0.76	0.11	1.31	0.33	0.08	0.90	0.10	0.00	0.11
NH_4^+ [mmol/l]	0.001	0.001	0.054	0.001	0.001	0.001	0.003	0.001	0.004
Ca^{2+} [mmol/l]	2.10	0.76	2.87	1.97	1.60	2.77	1.86	1.84	1.90
Mg^{2+} [mmol/l]	1.17	0.39	1.65	1.22	1.07	1.50	1.36	1.28	1.40
Na^+ [mmol/l]	0.25	0.13	0.45	0.16	0.13	0.38	0.23	0.17	0.24
K^+ [mmol/l]	0.02	0.01	0.16	0.02	0.01	0.04	0.03	0.02	0.03
Fe_{total} [mmol/l]	0.0	0.0	0.015	0.0	0.0	0.001	0.005	0.0	0.01

3.1.2 *Stable isotope composition of water (δ^2H & $\delta^{18}O$)*

The oxygen and hydrogen isotope ratios of groundwater (Figure S2 in Appendix A) varied between −10.2‰ and −9.1‰ for $\delta^{18}O_{water}$ and −72.2‰ to −63.4‰ for δ^2H in the PA. In the MA they varied between −10.2‰ and −9.6‰ for $\delta^{18}O_{water}$ and −73.9‰ to −69.2‰ for δ^2H. In the deep aquifer, $\delta^{18}O_{water}$ and δ^2H varied only within analytical uncertainty, ranging from −10.2‰ to −9.9‰ and from −73.6‰ to −71.4‰, respectively.

For monthly measurements of $\delta^{18}O_{water}$ and δ^2H in the GWM and springs in the PA a larger range from −10.5‰ to −6.9‰ and −71.7‰ to −59.0‰ respectively was observed. The amplitude between minimum and maximum δ^2H values showed a range from 1.0‰ to 3.9‰ for groundwater from GWM and shallow domestic wells in the PA and from 0.9‰ to 11.8‰ for springs in the PA with drainage 69 showing by far the largest variance of 11.8‰ over a period of one year.

The collected rainfall from the precipitation sampling point in the study area showed unweighted $\delta^{18}O$ values from −15.2‰ to −5.1‰ and δ^2H values from −116.4‰ to −36.4‰ in the timespan of 1.5 years. The amplitude of the unweighted $\delta^{18}O$ lies therefore at 10.1‰ and for δ^2H at 80.0‰.

3.1.3 *Stable isotope composition of nitrate ($\delta^{15}N$ & $\delta^{18}O$)*

Median, maximum and minimum $\delta^{15}N_{nitrate}$ and $\delta^{18}O_{nitrate}$ values are displayed in Table 3. The most ^{15}N and ^{18}O enriched nitrate isotope compositions were observed for groundwater from two shallow GWM wells in the PA, showing $\delta^{15}N_{nitrate}$ values of 13.1‰ ($\delta^{18}O_{nitrate}$ = 5.2‰) for GWM 65 and 19.7‰ ($\delta^{18}O_{nitrate}$ = 7.5‰) for GWM 64 and a spring pool with 13.6‰ ($\delta^{18}O_{nitrate}$ = 3.5‰) as shown in Figure 5.

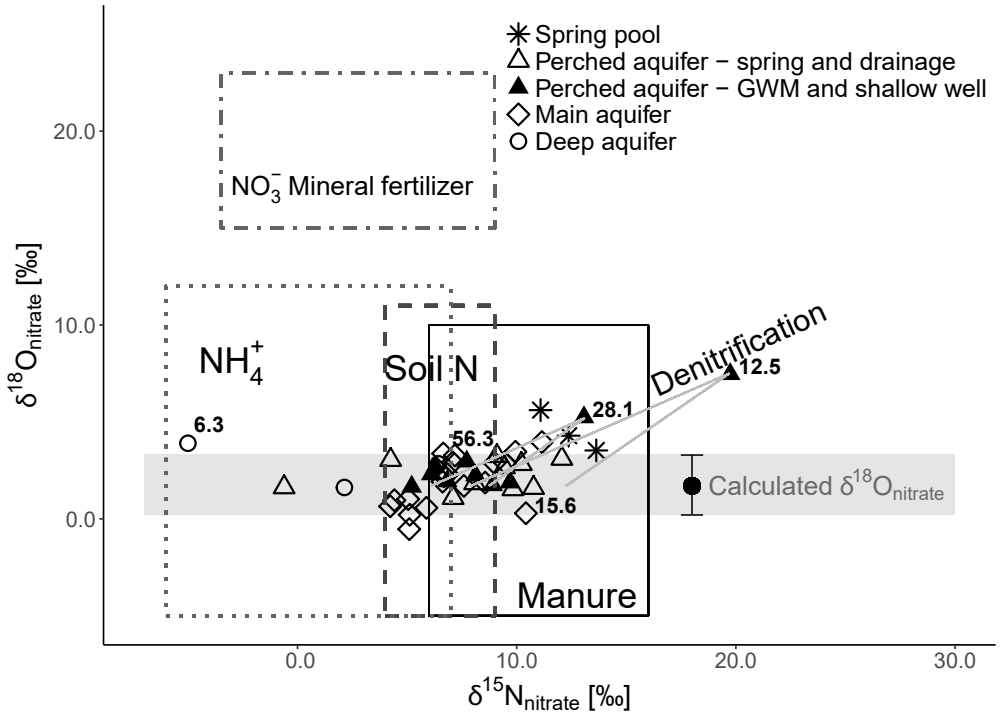

Figure 5: Plot of $\delta^{15}N_{nitrate}$ against $\delta^{18}O_{nitrate}$ to characterize nitrate sources and potential denitrification after Kendall and McDonnell (1998b) ; O_2 concentrations [µmol/L] of less than 60 µmol/L are displayed next to data points

Table 3: Median, Minimum and Maximum of $\delta^{15}N_{nitrate}$ and $\delta^{18}O_{nitrate}$ for the different aquifers

	Spring pools			PA			MA		
	M	Min	Max	M	Min	Max	M	Min	Max
$\delta^{15}N$ [‰]	12.4	11.1	13.6	8.5	-0.6	19.7	6.8	4.2	11.2
$\delta^{18}O$ [‰]	4.5	3.5	5.6	2.3	1.08	7.5	1.9	-0.5	4.0
	Deep aquifer			Overall					
	M	Min	Max	M	Min	Max			
$\delta^{15}N$ [‰]	2.1	-5.0	6.4	7.7	-5.0	19.7			
$\delta^{18}O$ [‰]	2.8	1.6	3.9	2.3	-0.5	7.5			

3.1.4 *Sulfur isotope composition of sulfate ($\delta^{34}S$)*

Groundwater obtained from six wells/GWMs and one spring was analysed for $\delta^{34}S$ in sulfate and values between -8.2‰ and 5.4‰ were observed. The measured $\delta^{34}S$ were plotted against $\delta^{15}N_{nitrate}$ in Figure 6 to identify chemo-lithotrophic dentirification by pyrite oxidation.

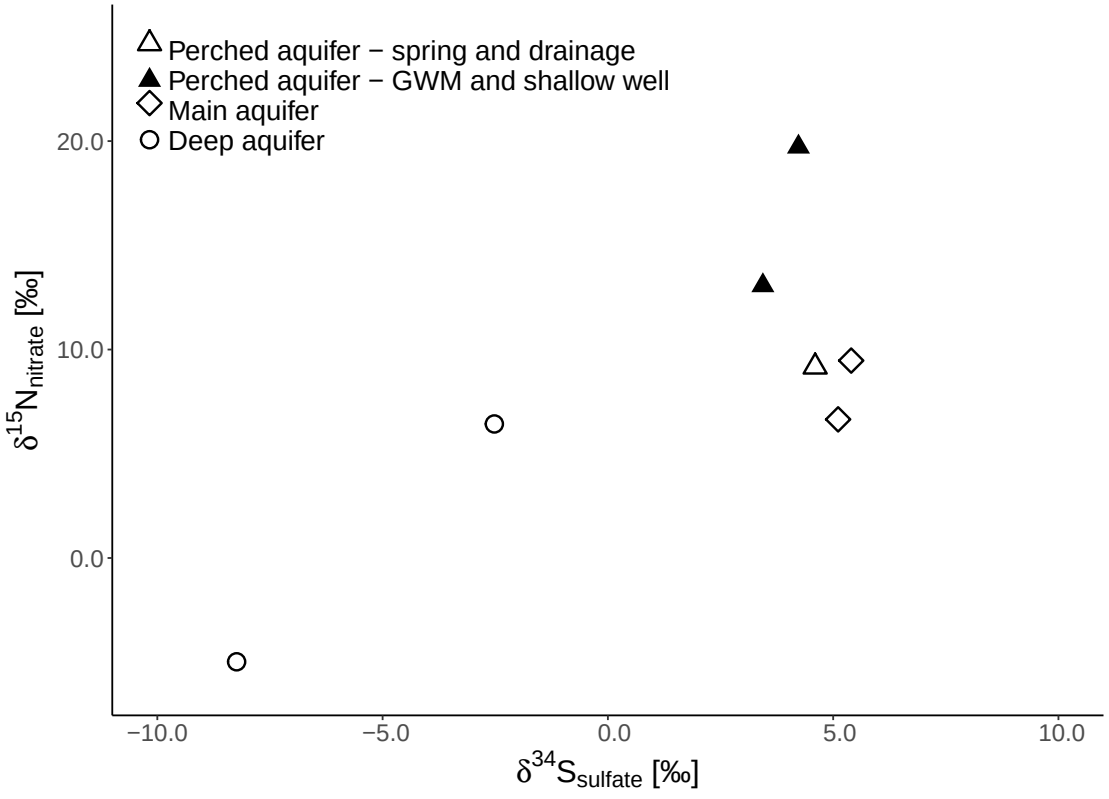

Figure 6: Plot of $\delta^{34}S_{sulfate}$ against $\delta^{15}N_{nitrate}$ to identify lithotrophic denitrification

3.1.5 *Calculation of apparent Mean Transit Times*

Apparent MTT for groundwater from wells screened in the PA varied between 5 and 20 years based on results from the dispersion model. P_D^* values ranged from 0.08 to 0.45. Groundwater MTT in the MA obtained with a dispersion model ranged between 14 and 122 years while P_D^* varied from 0.01 to 0.28. For wells completed in the MA with several screen horizons, the apparent MTT of the first groundwater component were between 14 and 36 years and P_D^* values ranged from 0.01 to 0.42, assuming a second component of ^{3}H free groundwater. Apparent MTTs for groundwater from wells in the deep aquifer were determined with a dispersion parameter and using the ^{3}H and ^{14}C concentrations. The dilution factor q describes the fractional reduction of $a_0^{14}C$ to determine a corrected $a^{14}C_{corr}$ input signal with less than 100 pMC. q values can range from 1 (no dilution, open system) to 0.75 (minor dilution from closed system exchange) to 0.5 (closed system carbonate weathering and exchange) to less than 0.5 (extensive carbonate exchange, possible bacterial sulfate reduction) (Clark, 2015). As a result, ^{14}C modeling revealed apparent MTTs from 965 to 6002 years for groundwater from wells in the deep aquifer depending on the q values ranging from 0.85 to 0.65.

3.1.6 *Calculation of O_2 reduction rates*

Figure 7 displays the apparent MTT against the O_2 concentrations of the groundwater samples showing a decrease of dissolved O_2 concentrations with increasing apparent MTT although O_2 concentration did not reach values below 6.3 µmol/L. As groundwater from wells modeled with a BMM (grey triangles) did not fit a linear regression line, they were separated from those modeled with a dispersion model (black dots) and excluded from the calculation of O_2 reduction rates.

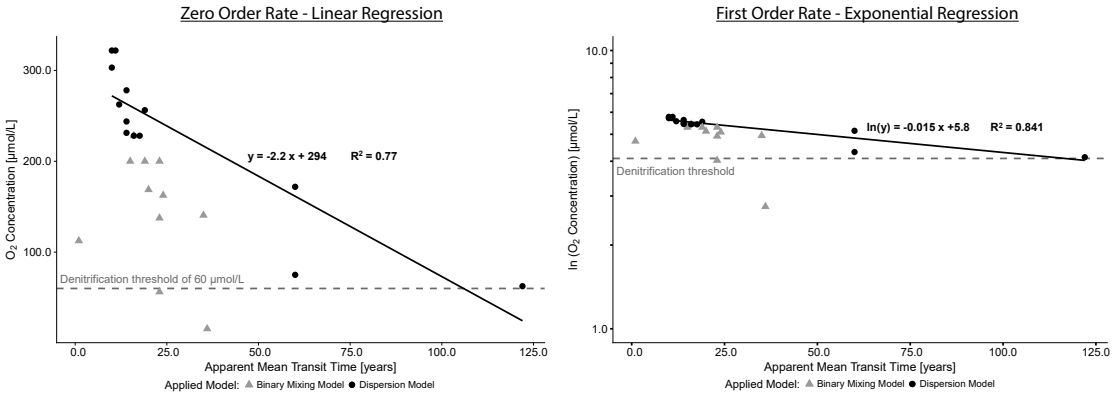

Figure 7: O_2 concentrations against the apparent MTT of groundwater modeled with a dispersion model (black dots) and a BMM (grey triangles); A) Determination of zero-order rate constant k_0 by fitting a linear regression line to O_2 concentrations (C) versus apparent MTT (dispersion model), B) Determination of first-order-rate constant k_1 by fitting a linear regression line to ln (C) versus apparent MTT (dispersion model).

A Zero-order rate constant k_0 was determined by fitting a linear regression line to a plot of O_2 concentration against the apparent groundwater MTT calculated by the dispersion model (Appelo and Postma, 2005; Bekins et al., 1998; Böhlke et al., 2002; Tesoriero and Puckett, 2011). The linear regression line of the dispersion model MTTs

showed a good coefficient of determination with R^2 = 0.77 and a negative slope of 2.2 suggesting a O_2 reduction rate of 2.2 µmol/(L×year). A first-order rate constant k_1 was determined by fitting a linear regression line to a plot of ln(c) versus the apparent groundwater MTT (Tesoriero and Puckett, 2011). The O_2 reduction rate, determined by the first-order, was 0.015 1/yr with R^2 = 0.84.

3.2 DISCUSSION

3.2.1 *Aqueous chemistry and stable isotopes of water*

The distribution of physico -chemical parameters and major ions were typical for groundwater in the UFM (Kainzmaier et al., 2007). Kainzmaier et al. (ibid.) found electrical conductivities in the range of 145 to 1070 µS/cm in the PA and 271 to 822 µS/cm in the MA, while in this study EC values of up to 969 µS/cm were measured in the PA, which may be explained by the high anthropogenic contamination of the groundwater system. Moreover, nitrate concentrations are elevated in the majority of the samples of the PA and the MA. In the PA, nitrate concentrations often exceed the drinking water limit of 0.8 mmol/L (The Council of the EU, 1998) and even the median nitrate concentration of 0.76 mmol/L for the PA is close to the drinking water limit of 0.8 mmol/L.

A plot of δ^2H against $\delta^{18}O$, displayed in Figure S2 in Appendix A, indicates that all sampled groundwater has a meteoric origin and that evaporation during recharge had little influence on the isotopic composition of the sampled groundwater. The measured groundwater isotope data fit well to the Local Meteoric Water Line (LMWL) with δ^2H [‰] = 7.9 $\delta^{18}O$ + 7.9 of Neuherberg, Munich, Germany (Stumpp et al., 2014).

3.2.2 *Constraints on apparent mean transit times*

Since the unweighted δ^2H values of precipitation samples that were collected in the study area vary up to 80‰ within the year, seasonal variations of groundwater with short apparent MTTs of up to four to five years should be detectable (Stichler and Herrmann, 1983). Based on the variation of δ^2H values of 11.8‰ (n=5) and an assumed P_D^* of 0.1, it can be concluded that groundwater of drainage 69 has a relatively short apparent MTT from a few weeks to less than one year. Variations in δ^2H values of more than 3‰ were also detected in groundwater from the PA in spring 30 with a δ^2H amplitude of 3.5‰ (n=13), and in spring 38 with 6.5‰ (n=2) indicating apparent MTTs of less than 4 years. Considering the measurement error of 1‰ for δ^2H, 8 out of 9 GWM/domestic wells and 9 out of 12 springs/drainages in the PA did not show a larger amplitude than 3‰, whereof only 6 of the springs and drainages and 5 of GWM/domestic wells were sampled regularly for δ^2H with at least 10 data points. These relatively low amplitudes and no seasonal variation in most of the springs, GWM and shallow domestic wells suggest an apparent MTT of more than four to five years (Maloszewski et al., 1983, 2002; Stichler and Herrmann, 1983). The stable isotope compositions of water suggest that the groundwater in the majority of springs, GWM and shallow domestic wells in the PA have an apparent MTT of more than 4 years.

MTT modeling results using the $^3H/^3He$ method and ^{14}C as a groundwater dating tool showed that the groundwater obtained from GWM and shallow wells, screened in the PA, is relatively young ranging from 5 to 20 years, whereas a wide range of MTTs between 14 and 122 years were calculated for groundwater from the MA. The large range of MTTs may be explained by the strong heterogeneity of the porous aquifer system and the varying depths of screens in the wells. In Figure 7, we display only the MTT modeling results with reasonable error percentages and P_D^* values between

0.01 and 0.3.

The plot of apparent MTTs versus O_2 concentrations (Figure 7) shows that MTTs obtained using a dispersion model can be well described with a linear regression, while apparent MTTs modeled with a BMM do not conform with the O_2 reduction of data points modeled with a simple dispersion model. Figure 7 also shows that all data points modeled with a BMM composed of two water components (grey triangles) lie below the regression line of the ones that were modeled with a dispersion model using one water component. This suggests that the groundwater in wells modeled with the BMM may be affected by mixing of at least two water components and the O_2 concentrations may be decreased only due to the influence of old, O_2-reduced water and not by O_2 reduction processes along the flow path.

3.2.3 *Limits of oxygen reduction rates*

Figure 4 displays the O_2 and DOC concentrations in different depths of the aquifer. The O_2 concentrations decrease only slightly from the springs and drainages connected to the PA (median = 258.1 µmol/L) to GWM and shallow wells up to 45 mbgl of the PA (median = 210.0 µmol/L), whereas the median DOC concentration decreases from 63.3 µmol/L to 20 µmol/L, respectively. Although there are considerable stochiometric variations (Taylor and Townsend, 2010), we assumed that 1 µmol/L DOC can reduce 1 µmol/L O_2. We found that only one third of the O_2 reduction appears to be caused by DOC oxidation. This indicates that the availability of easy degradable DOC may be the limiting factor for the lack of O_2 reduction as there is either too little DOC or it is not readily available for microorganisms (**Clark1997**; Aravena and Wassenaar, 1993; Einsiedl et al., 2007). However, there is a lack of information concerning the total organic carbon (TOC) content of the aquifer material. Within the scope of this project there was no core material available to determine the quantity and quality of TOC and its effect on O_2 reduction rates, but we suggest to further assess this in the future. Fe(II) as another electron donor may be excluded due to very low concentrations of total iron in all groundwater samples. It appears that the lack of electron donors in the aquifer may represent the limiting parameter for significant O_2 reduction and low O_2 reduction rates. Therefore, high O_2 concentrations in the groundwater may be the reason for high NO_3^- concentrations due to a lack of denitrification.

3.2.4 *Sources of nitrate in groundwater*

To characterize sources of nitrate and reveal potential denitrification in the groundwater system, the $\delta^{15}N$ and $\delta^{18}O$ values of dissolved nitrate from each groundwater sampling point were determined and are plotted in Figure 5. Literature sources reveal that nitrate derived from manure has typically $\delta^{15}N_{nitrate}$ values in the range of +7 to +16‰ and $\delta^{18}O$ values of $\leqslant$ +5‰ (Kendall and McDonnell, 1998b). This is consistent with the isotopic compositions of nitrate in the majority of the groundwater samples from the spring pools (median $\delta^{15}N$ value of 12.4‰), the PA (median $\delta^{15}N$ value of 8.5‰) and to some extent the MA with a median $\delta^{15}N$ value of 6.8‰, and $\delta^{18}O$ values of nitrate < 5‰ (Table 3, Figure 5). The elevated $\delta^{15}N$ values along with high nitrate concentrations as shown in Figure 9 suggest that, especially in

younger groundwater, nitrate is derived from manure (Kendall and McDonnell, 1998b).

During the microbial nitrification of manure-derived ammonium to nitrate, two thirds of the O_2 atoms in the newly formed nitrate are derived from water and one third from dissolved atmospheric O_2 (Amberger and Schmidt, 1987; Böhlke et al., 1997; Durka et al., 1994; Hollocher, 1984; Kendall and McDonnell, 1998b; Wassenaar, 1995). The theoretically expected $\delta^{18}O_{nitrate}$ derived from nitrification can therefore be calculated to an approximate value of 1.7‰ using a $\delta^{18}O_{water}$ value of −9.2‰ and a $\delta^{18}O_{O_2}$ value of 23.5±0.3‰ (Kroopnick and Craig, 1972). Voerkelius (1990) found in laboratory studies similar $\delta^{18}O$ values for nitrate that was formed by nitrification between −2 and +2‰ using $\delta^{18}O$ values for water of −10‰ that were very close to those in our study ($\delta^{18}O_{water}$ = −9.2‰). However, recent studies have shown that the O-exchange between water-oxygen, molecular O_2 and NO_2^-, as well as oxygen isotope fractionation can have a significant impact on the $\delta^{18}O_{nitrate}$ (Buchwald et al., 2012; Casciotti et al., 2010; Fang et al., 2012; Snider et al., 2010). Therefore, $\delta^{18}O$ values of nitrate from microbial nitrification can vary widely depending on soil types, pH and C content (Amberger and Schmidt, 1987; Einsiedl and Mayer, 2006; Mayer et al., 2001; Voerkelius, 1990). Consequently, we assigned an uncertainty of ±1.5‰ to the calculated $\delta^{18}O_{nitrate}$ value of 1.7‰ that assumed no O-exchange reactions and no oxygen isotope fractionation for nitrate derived from nitrification (see grey-shaded area in Figure 5). The majority of groundwater nitrate samples, except the samples from 2 GWMs, 3 spring pools and one well in the MA (well 50), fall into this predicted range of $\delta^{18}O_{nitrate}$ for nitrification processes.

In several wells, predominantly completed in the MA, nitrate was observed with $\delta^{15}N_{nitrate}$ values ranging from +4 to +7‰ and $\delta^{18}O$ values of < 5‰ (Figure 5). These isotope compositions are consistent with nitrate being derived from nitrification of soil N ($\delta^{15}N$ from +4 to +7‰) or possibly nitrate originating from synthetic fertilizers (typically around 0±3‰) (Einsiedl and Mayer, 2006; Kendall and McDonnell, 1998b).
Nitrate observed in groundwater from the deep aquifer with the highest MTTs had the lowest median $\delta^{15}N_{nitrate}$ value with 2.1‰ (Table 3) and $\delta^{18}O$ values < 5‰ (Table 3, Figure 5). This is consistent with nitrate being derived either from synthetic fertilizers or from nitrification processes in agricultural or forest soils throughout the catchment area (Einsiedl and Mayer, 2006). Nitrate from precipitation that undergoes immobilization with subsequent ammonification and nitrification in forest soils results in $\delta^{15}N_{nitrate}$ values of around −10‰ to +2‰ (Kendall and McDonnell, 1998b; Mayer et al., 2001). The latter process is likely also responsible for the nitrate in spring 27 with −0.6‰ and low NO_3^- concentrations of 0.27 mmol/L. Therefore, Figure 5 and Table 2 indicate that the isotopic compositions of nitrate in groundwater are consistent with nitrate being derived from manure predominantly in the younger groundwater and mineralization of organic nitrogen in agricultural and forest soil, and potentially nitrification of ammonia and urea containing fertilizers predominantly in the groundwater with higher MTTs.

3.2.5 *Processes regulating denitrification in groundwater*

The initial isotopic compositions of nitrate can be further modified by N and O isotope fractionation during processes such as denitrification. During this process, ^{15}N and

^{18}O are progressively enriched in the remaining nitrate as concentrations decrease. In laboratory studies, $\delta^{15}N$:$\delta^{18}O$ trajectories of 1 are observed for denitrification (Wunderlich et al., 2012). However, in freshwater systems empirical $\delta^{15}N$:$\delta^{18}O$ trajectories of 0.5 to 0.8 were detected (Amberger and Schmidt, 1987; Casciotti et al., 2002). Trajectories of < 1 in aquifers may be explained by changing redox conditions (oxic/anoxic) leading to a masking of isotopic systematics of denitrification with those of nitrification or by the back reaction of NO_2^- to NO_3^- and anammox (Granger and Wankel, 2016; Wunderlich et al., 2012). In Figure 5 two straight lines with a slope of 0.5 and 0.8 were inserted inversely from the two data points with the most elevated $\delta^{15}N$ and $\delta^{18}O$ in nitrate (GWM 64 and GWM 65 in the PA). Assuming an initial δ_{R_0} for $\delta^{18}O$ of 1.7‰, we determined the initial δ_{R_0} for $\delta^{15}N$ for GWM 64, GWM 65, the three spring pools and well 50.

$$\frac{\delta_{R_t}}{\delta_{R_0}} = \frac{C_t}{C_0}^{(\alpha-1)} \tag{30}$$

δ_{R_t} is the $\delta^{15}N$ value of the reactant nitrate at time t, δ_{R_0} is the initial $\delta^{15}N$ value of nitrate, C_t and C_0 represent the concentrations of nitrate at times t and zero, respectively, and α is the isotopic fractionation factor

To estimate the extent of biodegradation B along the flow path between two sampling points equation 31 can be used:

$$B\ [\%] = 1 - \frac{\delta_{R_t}}{\delta_{R_0}}^{\frac{1000}{\epsilon}} \tag{31}$$

B denotes the % of nitrate reduced from time zero to t, δ_{R_t} and δ_{R_0} are the $\delta^{15}N$ values of nitrate and ϵ is the N isotope enrichment factor.

Using equation 31, derived from equation 30 by Rayleigh (1896) and Mariotti et al. (1981) and a characteristic N isotope enrichment factor ϵ of -15.9‰ for porous groundwater systems (Boettcher et al., 1990), we calculated the initial nitrate concentration. The results in table 4 demonstrate that denitrification removed between 24 and 51% of the initial groundwater nitrate obtained from the two wells (GWM 64 and 65) displaying denitrification trends. Furthermore, nitrate reduction by denitrification was also assessed for the 3 spring pools. For spring pool 2 a nitrate reduction of 26 to 39% was calculated and 13 to 28% for spring pool 1 and 3, indicating only little nitrate reduction. Furthermore, one well (well 50) in the MA shows slightly elevated $\delta^{18}O$ values above the shaded area, but nitrate reduction calculated with the Rayleigh equation shows only minor reduction with less than 30% of the initial nitrate concentration reduced.

Only two wells in the PA (GWM 64 and 65) produced groundwater with elevated $\delta^{15}N$ values in combination with O_2 concentrations of less than 60 µmol/L and low NO_3^- concentrations potentially indicating some denitrification (Figure 8 and Figure 9). However, Figure 9 shows that $\delta^{15}N$ is not increasing with decreasing NO_3^- concentration and increasing depths within the aquifer and consequently increasing travel time, indicating that there is no general trend for denitrification in the dataset

Table 4: Calculated results to interpret the $\delta^{15}N_{nitrate}$ and $\delta^{18}O_{nitrate}$ values GWM 64 and 65, Spring pool 1,2 and 3 in the PA and well 50 in the MA

					$\delta^{18}O_0$ = 1,7‰		
	$C_{t-NO_3^-}$ [mmol/L]	$\delta^{15}N_t$ [‰]	$\delta^{18}O_t$ [‰]	slope [–]	$\delta^{15}N_0$ [‰]	$C_{0-NO_3^-}$ [mmol/L]	$\%_{red.}$ [%]
GWM 64	0.32	19.7	7.5	0.5	8.1	0.69	51%
				0.8	12.5	0.52	36%
GWM 65	0.14	13.1	5.2	0.5	6.1	0.22	35%
				0.8	8.7	0.19	24%
spring pool 1	0.38	13.6	3.5	0.5	10	0.48	20%
				0.8	11.4	0.44	13%
spring pool 2	0.85	11.1	5.6	0.5	3.3	1.42	39%
				0.8	6.2	1.17	26%
spring pool 3	0.57	12.4	4.3	0.5	7.2	1.1	28%
				0.8	9.2	0.97	18%
well 50	0.21	11.2	5.1	0.5	6.6	0.28	25%
				0.8	8.3	0.25	16%

of the study area.

At the two GWM sites, reducing redox conditions with dissolved O_2 concentrations of less than 60 µmol/L were observed (Böhlke et al., 2002; Tesoriero and Puckett, 2011) suggesting that denitrification occurs in this groundwater system at O_2 threshold concentrations of less than 60 µmol/L. Hence, there is some evidence for denitrification, if a combination of elevated $\delta^{15}N$ and $\delta^{18}O$ values and O_2 concentrations <60 µmol/L occur, which is the case for only two groundwater samples from GWM 65 and GWM 64 (Figure 8). However, GWM 64 is located in close proximity to an old landfill and is probably influenced by its highly reducing effluent. At GWM 65, there is a thick layer of silty sediments from 1 to 10 mbgl in the well log resulting in a untypical facies distribution for the entire study area that may be the reason for facilitating denitrification at this site.

Analyses of $\delta^{34}S$ in sulfate (Figure 6) indicate pyrite oxidation in the deep aquifer with negative $\delta^{34}S$ values of -8.2‰ from groundwater from well 73 and -2.5‰ from well 59. These observations are also in accordance with Schwientek et al. (2008), who found distinctly negative $\delta^{34}S_{sulfate}$ values of up to −15‰ in the groundwater of the South-German Molasse basin as a result of nitrate dependent pyrite oxidation. However, $\delta^{15}N$ values are low (-5.0‰ and 6.4‰ respectively) and therefore denitrification appears not to be prevalent. In addition, S and O isotope compositions in agricultural fertilizers and S isotope compositions of animal slurries have been reported by Moncaster et al. (2000) and Bartlett et al. (2010) (Fig. 6). Since the groundwater sulfate in the wells was characterized by $\delta^{34}S$ values of around 5‰ accompanied with moderate SO_4^{2-} concentrations of 0.2 to 0.4 mmol/L and elevated NO_3^- concentrations between

h!

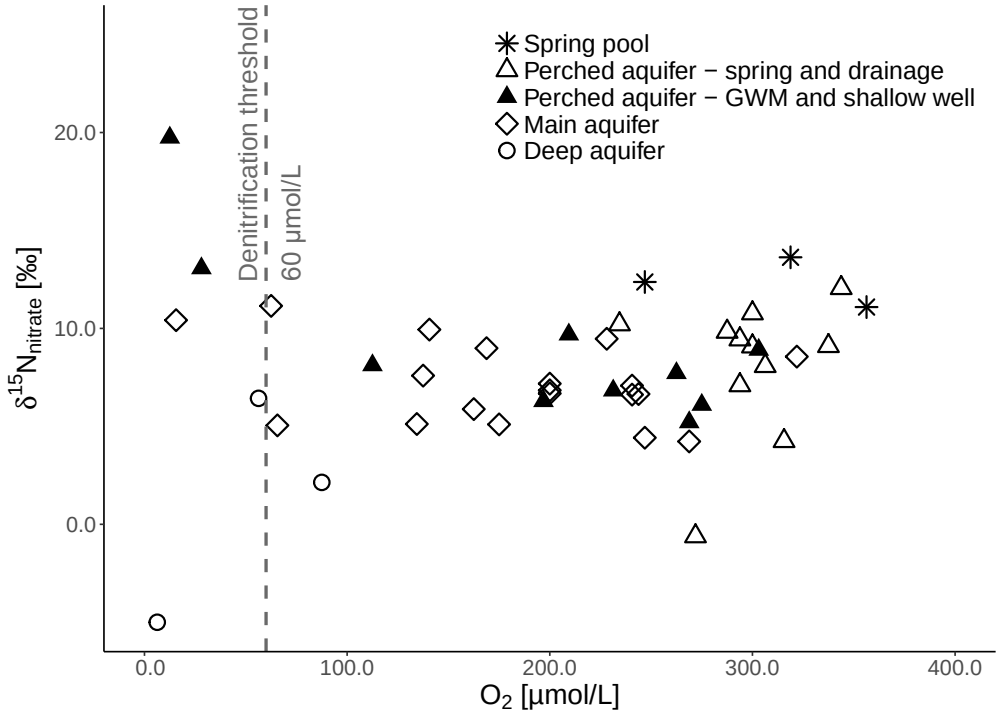

Figure 8: Plot of $\delta^{15}N_{nitrate}$ against O_2 concentrations to determine potential denitrification; The O_2 threshold concentration of 60 µmol/L has been drawn in with a dashed line

approximately 0.7 and 1 mmol/L, it is suggested that $\delta^{34}S$ values in dissolved SO_4^{2-} are predominantly affected by animal slurry or chemical S fertilizers derived S (Einsiedl, 2012). Hence, the presented results show that denitrification may occur only in two exceptional cases in the aquifers of the study area. The lack of denitrification appears to be caused by high O_2 concentrations in the groundwater. Therefore, we further explored the relation of O_2 reduction rates, denitrification lag times and denitrification potential.

3.2.6 *Denitrification lag times and O_2 reduction rates*

The O_2 concentration is a crucial parameter for preventing the occurrence of denitrification. In other field studies, a strong correlation of O_2 concentrations and denitrification potential was observed as there was only denitrification detected, when O_2 concentrations were less than 60 µmol/L (Böhlke et al., 2002; Tesoriero and Puckett, 2011). These results are consistent with our findings that denitrification does not occur when O_2 concentrations are above 60 µmol/L, which is the case in all, but two groundwater samples.

3.2.6.1 *Zero-order vs. first-order O_2 reduction rates*

To determine the lag-phase for denitrification, which is the time needed to lower the O_2 concentration below the denitrification threshold of 60 µmol/L, we calculated the O_2 reduction rate for the aquifer and estimated the availability of electron donors for nitrate reduction using zero-order (rate independent of concentration) and first-order

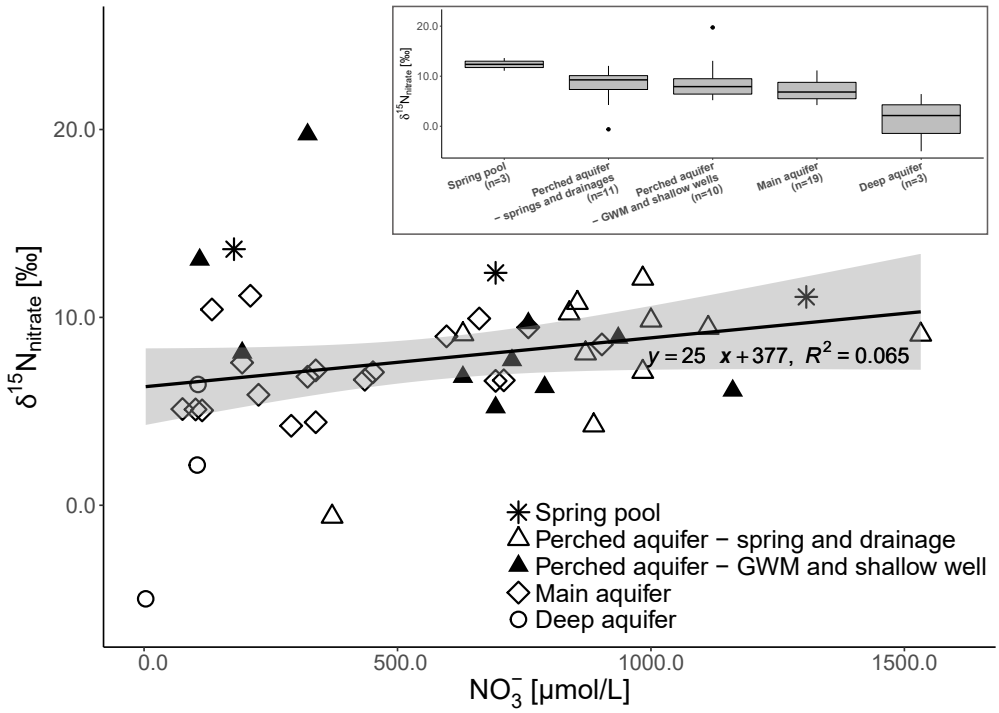

Figure 9: Plot of $\delta^{15}N_{nitrate}$ against NO_3^- concentrations to determine the denitrification potential, shaded area displays 95% confidence interval of data points; boxplot in the right corner shows $\delta^{15}N_{nitrate}$ distribution over the aquifer units

kinetics (rate dependent of concentration) (Appelo and Postma, 2005; Böhlke et al., 2002). In Figure 7, the O_2 concentrations of groundwater from the PA and MA are plotted against the apparent MTTs modeled with a dispersion model. As there were only few wells available in the MA for which the apparent groundwater MTT could be modeled with a simple dispersion model, where no mixing of old ^{3}H-free anoxic and young groundwater occurred, the data points with apparent MTT >25 years are relatively sparse, but reveal nevertheless a well-defined regression line for zero and first-order kinetics (R_0^2 = 0.77, R_1^2 = 0.84). First-order kinetics show a somewhat better fit (R_1^2 = 0.84) and are therefore the preferred model. However, first-order kinetics are only valid when the substrate concentration S is lower than the half-saturation constant K_s, whereas zero-order kinetics are only valid at high substrate concentrations (Bekins et al., 1998; Rifai and Bedient, 1990). This was not tested for the studied aquifer and consequently, both, zero-order and first-order, models are shown in Figure 7. We advise that future studies should determine K_s, v_{max} (maximal removal time), Y (yield) and the parameter b (microbial decay rate) to determine the degradation and the microbial growth rate over all concentration ranges of the substrate pool in laboratory studies. According to Figure 7, the O_2 reduction rate is 2.2 µmol/(L×year) for the zero-order kinetics and 0.015 1/year for the first-order kinetics, which is relatively low compared to DOC-rich waters in shallow riparian flow paths that have O_2 reduction rates of up to 140 µmol/(L×year) for zero-order kinetics (Tesoriero and Puckett, 2011). Assuming that the input is air saturated groundwater with an O_2 concentration of approximately 330 µmol/L (Appelo and Postma, 2005), it takes around 114 years assuming first-order kinetics until the O_2 concentration has been reduced to less than 60 µmol/L in order to obtain redox conditions favorable for denitrification. In

the literature, denitrification lag times vary widely between different study sites, ranging from <20 years at sites with high O_2 reduction rates and a high availability of electron donors to >60 years at sites with low O_2 reduction rates and a very limited supply of electron donors (Tesoriero and Puckett, 2011). Our findings of a denitrification lag time of >100 years are on the very high end of the previously reported range.

3.2.6.2 *Implications of O_2 reduction rates in porous aquifers*

We propose that the calculation of O_2 reduction rates in groundwater is of critical importance for estimating the time required until denitrification may commence in an aquifer and thereby accelerating nitrate removal. This approach may improve the assessment of the vulnerability of aquifers posed by dissolved nitrate and its persistence in drinking water resources. Fogg et al. (1999) have previously concluded that nitrate vulnerable areas may be best identified in combination with the assessment of MTTs. To further include areas with low nitrate reduction via denitrification, we propose that the assessment of O_2 reduction rates for potential nitrate reduction is a powerful tool to determine the potential of suboxic redox processes such as denitrification to occur and should be considered in future groundwater vulnerability studies. If the O_2 reduction is low in a groundwater system and there is no major change in the availability of reactive donors with increasing aquifer depth, denitrification will still not occur over extended time periods, also if O_2 concentrations fall below threshold values, where denitrification can occur. Consequently, elevated concentrations of nitrate will persist at timescales equal to the estimated apparent MTT of groundwater at drinking water wells. An intensive agriculturally used ecosystem with no or only little nitrate reduction potential, may therefore be of great risk for exceeding drinking water quality guidelines for many years or decades after contamination has occurred. Moreover, elevated nitrate concentrations in groundwater would be a concern for surface water quality (Carpenter et al., 1998), if a hydraulic connection between groundwater and the rivers Isar and Danube is present.

The obtained results illustrate the importance of the determination of apparent MTTs of groundwater linked with the calculation of O_2 reduction rates to predict the rate at which nitrate may be removed from groundwater through the process of denitrification. This approach increases the understanding of the groundwater ecosystem and facilitates the assessment of the vulnerability of aquifers posed by dissolved nitrate and its persistence in drinking water resources.

4

MONTE CARLO SIMULATIONS AS A DECISION SUPPORT TO INTERPRET $\delta^{15}N$ VALUES OF NITRATE IN GROUNDWATER

4.1 RESULTS AND DISCUSSION

PDFs were fitted to characteristic $\delta^{15}N$ values of nitrate sources reported by Kendall & of McDonnell (1998) (Figure S3 in Appendix B). A beta distribution was found as a best fit for manure (minimum = 3.25, maximum = 24.60, shape parameters α = 1.96 and β = 2.24). For precipitation and mineral fertilizer, we found normal distributions with mean value μ = 0.62, standard deviation σ = 3.47 and μ=2.06, σ=2.00, respectively. These PDFs were used as input for the Monte Carlo simulations in order to define the characteristics of different nitrate sources. PDFs were also fitted to $\delta^{15}N$ values observed in groundwater of the MA and the PA, respectively, where logistic distributions could describe observations best (with location α = 6.199, scale β = 1.952 for the MA and α = 9.221, β = 1.781 for the PA). Subsequently, Monte Carlo simulations were run (10,000 trials) applying these PDFs in order to generate 'measured' $\delta^{15}N$ frequency distributions that could be compared to modeled $\delta^{15}N$ values (as data pairs). Figure S4 in Appendix B shows measured values versus fitted distributions.

4.1.1 *Scenario 1: Mixing of different nitrate sources*

Simulation results considering the mixing of possible nitrate sources reveal that a range of different portions concerning land use and related nitrate input could explain observed $\delta^{15}N$ values in groundwater reasonably well. Those include agricultural (portion p_1) or non-agricultural land use ($1-p_1$), with manure (p_2) and mineral fertilizer ($1-p_2$) as nitrate sources for agricultural and precipitation for non-agricultural land use. Results are mainly discussed by means of cumulative frequency distributions and tile maps, but we also added some histograms in the SI to illustrate the resulting MAE and R^2. A selection of good simulation curve fits is shown in Figure 10 for simulated cumulative frequency distributions of $\delta^{15}N$. 'Good fits' were associated to a low range of MAE calculated for simulated versus observed $\delta^{15}N$ distributions. This corresponds to MAEs from 8.47 to 10.16 for the PA and 5.27 to 9.67 for the MA (Table 5, lowest MAE to 5^{th} percentile MAE of all realizations for each aquifer, cf. Materials and Methods and Figure S29). Figure 11 presents tilemaps of R^2 and MAE for the considered realizations of Sc. 1, where blue to green colors indicate good fit, and red indicates bad fit.

For the PA, good curve fits were found with 70 to 100% of agricultural land use and 60 to 100% of manure application (Figure 10a and 11, left hand side). The lowest MAE of 8.47 (with R^2= 0.907) was found for 100% agricultural land use and 60% manure (Table 5 and S6). However, such a high portion of agricultural land use is unrealistic: Burger (1993) estimated that 80% of the larger catchment area is agriculturally used, and from recent satellite images we estimated agricultural used areas to cover about 65-80%. Therefore, we can assume that 80% would be the maximum realistic percentage of

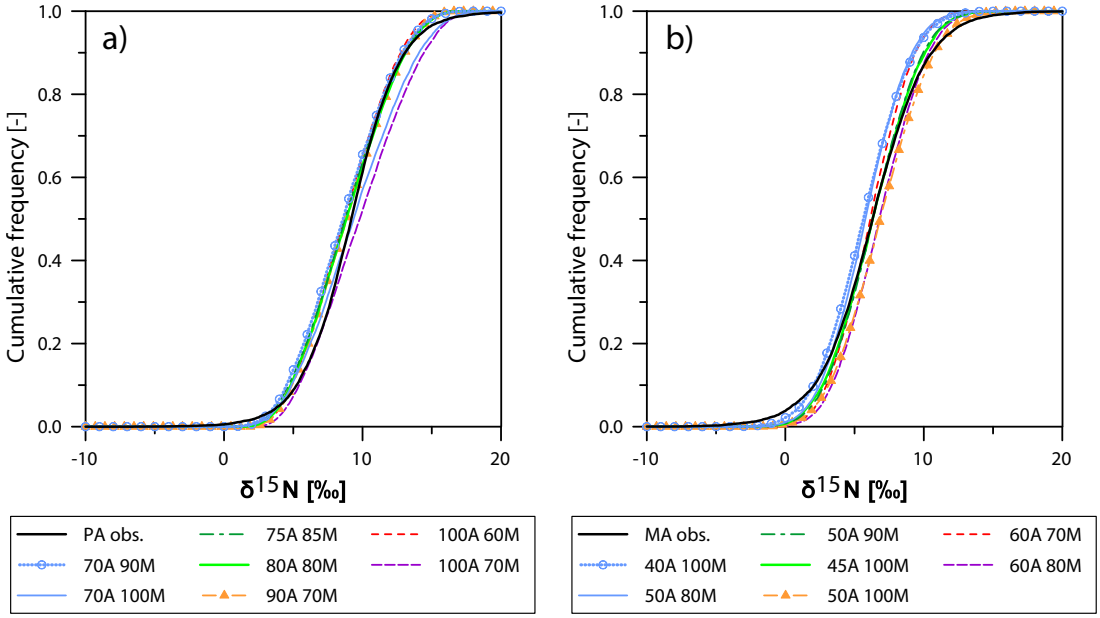

Figure 10: Cumulative frequency distributions of best fitting simulated $\delta^{15}N$ (source mixing, Sc. 1) and observed (obs.) $\delta^{15}N$ for a) the PA and b) the MA. Numbers in the legend refer to percentage of agricultural land use (A) and manure (M)

agricultural land use, where the simulated realization with 75% agricultural land use and 85% manure can be seen as the best estimate (MAE of 8.49, with R^2= 0.895). For the MA, best fits were found with lower portions of agricultural land use between 40 and 60% (best estimate 45%) and relatively high portions of manure between 70 and 100% (best estimate 100%; Figure 10b and 11, right hand side; Table 5 and S6).

Table 5: MAE and its corresponding R^2 for the frequency distribution of simulated versus measured $\delta^{15}N$ in groundwater of the PA and MA. Values refer to realizations within the best fit range for all scenarios. Cf. Figure S29 for more information on MAE.

Sc.	**Best fit range**	**PA**		**MA**	
		MAE [-]	**R^2 [-]**	**MAE [-]**	**R^2[-]**
1) Mixing	from	8.47	0.907	5.27	0.980
	to	10.2	0.871	9.67	0.953
2) Transport	from	6.37	0.950	5.97	0.977
	to	9.91	0.886	10.70	0.886
3a) Transport + microbial	from	6.31	0.947	3.57	0.984
denitrification (μ=1 a^{-1})	to	9.30	0.894	7.40	0.937
3b) Transport + microbial	from	6.59	0.947	5.16	0.984
denitrification (μ = 0.1 a^{-1})	to	10.0	0.880	9.26	0.966

The PA, located at shallow depths above 45 m bgl (meter below ground level), is characterized by relatively young groundwater with apparent MTT ranging from <4 years to 20 years. The deeper MA extends from 45 to 150 m bgl, and it contains older groundwater with apparent MTT between 14 and 122 years (Wild et al., 2018). Results from the simulations of Sc. 1, considering the impact of possible nitrate source mixing on

$\delta^{15}N$ distribution, indicate higher portions of agricultural land use (75 -80%) for the PA, compared to the MA (40-60%, best estimate (b.e.) 45%). Manure seems to have contributed with 60-100% (b.e.: 85%) for the PA, and with 70-100% (b.e.: 100%) for the MA. These findings point towards a change of land use within the past decade, characterized by an increase of the agriculturally used area within the catchment. Although relative contribution of manure (usage of manure versus mineral fertilizer) seems to be constant or slightly lower than mineral fertilizer, the total amount of released manure seems to have increased with time. Thus, these simulation results might indicate a source-driven isotopic shift to heavier $\delta^{15}N$ values of nitrate for the catchment area, away from less intensive farming with little livestock and mainly manure application (low use of mineral fertilizers) towards an increasingly intensive agricultural practice. This can be seen in Figure 10 (also Figure S30 and S31 in the SI), where curves for the PA (a) are shifted more to the right (higher $\delta^{15}N$), compared to the MA (b). Consequently, it can be estimated at which proportion a specific source might have contributed to observed nitrate contamination in groundwater, as similarly done for other sites by applying Bayesian framework studies (El Gaouzi et al., 2013; Korth et al., 2014; Xu et al., 2016; Zhang et al., 2015).

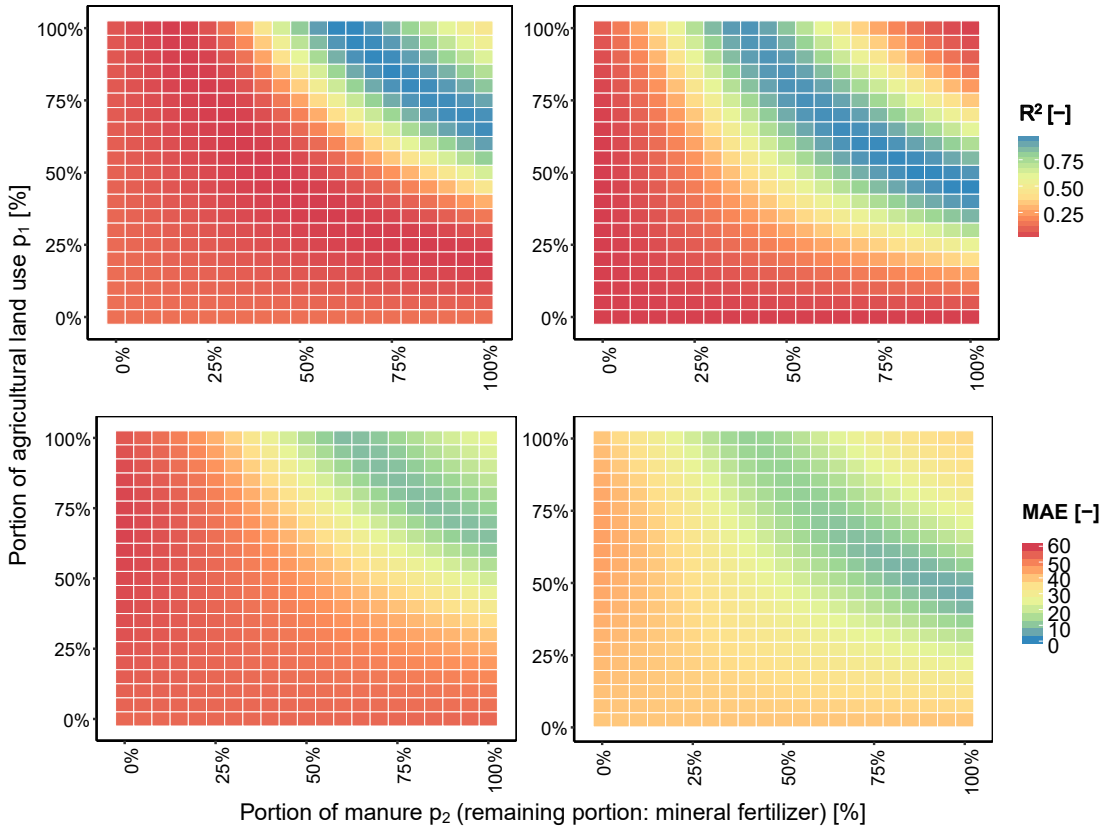

Figure 11: Coefficient of determination (R^2), top row, and mean absolute error (MAE), bottom row, for the frequency distribution of simulated versus measured $\delta^{15}N$ in groundwater of the PA (left) and MA (right). Comparison for all considered realizations of Sc. 1 (mixing of sources).

4.1.2 *Scenario 2: Hydrodynamic processes*

If hydrodynamic processes in groundwater (advection and dispersion) are considered, simulation results depend on the travel time of nitrate. As soon as the breakthrough of the isotopic signal, released at the source, has occurred at the observation well, good simulation curve fits were obtained (Figure S5-S8, Table S7). Simulated $\delta^{15}N$ frequency distributions (Figure 12 and Figure S32 in Appendix B, blue curves) are then similar to those obtained from Sc. 1 (Figure 10, as well as green curves in Figure 12 and S32). Indeed, good simulation curve fits were obtained for the same range of source composition. For the PA, depending on the percentage of agricultural use and manure, simulations were within the best fit range (as defined in Table 5) after a transport duration of 11 to 50 years (Figure S5 and S6, Table S7). Again, lowest MAE (6.37) was obtained for 100% agriculture and 60% manure (after 47 years), however this was not assumed realistic since not the whole catchment area is agriculturally used (see above). A more representative realization, considered as best estimate, was obtained for 80% agriculture with 80% manure after 50 years (MAE of 6.69). This source composition is similar to that yielding the best estimate for Sc. 1 (75% agriculture with 85% manure) and the MAEs of Sc.2 converge with time to the MAEs of Sc.1 as shown in Figure S17 and S18 in Appendix B.

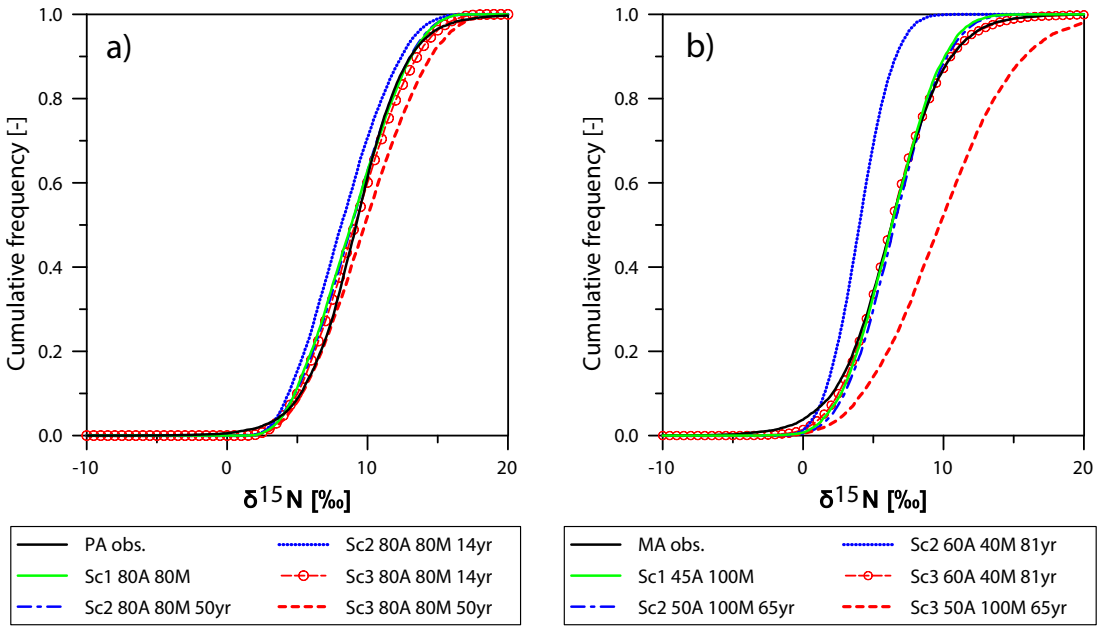

Figure 12: Cumulative frequency distributions of observed and simulated $\delta^{15}N$, comparison of Sc. 1-3. a) PA, b) MA. Percentage of agricultural land use A and manure M, with transport duration in years (yr).

For the MA, best fit ranges were obtained after longer transport duration from 28 to 100 years (Figure S7 and S8, Table S7). Associated source composition showed a wider range than for Sc. 1, with potentially 40-100% agriculture and 50-100% manure. The lowest MAE of 5.97 (R^2= 0.977) was found for 50% agricultural land use with 100% manure after 65 years, so that, like for the PA, the source composition coincides relatively well with that of Sc. 1 (with 45% agriculture and 100% manure as best estimate). Thus, the time of breakthrough (transport duration) is an important unknown for Sc. 2, which needs careful consideration in order to derive realistic

assumptions. It is mainly determined by advection (groundwater flow velocity v, in our case defined by the observed ranges and fitted PDFs for MTT and flow distance x), and it is also influenced by dispersion (PDF fitted for observed P_D). As soon as the breakthrough has taken place, transport processes revealed only a low influence on the frequency distribution of $\delta^{15}N$. While comparing Sc. 1 and 2, the lowest MAEs are found for similar or even the same mixing portions in the PA and MA (Figure S23 and S33 in Appendix B).

4.1.3 *Scenario 3: Hydrodynamic processes and microbial denitrification*

In this scenario, mixing and transport (hydrodynamic processes) along with microbial denitrification were considered. First, we simulated a hypothetically high microbial activity, using a generic degradation rate constant μ of 1 a^{-1}. In comparison to transport without microbial denitrification, we can see a shift towards lower portions of agriculture and/or manure, which would allow similar simulated $\delta^{15}N$ frequency distributions. This is illustrated in Figure 13, after a transport duration of 30 years for the PA and 60 years for the MA. Best simulation results (low MAE) are shifted to the left (less manure) and downwards (less agriculture) for Sc. 3, when comparing Fig. 13a with 13c and 13b with 13d. The best fit range was found for 60-100% agriculture with 50-100% manure (after 10 years or longer) for the PA, and 30-100% agriculture with 20-100% manure (after 28 years or longer) for the MA (Figure S9-S12, Table S8). This is a wider range for possible source compositions as compared to the previous scenarios.

For the PA, similar combinations concerning the sources (portion of agricultural land associated with portion of manure), compared to Sc. 2, yielded good curve fits (Figure 12a, red curves). Lowest MAE (6.31) was again found for 100% agriculture and 60% manure after 16 years and thus earlier than for Sc. 2 (with 47 years) as displayed in Figure S19 and S20 in Appendix B. Again, since 100% agricultural land use is not representative for the study area, a portion of 80% agriculture with 80% manure and a transport duration of 46 years resulted in the most realistic estimate (MAE of 6.49, R^2 of 0.939). For Sc. 2 the best fit was obtained for 80% agriculture with 80% manure after 50 years, thus being very close.

The source composition was different for the MA, where high portions of agriculture are associated with lower portions of manure, for obtaining similar $\delta^{15}N$ frequency distributions (Figure 12b). The lowest MAE with 3.57 (R^2= 0.984) was found for 60% agricultural land use with 40% manure after 81 years. Here we can see a clear difference compared to Sc. 2, where the best estimate was for a slightly lower portion of agricultural land use (50%) but much higher manure (100%), and after a shorter transport duration (65 years). The differences of the calculated MAE between Sc.2 and 3 are quite evident in Figure S25 in Appendix B.

The second assumption for Sc. 3, using a lower generic degradation rate constant μ of 0.1 a^{-1}, gave similar results compared to Sc. 2 (Figure S21, S22, S27 and S28 in Appendix B). In this case, microbial denitrification took only low influence on simulated $\delta^{15}N$ frequency distributions (Figure S13-S16). For oxic groundwater, Tesoriero and

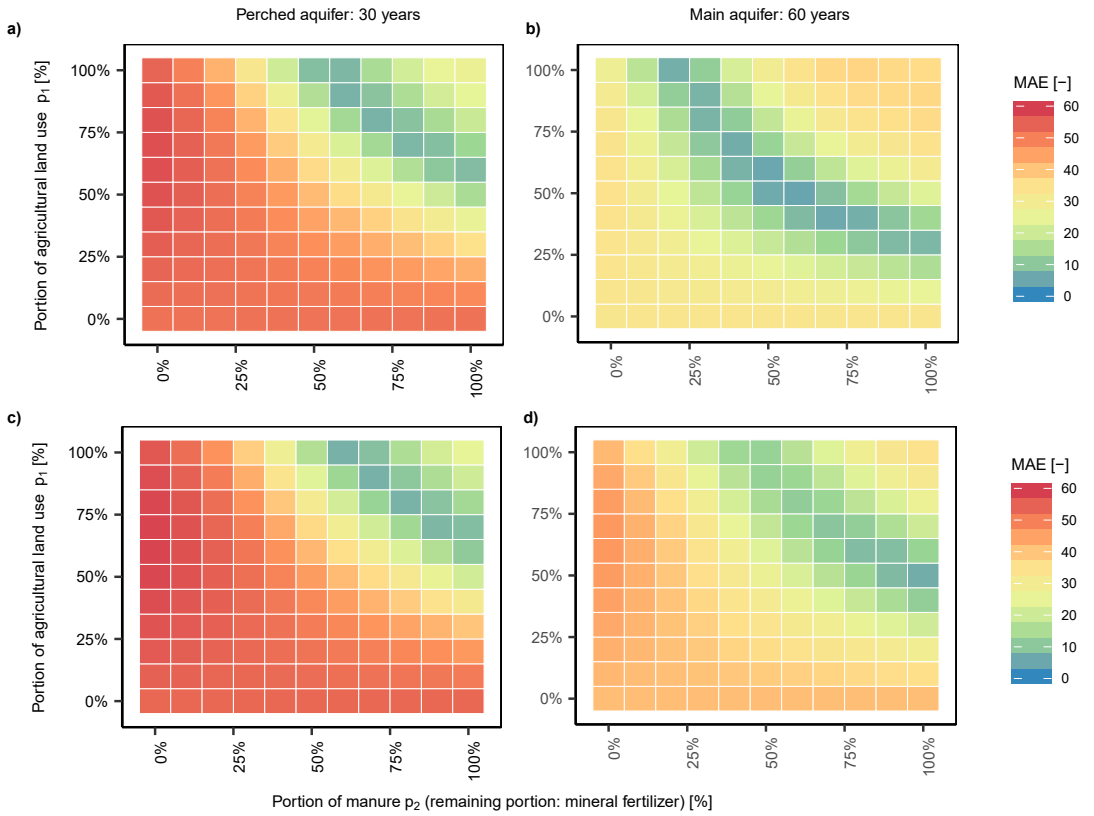

Figure 13: MAE for the frequency distribution of simulated versus measured $\delta^{15}N$ in groundwater of the PA after a transport duration of 30 years (a and c) and the MA after 60 years (b and d). Comparison of Sc. 2, transport (a and b) and Sc. 3, transport and microbial denitrification with μ of 1 a^{-1} (c and d).

Puckett (2011) found that significant changes due to microbial degradation may only be detectable for rates larger than 0.36 a^{-1}. This could explain the similarity to Sc. 2, which neglects microbial denitrification. For the PA, good estimates (as defined in Table 5) were obtained for 60-100% agriculture (slightly wider range as for Sc. 2) with 60-100% manure, after 11 to 50 years (as for Sc. 2). Lowest MAE was found for 100% agriculture and 60% manure (as for Sc. 2) after 32 years (for Sc. 2 it was 47 years). For the MA, good estimates resulted from 40-100% agriculture (as for Sc. 2), however, the manure best fit range started at a slightly lower percentage (40-100%). The best fit was found for 50% agriculture with 90-100% manure (similarly low MAE around 5.2) and thus very similar to Sc. 2.

Simulation results show that microbial denitrification might have taken place in the PA, but it is rather unlikely for the MA. For the PA, good simulation curve fits were obtained for Sc. 3 when considering transport and denitrification in groundwater combined with a nitrate input, which relates to expected portions of nitrate sources. This is also consistent with observations from the earlier results that revealed significant denitrification in two shallow wells in the PA but not in the residual shallow wells and springs. However, if assuming microbial denitrification for the MA, good curve fits were predominantly found for unrealistic (unexpected) percentages of either agricultural use or manure. The MA contains older groundwater (MTT of 14-122 years) compared to the PA (MTT <4 - 20 years, see above). Since the use of mineral fertilizers was lower in the past, we would expect a rather high percentage of manure. We can also assume a high percentage of agricultural use for the catchment area (80% was

reported by Burger 1993). However, better curve fits prevailed for other source compositions (best estimate for 50% manure and 50% agriculture, where at least the latter is lower than expected). Therefore, the presence of microbial denitrification is less likely in the MA as reasonable curve fits are not within a realistic range for the source composition (Table S8). These findings also agree with the calculated O_2 reduction rates and denitrification lag times of the investigated MA, which suggest that it will take many decades to significantly reduce nitrate concentrations in the MA via denitrification.

5

CONCLUSION AND OUTLOOK

The calculated O_2 reduction rate of 0.015 1/year for first-order kinetics is relatively low in the studied aquifer and leads to a high denitrification lag phase of approximately 114 years. In consequence, we suggest that the lack of microbial available electron donors in the aquifer is responsible for the low O_2 reduction rates and the high nitrate concentrations in this groundwater system. We, therefore, demonstrate that this approach is highly effective in estimating the approximate residence time of nitrate and the assessment of nitrogen loads in groundwater. Hence, the results provide critical information on the vulnerability of aquifers posed by dissolved nitrate and the time frames required to achieve water quality improvements in nitrate-polluted aquifers.

For groundwater ecosystems with a low potential for the reduction of redox sensitive parameters such as nitrate, we recommend a reduction of anthropogenic N inputs by applying agricultural beneficial management practices (Asgedom and Kebreab, 2011). In-situ groundwater remediation has also been shown to be suitable and effective to remove nitrate and consequently reach acceptable drinking water quality, however, this approach may be challenging in such heterogeneous groundwater systems and potentially too costly (Archna et al., 2012; Della Rocca et al., 2007; Janda et al., 1988). Future work could, however, include a remediation strategy that is feasible and applicable in nitrate contaminated catchment areas. This may be quite a complex task in such a heterogeneous study area but may be achieved by remediating the highly contaminated drinking water wells with push-pull tests or direct injection of a suitable e^--donor.

Moreover, we investigated MC simulations as a decision support to interpret $\delta^{15}N$ values of nitrate in groundwater. Different scenarios, such as mixing, combined with transport and microbial denitrification, were applied to study the influence of selected parameters on the evaluation of $\delta^{15}N$ values in groundwater. Results show that the portion (percentage) of nitrate-releasing land use and specific nitrate sources in a catchment area along with the MTT of nitrate dissolved in groundwater are crucial factors when evaluating influences related to the mixing of different nitrate sources linked with transport and denitrification processes. However, if the sensitive parameters are well documented for a catchment area, MC simulations have the potential to support decision makers in the assessment of nitrate isotope data.

To deepen this work, we suggest to also compare our results with a multidimensional numerical advection-dispersion model. This may need a complex hydrogeological structure, but with certain approximations and a statistical framework, good results could be obtained.

Amberger, A., & Schmidt, H. L. (1987). Natürliche Isotopengehalte von Nitrat als Indikatoren für dessen Herkunft. *Geochimica et Cosmochimica Acta*, *51*(10), 2699–2705.

Appelo, C. A. J., & Postma, D. (2005). *Geochemistry, groundwater and pollution* (2nd). A.A. Balkema Publishers, Taylor & Francis Group plc.

Aravena, R., Evans, M. L., & Cherry, J. A. (1993). Stable Isotopes of Oxygen and Nitrogen in Source Identification of Nitrate from Septic Systems. *Ground Water*, *31*(2), 7.

Aravena, R., & Wassenaar, L. I. (1993). Dissolved organic carbon and methane in a regional confined aquifer, southern Ontario, Canada: Carbon isotope evidence for associated subsurface sources. *Applied Geochemistry*, *8*(5), 483–493.

Aravena, R., Wassenaar, L. I., & Plummer, L. N. (1995). Estimating ^{14}C groundwater ages in a methanogenic aquifer. *Water Resources Research*, *31*(9), 2307–2317.

Archna, Sharma, S. K., & Sobti, R. C. (2012). Nitrate removal from ground water: a review. *E-Journal of Chemistry*, *9*(4), 1667–1675.

Asgedom, H., & Kebreab, E. (2011). Beneficial management practices and mitigation of greenhouse gas emissions in the agriculture of the Canadian Prairie: A review. *Agronomy for Sustainable Development*, *31*(3), 433–451.

Augenbraun, H., Matthews, E., & Sarma, D. (2010). GISS ICP: Global Methane Inventory.

Balci, N., Shanks, W. C., Mayer, B., & Mandernack, K. W. (2007). Oxygen and sulfur isotope systematics of sulfate produced by bacterial and abiotic oxidation of pyrite. *Geochimica et Cosmochimica Acta*, *71*(15), 3796–3811.

Bartlett, R., Bottrell, S. H., Sinclair, K., Thornton, S., Fielding, I. D., & Hatfield, D. (2010). Lithological controls on biological activity and groundwater chemistry in Quaternary sediments. *Hydrological Processes*, *24*(6), 726–735.

Bekins, B. A., Warren, E., & Godsy, E. M. (1998). A comparison of zero-order, first-order and Monod biotransformations models. *Groundwater*, *36*(2), 261–268.

Bender, M. M. (1971). Variations in the $^{13}C/^{12}C$ ratios of plants in relation to the pathway of photosynthetic carbon dioxide fixation. *Phytochemistry*, *10*, 1239–1244.

Bergersen, F. J., Turner, G. L., Bogusz, D., & Appleby, C. A. (2009). Fixation of N_2 by Bacteroids from Stem Nodules of Sesbania rostrata. *Microbiology*, *134*(7), 1807–1810.

Beven, K., & Freer, J. (2001). Equifinality, data assimilation, and uncertainty estimation in mechanistic modelling of complex environmental systems using the GLUE methodology. *Journal of Hydrology*, *249*(1-4), 11–29.

Bigeleisen, J. (1965). Chemistry of Isotopes. *Science*, *147*(3657), 463–471.

Bjerg, P. L., Ruegge, K., Pedersen, J. K., & Christensen, T. H. (1995). Distribution of redox-sensitive groundwater quality parameters downgradient of a landfill (Grindsted, Denmark). *Environmental Science & Technology*, *29*(5), 1387–1394.

Boettcher, J., Strebel, O., Voerkelius, S., & Schmidt, H. L. (1990). Using isotope fractionation of nitrate-nitrogen and nitrate-oxygen for evaluation of microbial denitrification in a sandy aquifer. *Journal of Hydrology*, *114*(3-4), 413–424.

Böhlke, J. K. (2002). Groundwater recharge and agricultural contamination. *Hydrogeology Journal*, *10*(1), 153–179.

Böhlke, J. K., & Coplen, T. B. (1995). Reference and intercomparison materials for stable isotopes of light elements. *IAEA TECDOC*, *825*, 51–66.

Böhlke, J. K., & Denver, J. M. (1995). Combined use of ground- water dating, chemical, and isotopic analyses to resolve the history and fate of nitrate contamination in two agricultural watersheds, atlantic coastal Plain, Maryland. *Water Resources Research*, *31*(9), 2319–2339.

Böhlke, J. K., Ericksen, G., & Revesz, K. (1997). Stable isotope evidence for an atmospheric origin of desert nitrate deposits in northern Chile and southern California, U.S.A. *Chemical Geology*, *136*(1-2), 135–152.

Böhlke, J. K., Smith, R. L., & Miller, D. N. (2006). Ammonium transport and reaction in contaminated groundwater: Application of isotope tracers and isotope fractionation studies. *Water Resources Research*, *42*(5), 1–19.

Böhlke, J. K., Wanty, R., Tuttle, M., Delin, G., & Landon, M. (2002). Denitrification in the recharge area and discharge area of a transient agricultural nitrate plume in a glacial outwash sand aquifer, Minnesota. *Water Resources Research*, *38*(7), 10–1–10–26.

Bond, A. L., & Diamond, A. W. (2011). Recent Bayesian stable-isotope mixing models are highly sensitive to variation in discrimination factors. *Ecological Applications*, *21*(4), 1017–1023.

Bonin, P., Gilewicz, M., & Bertrand, J. C. (1989). Effects of oxygen on each step of denitrification on Pseudomonas nautica. *Canadian Journal of Microbiology*, *35*(11), 1061–1064.

Bottrell, S. H., Parkes, R. J., Cragg, B. A., & Raiswell R. (2000). Isotopic evidence for anoxic pyrite oxidation and stimulation of bacterial sulphate reduction in marine sediments. *Journal of the Geological Society*, *157*(4), 711–714.

Brunner, B., Contreras, S., Lehmann, M. F., Matantseva, O., Rollog, M., Kalvelage, T., … Kuypers, M. M. M. (2013). Nitrogen isotope effects induced by anammox bacteria. *Proceedings of the National Academy of Sciences*, *110*(47), 18994–18999.

Buchwald, C., Santoro, A. E., McIlvin, M. R., & Casciotti, K. L. (2012). Oxygen isotopic composition of nitrate and nitrite produced by nitrifying cocultures and natural marine assemblages. *Limnology and Oceanography*, *57*(5), 1361–1375.

Burt, T. P., Matchett, L. S., Goulding, K. W. T., Webster, C. P., & Haycock, N. E. (1999). Denitrification in riparian buffer zones: the role of floodplain hydrology. *Hydrological Processes*, *13*(10), 1451–1463.

Buzek, F., Kadlecová, R., & Zák, K. (1997). Nitrate pollution of a karstic groundwater system. In *Isotope techniques in the study of environmental change* (Chap. Isotopic s, pp. 453–464). Vienna, Austria: IAEA.

Calderer, M., Gibert, O., Martí, V., Rovira, M., De Pablo, J., Jordana, S., … Bruno, J. (2010). Denitrification in presence of acetate and glucose for bioremediation of nitrate-contaminated groundwater. *Environmental Technology*, *31*(7), 799–814.

Campana, M. E., & Simpson, E. S. (1984). Groundwater residence times and recharge rates using a discrete-state compartment model and ^{14}C data. *Journal of Hydrology*, *72*, 171–185.

Carpenter, S. R., Caraco, N. F., Correll, D. L., W.Howarth, R., Sharpley, A. N., & Smith, V. H. (1998). Nonpoint pollution of surface waters with phosphorus and nitrogen. *Ecological Applications*, *8*(1998), 559–568. arXiv: arXiv:1011.1669v3

Casciotti, K. L., Sigman, D. M., Hastings, M. G., Bohlke, J. K., & Hilkert, A. (2002). Measurement of the oxygen isotopic composition of nitrate seawater and freshwater using the dentirifier method. *Analytical Chemistry*, *74*(19), 4905–4912.

Casciotti, K. L. (2009). Inverse kinetic isotope fractionation during bacterial nitrite oxidation. *Geochimica et Cosmochimica Acta*, *73*(7), 2061–2076.

Casciotti, K. L., McIlvin, M., & Buchwald, C. (2010). Oxygen isotopic exchange and fractionation during bacterial nitrite oxidation. *Limnology and Oceanography*, *55*(3), 1064–1074.

Castro, M. C., Stute, M., & Schlosser, P. (2000). Comparison of ^{4}He ages and ^{14}C ages in simple aquifer systems: Implications for groundwater flow and chronologies. *Applied Geochemistry*, *15*(8), 1137–1167.

Chai, T., & Draxler, R. R. (2014). Root mean square error (RMSE) or mean absolute error (MAE)? -Arguments against avoiding RMSE in the literature. *Geoscientific Model Development*, *7*(3), 1247–1250.

Choi, W. J., Han, G. H., Lee, S. M., Lee, G. T., Yoon, K. S., Choi, S. M., & Ro, H. M. (2007). Impact of land-use types on nitrate concentration and δ^{15}N in unconfined groundwater in rural areas of Korea. *Agriculture, Ecosystems and Environment*, *120*(2-4), 259–268.

Ciais, P., Tans, P. P., Troiler, M., White, J. W. C., & Francey, R. J. (1995). A large northern hemisphere terrestrial CO_2 sink indicated by the $^{13}C/^{12}C$ ratio of atmospheric CO_2. *Science*, *269*, 1098–1102.

Cirpka, O. A., & Helmig, R. (1999). Numerical simulation of biodegradation controlled by transverse mixing. *Journal of Contaminant Hydrology*, *40*, 159–182.

Clark, I. D. (2015). *Groundwater Geochemistry and Isotopes*. Boca Raton, USA: CRC Press.

Clark, I. D., & Fritz, P. (1997). *Environmental isotopes in hydrogeology*. Boca Raton, USA: CRC Press/Lewis Publishers.

Clark, I. D., Timlin, R., Bourbonnais, A., Jones, K., Lafleur, D., & Wickens, K. (2008). Origin and fate of industrial ammonium in anoxic ground water - ^{15}N evidence for anaerobic oxidation (anammox). *Ground Water Monitoring and Remediation*, *28*(3), 73–82.

Clarke, W. B., Jenkins, W. J., & Top, Z. (1976). Determination of tritium by mass spectrometric measurement of ^{3}He. *The International Journal Of Applied Radiation And Isotopes*, *27*(9), 515–522.

Cooper, L., Olsen, C. R., Solomon, D. K., Larsen, I. L., Cook, R., & Grebmeier, J. (1991). Isotopes of oxygen and natural and fallout radionuclides used for tracing runoff during snowmelt in an Arctic watershed. *Water Resources*, *27*(9), 2171–2179.

Craig, H. (1961). Isotopic Variations in Meteoric Waters. *Science*, *133*(3465), 1702–1703.

Currie, W. S., & Nadelhoffer, K. J. (1999). Dynamic redistribution of isotopically labeled cohorts of nitrogen inputs in two temperate forests. *Ecosystems*, *2*(1), 4–18.

Davidson, E. A., Hart, S. C., Firestone, M. K., & Aug, N. (2007). Internal Cycling of Nitrate in Soils of a Mature Coniferous Forest. *Ecology*, *73*(4), 1148–1156.

Davies, K. J. P., Lloyd, D., & Boddy, L. (1989). The Effect of Oxygen on Denitrification in Paracoccus denitrificans and Pseudomonas aeruginosa. *Microbiology*, *135*(9), 2445–2451.

Della Rocca, C., Belgiorno, V., & Meriç, S. (2007). Overview of in-situ applicable nitrate removal processes. *Desalination*, *204*(1-3 SPEC. ISS.), 46–62.

Dennard, S. T., McMeans, B. C., & Fisk, A. T. (2009). Preliminary assessment of Greenland halibut diet in Cumberland Sound using stable isotopes. *Polar Biology*, *32*(6), 941–945.

Deutzmann, J. S., & Schink, B. (2011). Anaerobic Oxidation of Methane in Sediments of Lake Constance, an Oligotrophic Freshwater Lake. *Applied and Environmental Microbiology*, *77*(13), 4429–4436.

Deutzmann, J. S., Stief, P., Brandes, J., & Schink, B. (2014). Anaerobic methane oxidation coupled to denitrification is the dominant methane sink in a deep lake. *Proceedings of the National Academy of Sciences*, *111*(51), 201411617.

Doppler, G., Heissig, K., & Reichenbacher, B. (2005). Die Gliederung des Tertiaers im sueddeutschen Molassebecken. *Newsletters on Stratigraphy*, *41*(1), 359–375.

Durka, W., Schulze, E.-D., Gebauer, G., & Voerkellus, S. (1994). Effects of forest decline on uptake and leaching of deposited nitrate determined from ^{15}N and ^{18}O measurements. *Nature*, *372*(22/29), 765–767.

Einsiedl, F. (2012). Sea-water/groundwater interactions along a small catchment of the European Atlantic coast. *Applied Geochemistry*, *27*(1), 73–80.

Einsiedl, F., Hertkorn, N., Wolf, M., Frommberger, M., Schmitt-Kopplin, P., & Koch, B. P. (2007). Rapid biotic molecular transformation of fulvic acids in a karst aquifer. *Geochimica et Cosmochimica Acta*, *71*(22), 5474–5482.

Einsiedl, F., Maloszewski, P., & Stichler, W. (2009). Multiple isotope approach to the determination of the natural attenuation potential of a high-alpine karst system. *Journal of Hydrology*, *365*(1-2), 113–121.

Einsiedl, F., & Mayer, B. (2006). Hydrodynamic and microbial processes controlling nitrate in a fissured-porous karst aquifer of the Franconian Alb, southern Germany. *Environmental Science & Technology*, *40*(21), 6697–702.

Einsiedl, F., & Mayer, B. (2005). Sources and processes affecting sulfate in a karstic groundwater system of the Franconian Alb, southern Germany. *Environmental Science & Technology*, *39*(18), 7118–7125.

El Gaouzi, F.-Z. J., Sebilo, M., Ribstein, P., Plagnes, V., Boeckx, P., Xue, D., … Zakeossian, M. (2013). Using $\delta^{15}N$ and $\delta^{18}O$ values to identify sources of nitrate in karstic springs in the Paris basin (France). *Applied Geochemistry*, *35*, 230–243.

Ettwig, K. F., van Alen, T., van de Pas-Schoonen, K. T., Jetten, M. S. M., & Strous, M. (2009). Enrichment and Molecular Detection of Denitrifying Methanotrophic Bacteria of the NC10 Phylum. *Applied and Environmental Microbiology*, *75*(11), 3656–3662.

Ettwig, K. F., Butler, M. K., Le Paslier, D., Pelletier, E., Mangenot, S., Kuypers, M. M. M., … Strous, M. (2010). Nitrite-driven anaerobic methane oxidation by oxygenic bacteria. *Nature*, *464*(7288), 543–548.

Ettwig, K. F., Shima, S., Van De Pas-Schoonen, K. T., Kahnt, J., Medema, M. H., Op Den Camp, H. J. M., … Strous, M. (2008). Denitrifying bacteria anaerobically oxidize methane in the absence of Archaea. *Environmental Microbiology*, *10*(11), 3164–3173.

European Commission. (2000). Directive 2000/60/EC of the European Parliament and of the Council of 23 October 2000 establishing a framework for Community action in the field of water policy. *Official Journal of the European Communities*, *L327*, 1–82. arXiv: 534

European Commission. (2012). *Commission StaffWorking Document, European Overview (2/2) Accompanying the Document: "Report From the Commission to the European*

Parliament and the Council on the Implementation of the Water Framework Directive (2000/60/EC) River Basin Management Plans". European Commision. Brussels.

European Commission. (2015). *The Water Framework Directive and the Floods Directive: Actions towards the ´good status´ of EU water and to reduce flood risks*. European Commission. Brussels.

Fang, Y., Koba, K., Makabe, A., Zhu, F., Fan, S., Liu, X., & Yoh, M. (2012). Low $\delta^{18}O$ values of nitrate produced from nitrification in temperate forest soils. *Environmental Science and Technology*, *46*(16), 8723–8730.

Fogel, M. L., & Cifuentes, L. A. (1993). Isotope Fractionation during Primary Production, 73–98.

Fogg, G. E., LaBolle, E. M., & Weissmann, G. S. (1999). Groundwater vulnerability assessment: Hydrologic perspective and example from Salinas Valley, California. *Assessment of Non-Point Source Pollution in the Vadose Zone (Geophysical Monograph 108)*, 45–61.

Fukada, T., Hiscock, K. M., Dennis, P. F., & Grischek, T. (2003). A dual isotope approach to identify denitrification in groundwater at a river-bank infiltration site. *Water Research*, *37*(13), 3070–3078.

Galloway, J. N., & Cowling, E. B. (2002). Reactive Nitrogen and The World: 200 Years of Change. *AMBIO: A Journal of the Human Environment*, *31*(2), 64–71.

Geyh, M. (2000). Groundwater - saturated and unsaturated zone. In *Environmental Isotopes in the Hydrological Cycle Principles and Applications* (Vol. 4, p. 196).

Glückauf, E., & Paneth, F. A. (1946). A micro-analysis of the helium and neon contents of air. *Proceedings of the Royal Society of London. Series A. Mathematical and Physical Sciences*, *185*, 98–119.

Grabczak, J., Rozanski, K., Maloszewski, P., & Zuber, A. (1984). Estimation of the tritium input function with the aid of stable isotopes. *Catena*, *11*(2-3), 105–114.

Granger, J., & Wankel, S. D. (2016). Isotopic overprinting of nitrification on denitrification as a ubiquitous and unifying feature of environmental nitrogen cycling. *Proceedings of the National Academy of Sciences*, *113*(42), E6391–E6400.

Hamdi, W., Gamaoun, F., Pelster, D. E., & Seffen, M. (2013). Nitrate sorption in an agricultural soil profile. *Applied and Environmental Soil Science*, *2013*(3).

Hansen, B., Thorling, L., Dalgaard, T., & Erlandsen, M. (2011). Trend reversal of nitrate in Danish groundwater - A reflection of agricultural practices and nitrogen surpluses since 1950. *Environmental Science & Technology*, *45*(1), 228–234.

Harper, B. H. J. (1924). The Accurate Determination of Nitrates in Soils - Phenoldisulfonic Acid Method. *Industrial and Engineering Chemistry*, *16*(2), 180–183.

Hochstein, L. I., Betlach, M., & Kritikos, G. (1984). The effect of oxygen on denitrification during steady-state growth of Paracoccus halodenitrificans. *Archives of Microbiology*, *137*(1), 74–78.

Hollocher, T. C. (1984). Source of the oxygen atoms of nitrate in the oxidation of nitrite by Nitrobacter agilis and evidence against a PON anhydride mechanism in oxidative phosphorylation. *Archives of Biochemistry and Biophysics*, *233*(2), 721–727.

Hooda, P., Edwards, A., Anderson, H., & Miller, A. (2000). A review of water quality concerns in livestock farming areas. *Science of The Total Environment*, *250*(1-3), 143–167.

Hu, B.-l., Shen, L.-d., Xu, X.-y., & Zheng, P. (2011). Anaerobic ammonium oxidation (anammox) in different natural ecosystems. *Biochemical Society Transactions*, *39*(6), 1811–1816.

Huber-Carol, C., Balakrishnan, N., Nikulin, M., & Mesbah, M. (2008). *Statistics for Industry and Technology*. Springer Science + Business Media, LLC.

Hübner, H. (1986). Isotope effects of nitrogen in the soil and biosphere. In P. Fritz & J.-C. Fontes (Eds.), *Handbook of environmental isotope geochemistry / edited by P. Fritz and J.Ch. Fontes. Vol.2., The terrestrial environment B* (Chap. Isotope ef, p. 557). Amsterdam, Oxford: Elsevier B.V.

Ibanez, J. G., Hernandez-Esparza, M., Doria-Serrano, C., Fregoso-Infante, A., & Singh, M. M. (2007). *Environmental Chemistry - Fundamentals*. arXiv: arXiv:1011.1669v3

Ikeda, H., Kubota, K., Kagawa, A., & Sota, T. (2010). Diverse diet compositions among harpaline ground beetle species revealed by mixing model analyses of stable isotope ratios. *Ecological Entomology*, *35*(3), 307–316.

Janda, V., Rudovský, J., Wanner, J., & Marha, K. (1988). In situ Denitrification of Drinking Water. *Water Science and Technology*, *20*(3), 215–219.

Jensen, M. M., Lam, P., Revsbech, N. P., Nagel, B., Gaye, B., Jetten, M. S. M., & Kuypers, M. M. (2011). Intensive nitrogen loss over the Omani Shelf due to anammox coupled with dissimilatory nitrite reduction to ammonium. *ISME Journal*, *5*(10), 1660–1670.

Jetten, M. S. M. (2001). New pathways for ammonia conversion in soil and aquatic systems. *Plant and Soil*, *230*(1), 9–19.

Jouzel, J., Alley, R. B., Cuffey, K. M., Dansgaard, W., Grootes, P., Hoffmann, G., … White, J. (1997). Validity of the temperature reconstruction from ice cores. *Journal of Geophysical Research*, *102*(C12), 26471–26487.

Jurgens, B. C., Böhlke, J. K., & Eberts, S. M. (2012). *TracerLPM (Version 1): An Excel Workbook for Interpreting Groundwater Age Distributions from Environmental Tracer Data* (tech. rep. No. Version 1). U.S. Department of the Interior, U.S. Geological Survey. Reston, Virginia.

Kainzmaier, B., Thom, P., Wrobel, M., & Pukowietz, C. (2007). *Geowissenschaftliche Landesaufnahme in der Planungsregion 13 Landshut: Erläuterungen zur Hydrogeologischen Karte*. Bayrisches Landesamt für Umwelt.

Katz, B. G., Chelette, A. R., & Pratt, T. R. (2004). Use of chemical and isotopic tracers to assess nitrate contamination and ground-water age, Woodville Karst Plain, USA. *Journal of Hydrology*, *289*(1-4), 36–61.

Kemper, K. E. (2004). Groundwater - from development to management. *Hydrogeology Journal*, *12*(1), 3–5.

Kendall, C., & McDonnell, J. J. (1998a). Isotopic variations in precipitation. In *Isotope Tracers in Catchment Hydrology* (Chap. 3, pp. 87–118). Oxford, United Kingdom: Elsevier B.V.

Kendall, C., & McDonnell, J. J. (1998b). Tracing nitrogen sources and cycling in catchments. In *Isotope Tracers in Catchment Hydrology* (Chap. 16, pp. 519–576). Oxford, United Kingdom: Elsevier B.V.

Knobeloch, L., Salna, B., Hogan, A., Postle, J., & Anderson, H. (2000). Blue babies and nitrate-contaminated well water. *Environmental Health Perspectives*, *108*(7), 675–678.

Knöller, K., Trettin, R., & Strauch, G. (2005). Sulphur cycling in the drinking water catchment area of Torgau - Mockritz (Germany): Insights from hydrochemical and stable isotope investigations. *Hydrological Processes*, *19*(17), 3445–3465.

Knöller, K., Vogt, C., Haupt, M., Feisthauer, S., & Richnow, H. H. (2011). Experimental investigation of nitrogen and oxygen isotope fractionation in nitrate and nitrite during denitrification. *Biogeochemistry*, *103*(1), 371–384.

Koh, D. C., Mayer, B., Lee, K. S., & Ko, K. S. (2010). Land-use controls on sources and fate of nitrate in shallow groundwater of an agricultural area revealed by multiple environmental tracers. *Journal of Contaminant Hydrology*, *118*(1-2), 62–78.

Kölle, W., Strebel, O., & Böttcher, J. (1985). Formation of sulfate by microbial denitrification in a reducing aquifer. *Water Supply*, *3*(1), 35–40.

Körner, H., & Zumft, W. G. (1989). Expression of denitrification enzymes in response to the dissolved oxygen level and respiratory substrate in continuous culture of *Pseudomonas stutzeri*. *Applied and Environmental Microbiology*, *55*(7), 1670–1676.

Korom, S. F. (1992). Natural denitrification in the saturated zone: A review. *Water Resources Research*, *28*(6), 1657.

Korth, F., Deutsch, B., Frey, C., Moros, C., & Voss, M. (2014). Nitrate source identification in the Baltic Sea using its isotopic ratios in combination with a Bayesian isotope mixing model. *Biogeosciences*, *11*(17), 4913–4924.

Kreft, A., & Zuber, A. (1978). On the physical meaning of the dispersion equation and its solutions for different initial and boundary conditions. *Chemical Enigneering Science*, *33*, 1471–1480.

Kroopnick, P., & Craig, H. (1972). Atmospheric Oxygen: Isotopic Composition and Solubility Fractionation. *Science*, *175*(4017), 54–55.

Krouse, H. R., & Grinenko, V. A. (1991). *Stable isotopes : natural and anthropogenic sulphur in the environment*. John Wiley and Sons.

Ledgard, S. F. (1989). Nutrition, moisture and rhizobial strain influence isotopic fractionation during N_2- fixation in pasture legumes. *Soil Biology and Biochemistry*, *21*(1), 65–68.

Lee, J.-E., & Fung, I. (2007). "Amount effect" of water isotopes and quantitative analysis of post-condensation processes. *Hydrological Processes*, *22*, 1–8.

Lehmann, M. F., Bernasconi, S. M., McKenzie, J. a., Barbieri, A., Simona, M., & Veronesi, M. (2004). Seasonal variation of the $\delta^{13}C$ and $\delta^{15}N$ of particulate and dissolved carbon and nitrogen in Lake Lugano: Constraints on biogeochemical cycling in a eutrophic lake. *Limnology and Oceanography*, *49*(2), 415–429.

Li, C., Li, S. L., Yue, F. J., Liu, J., Zhong, J., Yan, Z. F., … Xu, S. (2019). Identification of sources and transformations of nitrate in the Xijiang River using nitrate isotopes and Bayesian model. *Science of the Total Environment*, *646*, 801–810.

Lill, T. (2013). Schweinemast: Bayern wird zum riesigen Saustall.

Lucas, L., & Unterweger, M. (2012). Comprehensive review and critical evaluation of the half-life of tritium. *Journal of Research of the National Institute of Standards and Technology*, *105*(4), 541.

Maloszewski, P., Rauert, W., Stichler, W., & Herrmann, A. (1983). Application of Flow Models in an Alpine Catchment area using Tritium and Deuterium. *Journal of Hydrology*, *66*, 319–330.

Maloszewski, P., Stichler, W., Zuber, A., & Rank, D. (2002). Identifying the flow systems in a karstic-fissured-porous aquifer, the schneealpe, austria, by modelling of environmental ^{18}O and ^{3}H isotopes. *Journal of Hydrology*, *256*(1-2), 48–59.

Maloszewski, P., & Zuber, A. (1982). Determining the turnover time of groundwater systems with the aid of environmental tracers. *Journal of Hydrology*, *57*(3-4), 207–231.

Maloszewski, P., & Zuber, A. (1996). Lumped Parameter Models for the Interpretation of Environmental Tracer Data. *Manual on Mathematical Models in Isotope Hydrogeology, IAEA-TECDO*, 9–58.

Małoszewski, P., & Zuber, A. (1985). On the theory of tracer experiments in fissured rocks with a porous matrix. *Journal of Hydrology*, *79*(3-4), 333–358.

Maloszewski, P., Rauert, W., Trimborn, P., Herrmann, A., & Rau, R. (1992). Isotope hydrological study of mean transit times in an alpine basin (Wimbachtal, Germany). *Journal of Hydrology*, *140*(1-4), 343–360.

Mariotti, A., Germon, J. C., Hubert, P., Kaiser, P., Letolle, R., Tardieux, A., & Tardieux, P. (1981). Experimental determination of nitrogen kinetic isotope fractionation: Some principles; illustration for the denitrification and nitrification processes. *Plant and Soil*, *62*(3), 413–430.

Mariotti, A., Germon, J. C., & Leclerc, A. (1982). Nitrogen isotope fractionation associated with the NO_3^- -> N_2O step of denitrification in soils. *Canadian Journal of Soil Science*, (2).

Mariotti, A., Pierre, D., Vedy, J. C., Bruckert, S., & Guillemot, J. (1980). The Abundance of Natural Nitrogen 15 in Soils Along an Altitudinal Gradient. *Catena*, *7*(4), 293–300.

Mariotti, A., Landreau, A., & Simon, B. (1988). $\delta^{15}N$ isotope biogeochemistry and natural denitrification process in groundwater: Application to the chalk aquifer of northern France. *Geochimica et Cosmochimica Acta*, *52*(7), 1869–1878.

Massmann, G., Sültenfuß, J., Dünnbier, U., Knappe, A., Taute, T., & Pekdeger, A. (2007). Investigation of groundwater residence times during bank filtration in Berlin: a multi-tracer approach. *Hydrological Processes*, *22*(November 2008), 788–801.

Mayer, B., Bollwerk, S. M., Mansfeldt, T., Hütter, B., & Veizer, J. (2001). The oxygen isotope composition of nitrate generated by nitrification in acid forest floors. *Geochimica et Cosmochimica Acta*, *65*(16), 2743–2756.

Mayer, B., Fritz, P., Prietzel, J., & Krouse, H. R. (1995). The use of stable sulfur and oxygen isotope ratios for interpreting the mobility of sulfate in aerobic forest soils. *Applied Geochemistry*, *10*(2), 161–173.

Mayer, B., Boyer, E. W., Goodale, C., Jaworski, N. A., Van Breemen, N., Howarth, R. W., ... Paustian, K. (2002). Sources of nitrate in rivers draining sixteen watersheds in the northeastern U.S.: Isotopic constraints. *Biogeochemistry*, *57-58*(1), 171–197.

Mazor, E. (2004). *Chemical and isotopic groundwater hydrology*. Marcel Dekker, Inc. All.

McClellan, C. M., Braun-McNeill, J., Avens, L., Wallace, B. P., & Read, A. J. (2010). Stable isotopes confirm a foraging dichotomy in juvenile loggerhead sea turtles. *Journal of Experimental Marine Biology and Ecology*, *387*(1-2), 44–51.

Merkel, B. J., & Planer-Friedrich, B. (2008). *Groundwater Geochemistry* (D. K. Nordstrom, Ed.). Springer Verlag Berlin Heidelberg.

Mizota, C., & Sasaki, A. (1996). Sulfur isotope composition of soils and fertilizers: Differences between Northern and Southern Hemispheres. *Geoderma*, *71*(1-2), 77–93.

Moncaster, S., Bottrell, S., Tellam, J., Lloyd, J., & Konhauser, K. (2000). Migration and attenuation of agrochemical pollutants: insights from isotopic analysis of groundwater sulphate. *Journal of Contaminant Hydrology*, *43*(2), 147–163.

Montzka, S. A., Dlugokencky, E. J., & Butler, J. H. (2011). Non-CO_2 greenhouse gases and climate change. *Nature*, *476*(7358), 43–50.

Moore, J. W., & Semmens, B. X. (2008). Incorporating uncertainty and prior information into stable isotope mixing models. *Ecology Letters*, *11*, 470–480.

Mulder, A., van de Graaf, A. A., Robertson, L. A., & Kuenen, J. G. (1995). Anaerobic ammonium oxidation discovered in a denitrifying fluidized bed reactor. *FEMS Microbiology Ecology*, *16*(3), 177–183.

Newman, L., Krouse, H. R., & Grinenko, V. A. (1991). Sulphur Isotope Variations in the Atmosphere. *Stable Isotopes in the Assessment of Natural and Anthropogenic Sulphur in the Environment*, *19*(1983), 133–176.

Nordi, K. Á., & Thamdrup, B. (2014). Nitrate-dependent anaerobic methane oxidation in a freshwater sediment. *Geochimica et Cosmochimica Acta*, *132*, 141–150.

Nosrati, K., Collins, A. L., & Madankan, M. (2018). Fingerprinting sub-basin spatial sediment sources using different multivariate statistical techniques and the Modified MixSIR model. *Catena*, *164*(December 2017), 32–43.

Nosrati, K., Govers, G., Semmens, B. X., & Ward, E. J. (2014). A mixing model to incorporate uncertainty in sediment fingerprinting. *Geoderma*, *217-218*, 173–180.

Parnell, A. C., Phillips, D. L., Bearhop, S., Semmens, B. X., Ward, E. J., Moore, J. W., … Inger, R. (2013). Bayesian stable isotope mixing models. *Environmetrics*, *24*, 387–399.

Parnell, A. C., Inger, R., Bearhop, S., & Jackson, A. L. (2010). Source Partitioning Using Stable Isotopes: Coping with Too Much Variation. *PLoS ONE*, *5*(3), 1–5.

Pauwels, H., Foucher, J.-C., & Kloppmann, W. (2000). Denitrification and mixing in a schist aquifer : influence on water chemistry and isotopes. *Chemical Geology*, *168*(3), 307–324.

Payne, W. J. (1983). Bacterial Denitrification: Asset or Defect? *BioScience*, *33*(5), 319–325.

Pettitt, A., & Stephens, M. (1977). The Kolmogorov-Smirnov Goodness-of-Fit Statistic with Discrete and Grouped Data. *Technometrics*, *19*(2), 205–210.

Piotrowska, N. (2013). Status report of AMS sample preparation laboratory at GADAM Centre, Gliwice, Poland. *Nuclear Instruments and Methods in Physics Research B*, *294*, 176–181.

Postma, D., Boesen, C., Kristiansen, H., & Larsen, F. (1991). Nitrate Reduction in an Unconfined Sandy Aquifer: Water Chemistry, Reduction Processes, and Geochemical Modeling. *Water Resources Research*, *27*(8), 2027–2045.

Prosser, J. I. (1989). Autotrophic nitrification in bacteria. *Advances in Microbial Physiology*, *30*, 125.

Raghoebarsing, A. A., Pol, A., van de Pas-Schoonen, K. T., Smolders, A. J. P., Ettwig, K. F., Rijpstra, W. I. C., … Strous, M. (2006). A microbial consortium couples anaerobic methane oxidation to denitrification. *Nature*, *440*(7086), 918–921.

Rasigraf, O., Vogt, C., Richnow, H.-H., Jetten, M. S. M., & Ettwig, K. F. (2012). Carbon and hydrogen isotope fractionation during nitrite-dependent anaerobic methane oxidation by Methylomirabilis oxyfera. *Geochimica et Cosmochimica Acta*, *89*, 256–264.

Rayleigh, L. (1896). L. Theoretical considerations respecting the separation of gases by diffusion and similar processes. *The London, Edinburgh, and Dublin Philosophical Magazine and Journal of Science*, *42*(259), 493–498.

Rifai, H. S., & Bedient, P. B. (1990). Comparison of biodegradation kinetics with an instantaneous reaction model for groundwater. *Water Resources Research*, *26*(4), 637–645.

Rivett, M. O., Buss, S. R., Morgan, P., Smith, J. W., & Bemment, C. D. (2008). Nitrate attenuation in groundwater: A review of biogeochemical controlling processes. *Water Research*, *42*(16), 4215–4232.

Robertson, L. A., & Kuenen, J. G. (1984). Aerobic denitrification: a controversy revived. *Archives of Microbiology*, *139*(4), 351–354.

Rodhe, A., Nyberg, L., & Bishop, K. (1996). Transit times for water in a small till catchment from a step shift in the oxygen 18 content of the water input. *Water Resources*, *32*(12), 3497–3511.

Ryabenko, E. (2013). Stable Isotope Methods for the Study of the Nitrogen Cycle. In E. Zambianchi (Ed.), *Topics in Oceanography* (Chap. 3).

Sadegh, M., & Vrugt, J. A. (2014). Approximate Bayesian computation using markov chain Monte Carlo simulation: DREAM(ABC). *Water Resources Research*, *50*(8), 6767–6787.

Schubert, C. J., Durisch-Kaiser, E., Wehrli, B., Thamdrup, B., Lam, P., & Kuypers, M. M. (2006). Anaerobic ammonium oxidation in a tropical freshwater system (Lake Tanganyika). *Environmental Microbiology*, *8*(10), 1857–1863.

Schwientek, M., Einsiedl, F., Stichler, W., Stögbauer, A., Strauss, H., & Maloszewski, P. (2008). Evidence for denitrification regulated by pyrite oxidation in a heterogeneous porous groundwater system. *Chemical Geology*, *255*(1-2), 60–67.

Sebilo, M., Billen, G., Mayer, B., Billiou, D., Grably, M., Garnier, J., & Mariotti, A. (2006). Assessing nitrification and denitrification in the Seine river and estuary using chemical and isotopic techniques. *Ecosystems*, *9*(4), 564–577.

Sebilo, M., Mayer, B., Nicolardot, B., Pinay, G., & Mariotti, A. (2013). Long-term fate of nitrate fertilizer in agricultural soils. *Proceedings of the National Academy of Sciences*, *110*(45), 18185–18189.

Shearer, G., Kohl, D. H., Jones, J. R., & Kohl, D. H. (1986). N_2-fixation in field settings: Estimations based on natural ^{15}N abundance. *Aust. J. Plant Physiol.*, *13*, 699–756.

Silva, S., Kendall, C., Wilkison, D., Ziegler, A., Chang, C., & Avanzino, R. (2000). A new method for collection of nitrate from fresh water and the analysis of nitrogen and oxygen isotope ratios. *Journal of Hydrology*, *228*(1-2), 22–36.

Simmons, C. S., Ginn, T. R., & Wood, B. D. (1995). Stochastic-convective transport with nonlinear reaction : *Water Resources Research*, *31*(11), 2675–2688.

Singh, B. R., & Kanehiro, Y. (1969). Adsorption of Nitrate in Amorphous and Kaolinitic Hawaiian Soils. *Soil Science Society of America Journal*, *33*, 681–683.

Smith, B. N., & Epstein, S. (1971). Two Categories of ^{13}C / ^{12}C Ratios for Higher Plants. *Plant Physiol*, *47*, 380–384.

Smith, R. L., Böhlke, J. K., Song, B., & Tobias, C. R. (2015). Role of Anaerobic Ammonium Oxidation (Anammox) in Nitrogen Removal from a Freshwater Aquifer. *Environmental Science and Technology*, *49*(20), 12169–12177.

Smith, R. L., Howes, B. L., & Garabedian, S. P. (1991). In situ measurement of methane oxidation in groundwater by using natural gradient tracer tests. *Applied and Environmental Microbiology*, *57*(7), 1997–2004.

Smith, R. L., Kent, D. B., Repert, D. A., & Böhlke, J. K. (2016). Anoxic Nitrate Reduction Coupled with Iron Oxidation and Attenuation of Dissolved Arsenic and Phosphate in a Sand and Gravel Aquifer. *Geochimica et Cosmochimica Acta*, *196*, 102–120.

Snider, D. M., Spoelstra, J., Schiff, S. L., & Venkiteswaran, J. J. (2010). Stable Oxygen Isotope Ratios of Nitrate Produced from Nitrification: ^{18}O-Labeled Water Incubations of Agricultural and Temperate Forest Soils. *Environmental Science & Technology*, *44*(14), 100615134113072.

Starr, R. C., & Gillham, R. W. (1993). Denitrification and Organic Carbon Availability in Two Aquifers. *Ground Water*, *31*(6), 934–947.

Stichler, W., & Herrmann, A. (1983). Application of environmental isotope techniques in water balance studies of small basins. *New Approaches in Water Balance Computations*, *18*(148), 93–112.

Stoewer, M., Knöller, K., & Stumpp, C. (2015). Tracing freshwater nitrate sources in prealpine groundwater catchments using environmental tracers. *Journal of Hydrology*, *524*, 753–767.

Stumpp, C., Stichler, W., & Maloszewski, P. (2009). Application of the environmental isotope $\delta^{18}O$ to study water flow in unsaturated soils planted with different crops: Case study of a weighable lysimeter from the research field in Neuherberg, Germany. *Journal of Hydrology*, *368*(1-4), 68–78.

Stumpp, C., Klaus, J., & Stichler, W. (2014). Analysis of long-term stable isotopic composition in German precipitation. *Journal of Hydrology*, *517*, 351–361.

Suchy, M., Wassenaar, L. I., Graham, G., & Zebarth, B. (2018). High-frequency NO_3^- isotope ($\delta^{15}N$, $\delta^{18}O$) patterns in ground water recharge reveal that short-term land use and climatic changes influence nitrate contamination trends. *Hydrology and Earth System Sciences Discussion*, (February), 1–27.

Sültenfuß, J. (1998). *The radionuclide Tritium in the ocean: measurement and distribution of Tritium in the South Atlantic and Weddell Sea* (Doctoral dissertation, Bremen University).

Sültenfuß, J., Purtschert, R., & Führböter, J. F. (2011). Age structure and recharge conditions of a coastal aquifer (northern Germany) investigated with ^{39}Ar, ^{14}C, ^{3}H, ^{3}He isotopes and Ne. *Hydrogeology Journal*, *19*(1), 221–236.

Sültenfuß, J., Roether, W., & Rhein, M. (2009). The Bremen mass spectrometric facility for the measurement of helium isotopes, neon, and tritium in water. *Isotopes in Environmental and Health Studies*, *45*(2), 83–95.

Sültenfuß, J., & Massmann, G. (2004). Datierung mit der ^{3}He-Tritium-Methode am Beispiel der Uferfiltration im Oderbruch. *Grundwasser*, *9*(4), 221–234.

Taylor, P. G., & Townsend, A. R. (2010). Stoichiometric control of organic carbon-nitrate relationships from soils to the sea. *Nature*, *464*(7292), 1178–1181.

Teodosiu, C., Barjoveanu, G., & Teleman, D. (2018). Sustainable water resources management 1. river basin management and the EC Water Framework Directive. *Environmental Engineering and Management Journal*, *2*(4), 377–394.

Tesoriero, A. J., & Puckett, L. J. (2011). O_2 reduction and denitrification rates in shallow aquifers. *Water Resources Research*, *47*(12), 1–17.

Tesoriero, A. J., Liebscher, H., & Cox, S. E. (2000). Mechanism and rate of denirification in an agricultural watershed: Electron and mass balance along groundwater flow paths. *Water Resources Research*, *36*(6), 1545–1559.

The Council of the EU. (1998). Council Directive 98/83/EC of 3 November 1998 on the quality of water intended for human consumption. *Official Journal of the European Communities*, *L330*, 32–54.

Tiedje, J. M. (1988). Ecology of denitrification and dissimilatory nitrate reduction to ammonium. In *Environmental Microbiology on Anaerobes* (pp. 179–244).

Torrentó, C., Cama, J., Urmeneta, J., Otero, N., & Soler, A. (2010). Denitrification of groundwater with pyrite and Thiobacillus denitrificans. *Chemical Geology*, *278*(1-2), 80–91.

Trcek, B., & Zojer, H. (2010). Groundwater hydrology of springs - Engineering, theory, management, and sustainability. In N. Kresic & Z. Stevanovic (Eds.), *Groundwater hydrology of springs - Engineering, theory, management, and sustainability* (pp. 1–515).

Van Dongen, U., Jetten, M. S. M., & van Loosdrecht, M. C. M. (2001). The SHARON ® - Anammox ® - process for treatment of ammonium rich wastewater. *Water Science and Technology*, *44*(1), 153–160.

van Kessel, M. A., Speth, D. R., Albertsen, M., Nielsen, P. H., Op Den Camp, H. J., Kartal, B., … Lücker, S. (2015). Complete nitrification by a single microorganism. *Nature*, *528*(7583), 555–559.

van Genuchten, M., & Alves, W. (1982). Analytical solutions of the one-dimensional convective-dispersive solute transport equation. *U. S. Department of Agriculture, Agricultural Research Service, Technical Bulletin*, *1661*, 1–151.

Visser, A., Broers, H. P., Purtschert, R., Sültenfuß, J., & De Jonge, M. (2013). Groundwater age distributions at a public drinking water supply well field derived from multiple age tracers (^{85}Kr, ^{3}H/ ^{3}He, and ^{39}Ar). *Water Resources Research*, *49*(11), 7778–7796.

Voerkelius, S. (1990). *Isotopendiskriminierungen bei der Nitrifikation und Denitrifikation: Grundlagen und Anwendungen der Herkunfts-Zuordnung von Nitrat und Distickstoffmonoxid* (Doctoral dissertation, TU, München).

Vogel, J. C., Talma, A. S., & Heaton, T. H. E. (1981). Gaseous Nitrogen as Evidence for Denitrification in Groundwater. *Journal of Hydrology*, *50*, 191–200.

Voulvoulis, N., Arpon, K. D., & Giakoumis, T. (2017). The EU Water Framework Directive: From great expectations to problems with implementation. *Science of the Total Environment*, *575*, 358–366.

Ward, B. B., Devol, A. H., Rich, J. J., Chang, B. X., Bulow, S. E., Naik, H., … Jayakumar, A. (2009). Denitrification as the dominant nitrogen loss process in the Arabian Sea. *Nature*, *461*(7260), 78–81.

Ward, E. J., Semmens, B. X., & Schindler, D. E. (2010). Including Source Uncertainty and Prior Information in the Analysis of Stable Isotope Mixing Models. *Environmental Science & Technology*, *44*(12), 4645–4650.

Wassenaar, L. I. (1995). Evaluation of the origin and fate of nitrate in the Abbbotsford Aquifer using isotopes of δ^{15}N and δ^{18}O in NO_3^-O. *Applied Geochemistry, 1995*, *10*, 391–405.

Wassenaar, L. I., Hendry, M. J., & Harrington, N. (2006). Decadal geochemical and isotopic trends for nitrate in a transboundary aquifer and implications for agricultural beneficial management practices. *Environmental Science & Technology*, *40*(15), 4626–4632.

Werner, B., & O'Doherty, J. J. (2012). *European waters — current status and future challenges*. Copenhagen: EEA.

Wick, K., Heumesser, C., & Schmid, E. (2012). Groundwater nitrate contamination: Factors and indicators. *Journal of Environmental Management*, *111*, 178–186.

Widory, D., Petelet-Giraud, E., Négrel, P., & Ladouche, B. (2005). Tracking the sources of nitrate in groundwater using coupled nitrogen and boron isotopes: A synthesis. *Environmental Science & Technology*, *39*(2), 539–548.

Wild, L. M., Mayer, B., & Einsiedl, F. (2018). Decadal delays in groundwater recovery from nitrate contamination caused by low O_2 reduction rates. *Water Resources Research*, *54*(12), 9996–10012.

Willmott, C. J., & Matsuura, K. (2005). Advantages of the mean absolute error (MAE) over the root mean square error (RMSE) in assessing average model performance. *Climate Research*, *30*(1), 79–82.

World Health Organisation. (2004). *Guidelines for Drinking-Water Quality - Second Edition*. World Health Organization. Geneva: World Health Organization.

World Health Organisation. (2007). *Nitrate and Nitrite in Drinking Water*. World Health Organization.

Wunderlich, A., Meckenstock, R., & Einsiedl, F. (2012). Effect of different carbon substrates on nitrate stable isotope fractionation during microbial denitrification. *Environmental Science & Technology*, *46*(9), 4861–4868.

Wunderlich, A., Meckenstock, R. U., & Einsiedl, F. (2013). A mixture of nitrite-oxidizing and denitrifying microorganisms affects the $\delta^{18}O$ of dissolved nitrate during anaerobic microbial denitrification depending on the $\delta^{18}O$ of ambient water. *Geochimica et Cosmochimica Acta*, *119*, 31–45.

Xia, Y., Li, Y., Zhang, X., & Yan, X. (2017). Nitrate source apportionment using a combined dual isotope, chemical and bacterial property, and Bayesian model approach in river systems. *Journal of Geophysical Research: Biogeosciences*, *122*(1), 2–14.

Xu, W., Cai, Y., Tan, Q., & Xu, Y. (2016). Estimating the Proportional Contributions of Multiple Nitrate Sources in Shallow Groundwater with a Bayesian Isotope Mixing Model. *International Journal of Environmental Science and Development*, *7*(8), 581–585.

Xue, D., Botte, J., De Baets, B., Accoe, F., Nestler, A., Taylor, P., ... Boeckx, P. (2009). Present limitations and future prospects of stable isotope methods for nitrate source identification in surface- and groundwater. *Water Research*, *43*(5), 1159–1170.

Yue, F.-J., Li, S.-L., & Hu, J. (2015). The contribution of nitrate sources in Liao Rivers, China, based on isotopic fractionation and Bayesian Mixing Model. *Procedia Earth and Planetary Science*, *13*, 16–20.

Zhang, Q., Wang, X., Sun, F., Sun, J., Liu, J., & Ouyang, Z. (2015). Assessment of temporal and spatial differences of source apportionment of nitrate in an urban river in China, using $\delta^{15}N$ and $\delta^{18}O$ values and an isotope mixing model. *Environmental Science and Pollution Research*, *22*(24), 20226–20233.

Zuber, A. (1986). Mathematical models for the interpretation of environmental radioisotopes in groundwater systems. *Handbook of environmental isotope geochemistry*.

Zumft, W. G. (1997). Cell biology and molecular basis of denitrification. *Microbiology and molecular biology reviews*, *61*(4), 533–616.

APPENDIX A

A.1 SUPPORTING INFORMATION ON THE WATER CHEMISTRY DATA

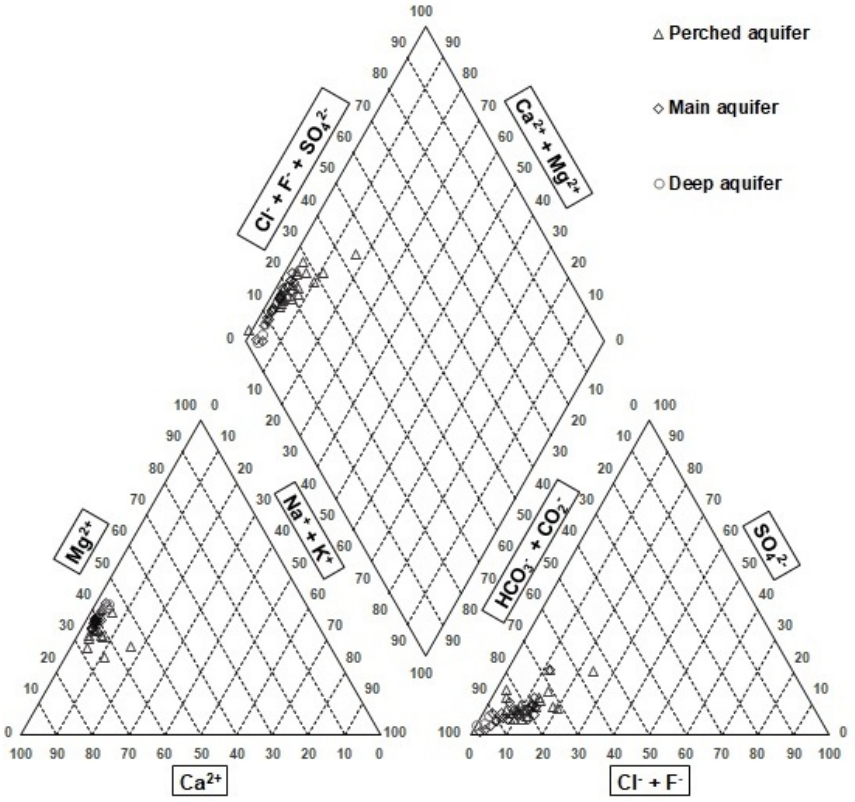

Figure S1: Piperplot for all sampling points in the different aquifers

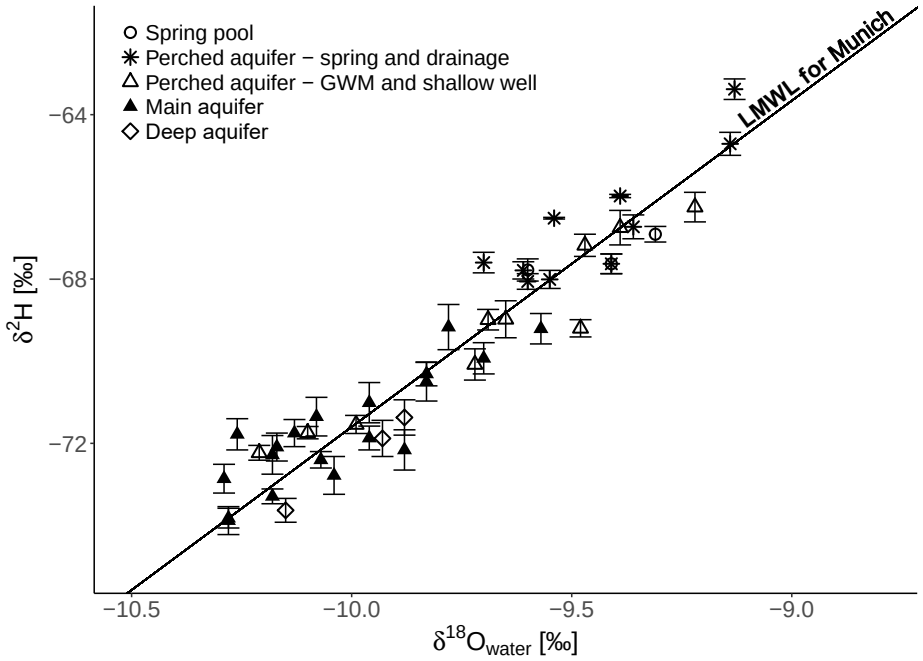

Figure S2: Stable isotopes of water with the Local Meteoric Water Line (LMWL) for Neuherberg, Munich

Table S1: Standard parameters and major ions for all sampling points.

Name	Aquifer	Sampling date	O_2 [µmol/L]	O_2 [mg/l]	O_2 [%]	pH [-]	LF 25°C [µS/cm]	Temp [°C]	Redox [mV]	DOC [µmol/L]	SO_4^{2-} [mmol/L]	Cl^- [mmol/L]	FL^- [mmol/L]	Ca^{2+} [mmol/L]	Mg^{2+} [mmol/L]	Na^+ [mmol/L]	K^+ [mmol/L]	HCO_3^- [mmol/L]	Depth [mbgl]	DGM [m asl]
SP114	Spring pool	12/15/15	368.76	11.82	96.60	7.66	705.00	4.70	103.50	163.2	0.31	0.62	0.03	1.75	0.77	0.57	0.11	4.36	0.0	482.0
SP18	Spring pool	05/25/16	135.01	4.32	41.70	7.49	488.00	11.30	94.50	153.2	0.20	0.59	0.01	1.58	0.75	0.25	0.06	3.31	0.0	453.1
SP57	Spring pool	12/15/15	N/A	N/A	N/A	7.33	661.00	4.90	N/A	63.3	0.42	0.87	0.01	2.59	1.46	0.30	0.02	5.18	0.0	444.7
drainage 157	Perched aquifer - spring & drainage	06/08/16	233.13	7.46	77.10	6.68	496.00	14.60	295.70	50.0	0.11	0.45	0.01	1.57	0.68	0.52	0.07	3.93	0.0	477.0
drainage 69	Perched aquifer - spring & drainage	06/02/16	232.82	7.45	74.60	7.08	843.00	12.50	253.40	50.0	0.30	0.71	0.01	2.97	1.38	0.29	0.03	6.21	0.0	460.1
spring 109	Perched aquifer - spring & drainage	05/31/16	N/A	N/A	N/A	8.06	627.00	13.30	208.90	123.2	0.25	0.56	0.01	2.04	1.00	0.26	0.02	3.78	0.0	441.3
spring 155	Perched aquifer - spring & drainage	05/25/16	267.20	8.55	79.30	7.46	502.00	10.10	237.70	23.3	0.29	0.73	0.01	2.10	1.07	0.38	0.12	4.68	0.0	448.1
spring 156	Perched aquifer - spring & drainage	05/25/16	270.64	8.66	80.90	6.08	313.00	9.70	292.90	43.3	0.21	0.48	0.01	0.76	0.39	0.30	0.16	1.13	0.0	485.0
spring 20	Perched aquifer - spring & drainage	05/25/16	249.07	7.97	71.70	7.14	841.00	8.80	227.40	16.7	0.31	0.45	0.01	2.74	1.65	0.18	0.01	6.48	0.0	448.7
spring 27	Perched aquifer - spring & drainage	05/25/16	306.89	9.82	93.70	8.01	746.00	10.40	191.40	46.6	0.57	0.21	0.01	2.57	1.49	0.21	0.01	6.58	0.0	445.4
spring 30	Perched aquifer - spring & drainage	05/24/16	221.26	7.08	66.80	6.96	808.00	10.40	96.70	89.9	0.33	0.65	0.01	2.87	1.17	0.31	0.07	5.76	0.0	461.9
spring 37	Perched aquifer - spring & drainage	05/24/16	245.32	7.85	72.90	6.96	969.00	9.70	248.00	33.3	0.35	0.76	0.01	2.34	1.09	0.25	0.02	4.42	0.0	459.8
spring 38	Perched aquifer - spring & drainage	05/24/16	297.51	9.52	88.40	7.47	401.00	7.90	245.20	466.3	0.23	0.16	0.01	1.36	0.72	0.13	0.04	3.27	0.0	459.8
spring 66	Perched aquifer - spring & drainage	06/02/16	148.44	4.75	44.90	6.89	691.00	10.00	44.20	166.5	0.24	0.56	0.01	2.37	1.13	0.23	0.06	5.05	0.0	455.9
spring 68	Perched aquifer - spring & drainage	05/24/16	221.88	7.10	68.10	6.86	809.00	11.00	N/A	99.9	0.30	1.41	0.01	2.69	1.01	0.77	0.04	5.02	0.0	467.0
spring 7	Perched aquifer - spring & drainage	05/30/16	288.45	9.23	91.00	7.24	472.00	11.80	191.50	76.6	0.42	0.48	0.01	1.38	0.53	0.42	0.04	2.73	0.0	484.9
GWM 62	Perched aquifer - GWM and shallow well	05/03/16	263.45	8.43	81.10	7.24	738.00	11.40	154.30	26.6	0.29	0.62	0.01	2.46	1.32	0.26	0.06	5.94	9.7	447.5
GWM 63	Perched aquifer - GWM and shallow well	04/22/16	275.32	8.81	85.60	7.31	806.00	7.31	104.00	33.3	0.32	1.33	0.00	2.16	1.54	0.45	0.02	5.17	21.7	471.1
GWM 64	Perched aquifer - GWM and shallow well	04/21/16	10.94	0.35	3.40	7.07	834.00	11.20	86.60	40.0	0.47	0.51	0.00	2.67	1.62	0.26	0.02	7.45	14.3	454.4
GWM 65	Perched aquifer - GWM and shallow well	04/22/16	28.75	0.92	8.60	7.40	675.00	11.70	69.40	20.0	0.19	0.85	0.02	2.09	1.44	0.15	0.02	5.96	4.8	457.3
well 1	Perched aquifer - GWM and shallow well	04/13/16	209.70	6.71	64.80	7.14	722.00	10.80	115.50	11.8	0.26	0.54	0.01	2.36	1.24	0.25	0.02	2.67	30.0	483.4
well 27	Perched aquifer - GWM and shallow well	04/13/16	303.14	9.70	93.20	7.10	595.00	10.80	129.00	11.8	0.21	0.59	0.00	1.83	0.93	0.37	0.02	4.11	11.0	431.3
well 37	Perched aquifer - GWM and shallow well	04/13/16	195.32	6.25	60.50	7.09	641.00	10.80	118.50	11.8	0.27	0.71	0.01	2.09	1.02	0.19	0.02	3.74	13.7	464.1
well 48	Perched aquifer - GWM and shallow well	04/13/16	112.19	3.59	34.90	6.56	375.00	10.80	104.00	23.3	0.14	0.68	0.01	1.11	0.49	0.41	0.04	2.59	15.0	487.2
well 9	Perched aquifer - GWM and shallow well	05/03/16	232.20	7.43	71.00	7.40	622.00	11.00	103.70	11.8	0.18	0.73	0.01	1.99	1.18	0.15	0.02	4.78	43.0	450.3
well 110	Main aquifer	04/20/16	133.44	4.27	40.50	7.40	559.00	11.60	23.40	11.8	0.04	0.16	0.01	1.68	1.20	0.24	0.04	4.88	60.0	408.6
well 122	Main aquifer	05/02/16	163.13	5.22	49.20	7.39	561.00	10.90	274.80	11.8	0.10	0.25	0.00	1.85	1.13	0.13	0.02	5.36	60.5	419.7
well 123	Main aquifer	05/02/16	200.32	6.41	60.20	7.36	607.00	10.80	198.60	11.8	0.17	0.39	0.01	1.99	1.28	0.16	0.02	5.50	47.0	423.7
well 124	Main aquifer	05/03/16	199.69	6.39	60.50	7.38	616.00	10.80	269.20	11.8	0.16	0.48	0.00	1.99	1.23	0.15	0.02	5.35	92.5	425.8
well 126	Main aquifer	05/03/16	241.57	7.73	72.80	7.39	591.00	10.60	195.40	11.8	0.15	0.45	0.01	1.88	1.17	0.14	0.02	5.04	120.0	441.2
well 14	Main aquifer	05/02/16	245.63	7.86	73.40	7.40	585.00	10.20	220.20	11.8	0.21	0.31	0.01	1.95	1.11	0.15	0.02	5.18	103.0	478.5
well 36	Main aquifer	05/03/16	137.19	4.39	42.80	7.41	547.00	12.00	14.30	11.8	0.14	0.26	0.01	1.74	1.14	0.15	0.02	5.27	120.0	478.1
well 47	Main aquifer	05/02/16	139.07	4.45	41.70	7.20	814.00	10.50	249.60	11.8	0.26	0.87	0.01	2.77	1.48	0.21	0.03	6.66	103.6	456.5
well 48	Main aquifer	05/02/16	226.88	7.26	68.20	7.22	779.00	10.50	295.50	11.8	0.25	0.73	0.00	2.64	1.43	0.20	0.02	6.32	92.0	460.7
well 50	Main aquifer	04/12/16	63.44	2.03	19.40	7.27	767.00	10.70	174.00	11.8	0.21	1.10	0.01	2.46	1.50	0.16	0.03	6.56	61.0	463.8
well 51	Main aquifer	04/21/16	16.56	0.53	5.10	7.36	669.00	11.50	85.90	11.8	0.42	0.82	0.01	2.08	1.25	0.14	0.02	5.30	126.5	486.0
well 53	Main aquifer	04/12/16	198.76	6.36	61.90	7.41	586.00	11.40	227.90	11.8	0.14	0.31	0.01	1.88	1.16	0.13	0.02	5.36	44.5	423.4
well 6	Main aquifer	04/21/16	322.82	10.33	96.50	7.28	693.00	10.60	212.60	40.0	0.26	0.73	0.01	2.18	1.15	0.19	0.01	4.99	32.0	426.6
well 67	Main aquifer	05/12/16	240.63	7.70	72.00	7.40	590.00	11.70	100.00	23.3	0.29	0.79	0.00	0.00	0.00	0.00	0.00	0.00	108.5	474.1
well 68	Main aquifer	05/10/16	243.76	7.80	72.00	7.10	610.00	11.30	N/A	50.0	0.29	0.90	0.01	2.28	1.39	0.30	0.02	4.98	59.0	474.6
well 76	Main aquifer	05/02/16	267.20	8.55	79.30	7.44	546.00	10.00	173.20	11.8	0.14	0.28	0.01	1.82	1.07	0.13	0.02	2.86	87.0	463.6
well 86	Main aquifer	04/20/16	169.38	5.42	50.40	7.26	791.00	10.60	221.30	11.8	0.25	1.13	0.01	2.50	1.31	0.38	0.02	6.15	59.0	405.8
well 87	Main aquifer	04/20/16	175.01	5.60	52.90	7.42	552.00	11.20	220.50	11.8	0.04	0.11	0.01	1.60	1.21	0.13	0.02	5.75	113.0	436.5
well 91	Main aquifer	04/21/16	66.88	2.14	23.20	7.29	576.00	17.20	172.30	20.0	0.22	0.17	0.01	1.75	1.17	0.16	0.02	5.55	158.0	447.8
well 5	Deep aquifer	08/10/16	87.19	2.79	32.20	7.14	582.00	16.80	162.70	11.8	0.19	0.14	0.01	1.90	1.28	0.17	0.02	5.70	185.0	454.4
well 59	Deep aquifer	08/09/16	57.50	1.84	18.40	7.28	504.00	13.00	-84.40	11.8	0.11	0.14	0.01	1.86	1.36	0.23	0.03	6.00	134.5	425.3
well 73	Deep aquifer	08/09/16	1.88	0.06	0.60	7.30	593.00	12.90	182.00	11.8	0.10	0.03	0.01	1.84	1.40	0.24	0.03	6.34	162.4	451.9

Table S2: Measured $\delta^{15}N_{nitrate}$ and $\delta^{18}O_{nitrate}$ values with O_2 concentrations [µmol/L] for all sampling points.

Name	Aquifer	Sampling date	O_2 [µmol/L]	$\delta^{15}N$ [‰]	$\delta^{18}O$ [‰]
spring pool 114	Spring pool	15-Dec-2015	318.8	13.6	3.5
spring pool 18	Spring pool	8-Dec-2015	246.9	12.4	4.3
spring pool 57	Spring pool	15-Dec-2015	356.3	11.1	5.6
drainage 69	Perched aquifer - spring & drainage	15-Dec-2015	343.8	12.1	3.1
spring 66	Perched aquifer - spring & drainage	1-Mar-2016	300	10.8	1.6
spring 109	Perched aquifer - spring & drainage	1-Mar-2016	300	9.1	5.1
spring 68	Perched aquifer - spring & drainage	7-Dec-2015	234.4	10.2	2.8
spring 27	Perched aquifer - spring & drainage	17-Dec-2015	271.9	-0.6	1.6
spring 20	Perched aquifer - spring & drainage	15-Dec-2015	315.6	4.3	3.0
spring 156	Perched aquifer - spring & drainage	8-Dec-2015	287.5	9.8	1.5
spring 155	Perched aquifer - spring & drainage	8-Dec-2015	306.3	8.1	1.8
spring 37	Perched aquifer - spring & drainage	7-Dec-2015	293.8	9.4	2.7
spring 38	Perched aquifer - spring & drainage	7-Dec-2015	337.5	9.1	3.2
spring 7	Perched aquifer - spring & drainage	25-Feb-2016	293.8	7.1	1.1
well 1	Perched aquifer - GWM and shallow well	13-Apr-2016	209.4	9.7	1.9
well 9	Perched aquifer - GWM and shallow well	3-May-2016	231.3	6.8	1.9
well 27	Perched aquifer - GWM and shallow well	13-Apr-2016	303.1	8.9	1.7
well 48	Perched aquifer - GWM and shallow well	13-Apr-2016	112.5	8.1	2.2
well 37	Perched aquifer - GWM and shallow well	13-Apr-2016	196.9	6.3	2.7
GWM 62	Perched aquifer - GWM and shallow well	3-May-2016	262.5	7.7	3.0
GWM 63	Perched aquifer - GWM and shallow well	22-Apr-2016	275	6.1	2.3
GWM 64	Perched aquifer - GWM and shallow well	21-Apr-2016	12.5	19.7	7.5
GWM 65	Perched aquifer - GWM and shallow well	22-Apr-2016	28.1	13.1	5.2
well 6	Main aquifer	21-Apr-2016	321.9	8.6	1.9
well 124	Main aquifer	3-May-2016	200	6.7	2.2
well 86	Main aquifer	20-Apr-2016	168.8	9.0	2.9
well 48	Main aquifer	2-May-2016	228.1	9.5	2.9
well 36	Main aquifer	3-May-2016	137.5	7.6	1.7
well 122	Main aquifer	2-May-2016	162.5	5.9	0.6
well 123	Main aquifer	2-May-2016	200	6.8	2.3
well 76	Main aquifer	2-May-2016	268.8	4.2	0.7
well 47	Main aquifer	2-May-2016	140.6	9.9	3.5
well 53	Main aquifer	12-Apr-2016	200	7.2	3.3
well 50	Main aquifer	12-Apr-2016	62.5	11.2	4.0
well 14	Main aquifer	2-May-2016	246.9	4.4	1.0
well 110	Main aquifer	20-Apr-2016	134.4	5.1	0.2
well 126	Main aquifer	3-May-2016	240.6	7.1	2.9
well 87	Main aquifer	20-Apr-2016	175	5.1	-0.5
well 91	Main aquifer	21-Apr-2016	65.6	5.1	1.0
well 51	Main aquifer	21-Apr-2016	15.6	10.4	0.3
well 68	Main aquifer	10-May-2016	243.8	6.7	3.4
well 67	Main aquifer	12-May-2016	240.6	6.6	1.9
well 59	Deep aquifer	9-Aug-2016	56.3	6.4	2.8
well 5	Deep aquifer	10-Aug-2016	87.5	2.1	1.6
well 73	Deep aquifer	9-Aug-2016	6.3	-5.0	3.9

Table S3: Results of mean transit time modeling for all sampled wells.

Sample name	Aquifer	Sampling date	^3H [TU]	^3He [TU]	$^3He_0$ [TU]	MTT of young component [years]	Model	p_D [-]	MTT of old component [years]	Mixing fraction 1st comp [%]	P_D of old component [-]	Dilution factor	Number of screens	Included in graph	construction depth [mbgl]
GWM 65	Perched aquifer - GWM and shallow well	22-Apr-2016	6.1	21.6	27.9	15	DM	0.35		100			1	no, evidence of abnormity	17.7
GWM 64	Perched aquifer - GWM and shallow well	21-Apr-2016	6.1	2.5	8.3	6	DM	0.08		100			1	no, evidence of abnormity	14.3
GWM 63	Perched aquifer - GWM and shallow well	22-Apr-2016	5.3	1.3	6.6	5	DM	0.17		100			1	no, large modelling error	21.7
GWM 62	Perched aquifer - GWM and shallow well	3-May-2016	5.3	6.7	12.1	12	DM	0.15		100			1	yes	9.7
well 9	Perched aquifer - GWM and shallow well	3-May-2016	6.2	7.5	13.6	9	DM	0.45		100			1	yes	43
well 1	Perched aquifer - GWM and shallow well	13-Apr-2016	5.9	2.3	8.1	20	DM	0.28		100			N/A	no, large modelling error	40
well 27	Perched aquifer - GWM and shallow well	13-Apr-2016	5.5	4.0	9.5	10	DM	0.12		100			N/A	yes	11
well 68	Main aquifer	10-May-2016	6.4	7.3	13.6	14	DM	0.04		100			1	yes	50
well 67	Main aquifer	12-May-2016	6.4	21.9	28.3	28	DM	0.05		100			3	no, large modelling error	100
well 110	Main aquifer	20-Apr-2016	0.6	1.8	2.4	57	DM	0.03		100			1	yes	60
well 47	Main aquifer	2-May-2016	7.0	37.2	44.2	35	BMM	0.03	500	33	0.1		4	yes	103.6
well 47, 48 mbgl	Main aquifer	8-Jun-2016	7.0	50.5	57.5	60	DM	0.25		100			4	yes	103.6
well 50	Main aquifer	12-Apr-2016	7.3	68.6	76.3	122	DM	0.2		100			1	yes	61
well 48	Main aquifer	2-May-2016	5.7	22.4	27.9	18	DM	0.19		100			3	no, large modelling error	92
well 86	Main aquifer	20-Apr-2016	6.5	24.2	30.7	20	BMM	0.3	500	60	0.1		3	yes	59
well 53	Main aquifer	12-Apr-2016	2.8	10.5	13.2	15	TTM-BMM	0.23	500	49	0.1		2	yes	44.5
well 51	Main aquifer	21-Apr-2016	5.8	51.6	57.5	36	TTM-BMM	0.01	500	61	0.1		4	no, large modelling error	126.5
well 123	Main aquifer	2-May-2016	2.9	16.9	19.8	19	TTM-BMM	0.29	500	46	0.1		3	yes	47
well 14	Main aquifer	2-May-2016	3.8	13.5	17.2	24	DM	0.01		100			2	no, large modelling error	103
well 14	Main aquifer	2-May-2016	3.8	13.5	17.2	14	TTM-BMM	0.42	500	61	0.1		2	no, pd too high	103
well 36	Main aquifer	3-May-2016	1.3	9.0	10.3	23	BMM	0.07	500	24	0.1		N/A	yes	123
well 122	Main aquifer	2-May-2016	1.8	15.4	17.2	24	TTM-BMM	0.23	500	26	0.1		2	yes	60.5
well 124	Deep aquifer	3-May-2016	4.2	29.2	33.4	23	TTM-BMM	0.15	500	65	0.08		4	yes	92.5
well 126	Deep aquifer	3-May-2016	3.1	18.4	21.5	21	TTM-BMM	0.15	500	52	0.1		4	no, large modelling error	120
well 59	Deep aquifer	9-Aug-2016	1.7	13.1	14.7	23	BMM	0.1	6455	25	0.5		4	no	134.5
well 5	Deep aquifer	10-Aug-2016	1.9	2.1	3.9	965	DM	0.11		100		0.65	5	no	185
well 5	Deep aquifer	10-Aug-2016	1.9	2.1	3.9	3603	DM	0.2		100		0.85	5	no	185
well 73	Deep aquifer	9-Aug-2016	0.0	1.0	1.1	5883	DM	0.23		100		0.85	1	no	162.4
well 73	Deep aquifer	9-Aug-2016	0.0	1.0	1.1	2884	DM	0.28		100		0.65	1	no	162.4
well 59	Main aquifer	9-Aug-2016	1.7	13.1	14.7	6002	DM	0.06		100		0.85	4	no	134.5
well 59	Main aquifer	9-Aug-2016	1.7	13.1	14.7	3364	DM	0.17		100		0.65	4	no	134.5
well 91	Main aquifer	21-Apr-2016	2.2	2.5	4.6	1	TTM-BMM	0.67	500	41	0.1		6	no	158
well 76	Main aquifer	2-May-2016	2.8	14.7	17.3	70	BMM	0.1	500	20	0.1		5	no, large modelling error	87
well 48	Main aquifer	13-Apr-2016	5.8	1.2	7.1	1	BMM-DM-DM	0.2	500	86	0.1		N/A	yes	15
well 152, 40 mgbl	Main aquifer	25-Oct-2016	6.3	7.4	13.6	11	DM	0.27		100				yes, additional to planned sampling	89.4
well 106	Main aquifer	21-Apr-2016	6.5	10.4	17.1	12	DM	0.3		100				yes	32
well 118, 53 mbgl	Main aquifer	3-Nov-2016	5.7	4.7	10.4	10	DM	0.01		100				yes, additional to planned sampling	116

Table S4: Measured stable isotopes of water ($\delta^{18}O$ and $\delta^{2}H$) for all sampling points.

Name	Aquifer	Sample Date	$\delta^{18}O$ [‰]	$\delta^{2}H$ [‰]
spring pool 114	Spring pool	15-Dec-2015	-9.4	-67.6
spring pool 18	Spring pool	8-Dec-2015	-9.6	-67.8
spring pool 57	Spring pool	15-Dec-2015	-9.3	-66.9
drainage 69	Perched aquifer - spring & drainage	15-Dec-2015	-9.1	-63.4
spring 27	Perched aquifer - spring & drainage	15-Dec-2017	-9.6	-68.0
spring 20	Perched aquifer - spring & drainage	28-Apr-2016	-9.6	-68.1
spring 156	Perched aquifer - spring & drainage	8-Dec-2015	-9.7	-67.6
spring 155	Perched aquifer - spring & drainage	8-Dec-2015	-9.4	-66.7
spring 37	Perched aquifer - spring & drainage	7-Dec-2015	-9.1	-64.7
spring 38	Perched aquifer - spring & drainage	7-Dec-2015	-9.5	-66.5
spring 7	Perched aquifer - spring & drainage	25-Feb-2016	-9.6	-67.8
spring 68	Perched aquifer - spring & drainage	7-Dec-2015	-9.4	-66.0
well 1	Perched aquifer - GWM and shallow well	13-Apr-2016	-9.5	-67.2
well 37	Perched aquifer - GWM and shallow well	13-Apr-2016	-9.2	-66.3
GWM 65	Perched aquifer - GWM and shallow well	22-Apr-2016	-9.7	-70.1
well 27	Perched aquifer - GWM and shallow well	13-Apr-2016	-9.7	-69.0
GWM 63	Perched aquifer - GWM and shallow well	22-Apr-2016	-9.7	-69.0
GWM 62	Perched aquifer - GWM and shallow well	31-May-2016	-9.5	-69.2
well 9	Perched aquifer - GWM and shallow well	25-Aug-2016	-10.1	-71.7
GWM 64	Perched aquifer - GWM and shallow well	21-Apr-2016	-9.4	-66.8
well 48	Perched aquifer - GWM and shallow well	13-Apr-2016	-10.2	-72.2
well 6	Main aquifer	21-Apr-2016	-9.6	-69.2
well 124	Main aquifer	3-May-2016	-10.3	-72.9
well 86	Main aquifer	20-Apr-2016	-9.8	-69.2
well 48	Main aquifer	2-May-2016	-9.7	-69.9
well 36	Main aquifer	3-May-2016	-10.2	-73.3
well 122	Main aquifer	2-May-2016	-10.3	-71.8
well 123	Main aquifer	2-May-2016	-10.1	-71.8
well 76	Main aquifer	2-May-2016	-9.9	-72.2
well 47	Main aquifer	2-May-2016	-9.8	-70.3
well 53	Main aquifer	12-Apr-2016	-10.2	-72.1
well 50	Main aquifer	12-Apr-2016	-10.1	-72.4
well 14	Main aquifer	2-May-2016	-10.0	-71.0
well 110	Main aquifer	20-Apr-2016	-10.3	-73.8
well 126	Main aquifer	3-May-2016	-10.1	-71.4
well 87	Main aquifer	20-Apr-2016	-10.3	-73.9
well 91	Main aquifer	21-Apr-2016	-10.0	-71.9
well 51	Main aquifer	21-Apr-2016	-10.2	-72.3
well 68	Main aquifer	10-May-2016	-9.8	-70.5
well 67	Main aquifer	12-May-2016	-10.0	-72.8
well 73	Deep aquifer	9-Aug-2016	-9.9	-71.4
well 59	Deep aquifer	9-Aug-2016	-10.2	-73.6
well 5	Deep aquifer	10-Aug-2016	-9.9	-71.9

Table S5: Monthly measured stable isotopes of water ($\delta^{18}O$ and $\delta^{2}H$) for selected drainages and springs.

Name	Aquifer	n	Amplitude $\delta^{18}O$ [‰]	$\delta^{18}O$ - Max [‰]	$\delta^{18}O$ - Min [‰]	Amplitude $\delta^{2}H$ [‰]	$\delta^{2}H$ - Max [‰]	$\delta^{2}H$ - Min [‰]
GWM 64	Perched aquifer - GWM and shallow well	12	0.4	-9.3	-9.7	1.9	-65.6	-67.5
GWM 62	Perched aquifer - GWM and shallow well	11	0.8	-9.1	-9.9	1.0	-68.5	-69.5
GWM 63	Perched aquifer - GWM and shallow well	15	1.4	-9.0	-10.4	3.9	-65.7	-69.6
GWM 65	Perched aquifer - GWM and shallow well	9	0.4	-9.5	-9.9	1.0	-69.1	-70.1
well 9	Perched aquifer - GWM and shallow well	10	0.3	-9.9	-10.2	2.7	-69.0	-71.7
well 27	Perched aquifer - GWM and shallow well	9	1.0	-9.5	-10.5	1.5	-69.0	-70.5
well 37	Perched aquifer - GWM and shallow well	6	0.4	-9.0	-9.4	2.0	-64.5	-66.5
well 1	Perched aquifer - GWM and shallow well	12	0.6	-9.0	-9.6	1.8	-65.7	-67.5
well 48	Perched aquifer - GWM and shallow well	2	0.4	-9.8	-10.2	2.7	-69.5	-72.2
wells and GWM_Min			**0.3**	**-9.9**	**-10.5**	**1.0**	**-69.5**	**-72.2**
wells and GWM_Max			**1.4**	**-9.0**	**-9.4**	**3.9**	**-64.5**	**-66.5**
drainage 1	Perched aquifer - spring & drainage	**6**	0.3	-9.6	-9.9	1.1	-68.7	-69.8
spring 27	Perched aquifer - spring & drainage	12	0.8	-9.4	-10.2	1.9	-68.0	-69.9
spring 30	Perched aquifer - spring & drainage	13	0.5	-9.2	-9.7	3.5	-65.0	-68.5
spring 20	Perched aquifer - spring & drainage	12	0.9	-8.9	-9.8	1.6	-66.5	-68.1
spring 156	Perched aquifer - spring & drainage	15	0.6	-9.4	-10.0	1.9	-67.6	-69.5
drainage 6	Perched aquifer - spring & drainage	5	2.9	-6.9	-9.7	11.8	-59.0	-70.8
spring 66	Perched aquifer - spring & drainage	4	0.1	-9.6	-9.7	0.9	-67.9	-68.8
spring 68	Perched aquifer - spring & drainage	**15**	0.4	-9.3	-9.7	2.6	-66.0	-68.6
spring 7	Perched aquifer - spring & drainage	12	0.6	-9.3	-9.8	1.1	-66.8	-67.9
spring 37	Perched aquifer - spring & drainage	2	0.2	-9.1	-9.4	2.3	-64.7	-67.1
spring 38	Perched aquifer - spring & drainage	2	0.7	-9.5	-10.3	6.5	-66.5	-73.1
spring 155	Perched aquifer - spring & drainage	2	0.3	-9.4	-9.7	2.6	-66.7	-69.3
springs and drainages_Min			**0.1**	**-9.6**	**-10.3**	**0.9**	**-68.7**	**-73.1**
springs and drainages_Max			**2.9**	**-6.9**	**-9.4**	**11.8**	**-59.0**	**-67.1**

B

APPENDIX B

B.1 S1 MODELING OF MICROBIAL DENITRIFICATION AND ISOTOPIC ENRICHMENT

Considering first-order degradation, the change of substance concentration X_l with time t can be described as:

$$\frac{dX_l}{dt} = -\mu \cdot X_l \tag{S1}$$

where μ is a first-order rate constant describing degradation [a^{-1}], and X_l is concentration of the substrate, i. e.the more abundant (lighter) isotope.

The well-known Rayleigh equations are based upon an exponential relation describing the partitioning of isotopes between two reservoirs as one reservoir decreases in size (Kendall and McDonnell, 1998b). The equations can be used to describe an isotope fractionation process if: (i) material is continuously removed from a mixed system containing molecules of two or more isotopic species, (ii) the fractionation accompanying the removal process at any instance is described by the fractionation factor α, and (iii) α does not change during the process (ibid.). Under these conditions, the evolution of the isotopic composition in the residual (reactant) material can be described by the following differential equation:

$$\frac{dR}{dX_l} = \frac{R}{X_l} \cdot (\alpha - 1) \tag{S2}$$

where R is the isotopic ratio. With initial condition $R(X_l = X_{l,o}) = R_o$, where R_o is the isotopic ratio at initial concentration, the solution of Eq. S2 is (ibid.)

$$\frac{R}{R_0} = \left(\frac{X_l}{X_{l,0}}\right)^{(\alpha-1)} \tag{S3}$$

Equation S2 can be rearranged to:

$$dR = \frac{R}{X_l} \cdot (\alpha - 1) \cdot dX_l \tag{S4}$$

Rearranging equation S1 to $dX_l = -\mu \cdot X_l$ and inserting into equation S4 yields:

$$\frac{dR}{dt} = -\mu \cdot (\alpha - 1) \cdot R \tag{S5}$$

Thus, degradation plus isotopic enrichment can be considered by implementing a first-order constant $k=\mu(\alpha-1)$. This has been done for equation 28 (where k is part of coefficient u) and Sc. 3.

B.2 REPORTED δ^{15}N FREQUENCY DISTRIBUTIONS OF NITRATE SOURCES

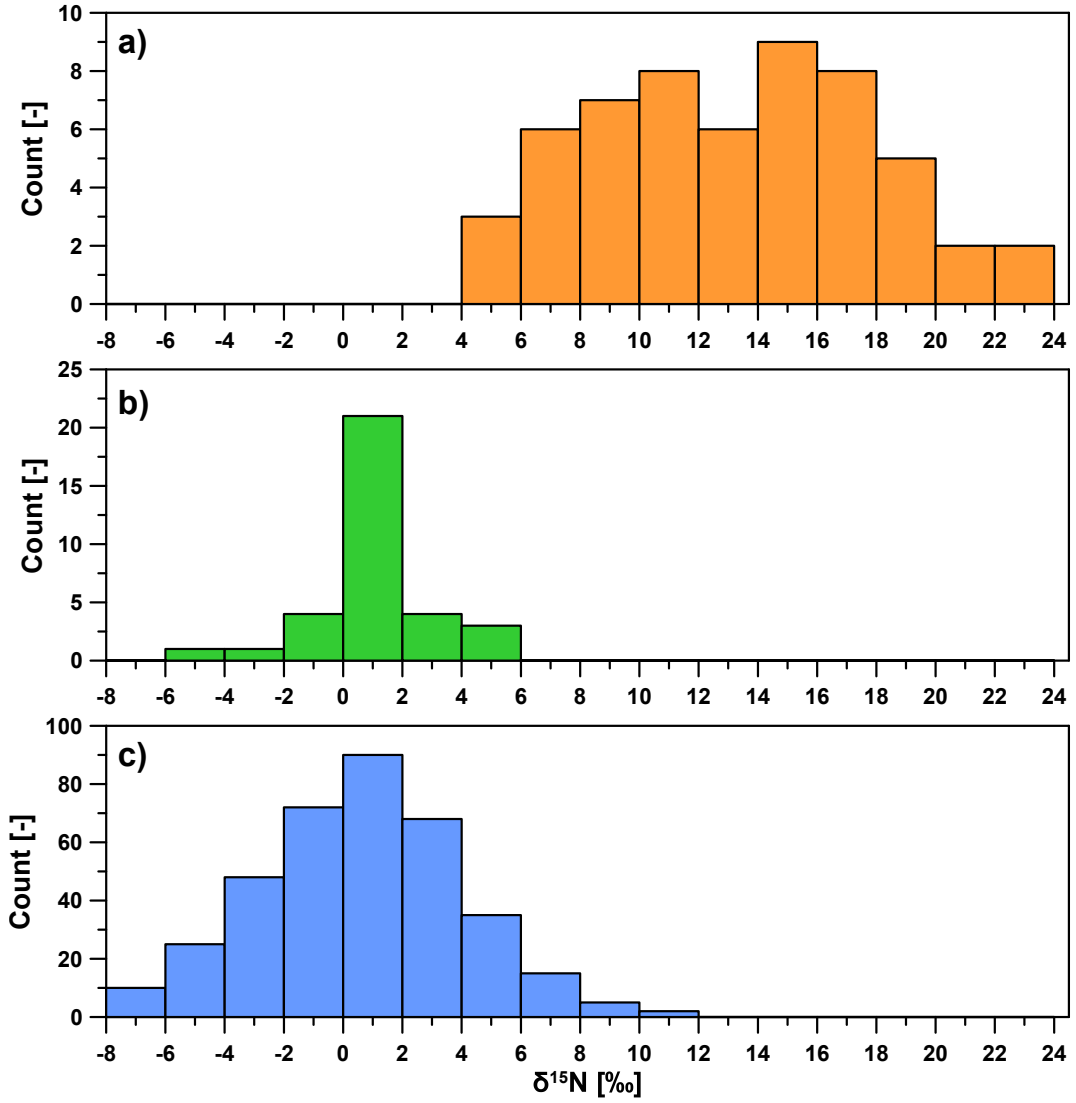

Figure S3: Typical δ^{15}N frequency distributions of different nitrate sources, including a) manure, b) mineral fertilizer and c) precipitation (after (Kendall and McDonnell, 1998b))

B.3 OBSERVED $\delta^{15}N$ (NITRATE) IN GROUNDWATER AND FITTED FREQUENCY DISTRIBUTIONS

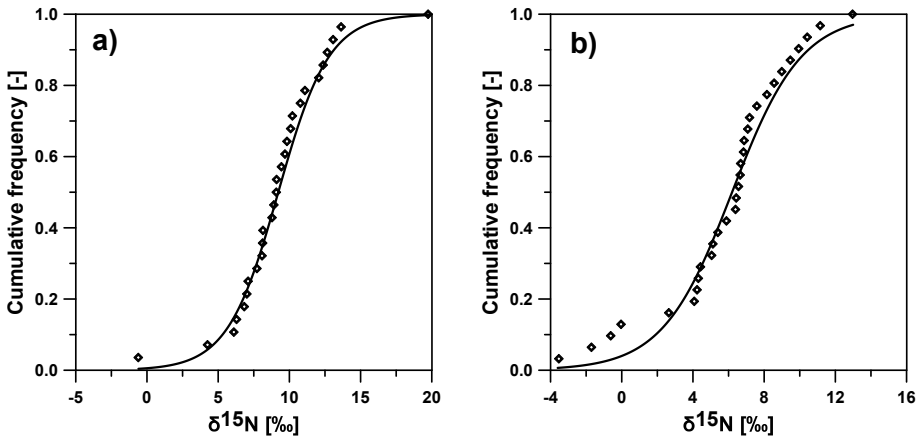

Figure S4: Measured (diamonds) and fitted (lines) cumulative frequency distributions for $\delta^{15}N$ (nitrate) in a) the perched aquifer and b) the main aquifer. Numbers of measured $\delta^{15}N$ values are n = 31 for the main aquifer and n = 28 for the perched aquifer. Logistic distributions were fitted.

B.4 EVALUATION OF SC. 1 REALIZATIONS (MIXING OF NITRATE SOURCES)

Table S6: MAE and R^2 for the frequency distribution of simulated versus measured $\delta^{15}N$ in groundwater of the perched and main aquifer. Realization of Sc. 1 within the best fit range (with MAE <10.2 for the perched aquifer and <9.67 for the main aquifer, i. e.below 5th percentile MAE). Green via yellow to red indicates decreasing goodness of fit.

Perched Aquifer				Main Aquifer			
p_1, portion agriculture [%]	p_2, portion manure [%]	MAE [-]	R^2 [-]	p_1, portion agriculture [%]	p_2, portion manure [%]	MAE [-]	R^2 [-]
65	95	9.27	0.875	40	95	9.01	0.929
65	100	8.82	0.893	40	100	7.51	0.952
70	90	8.71	0.891	45	85	9.17	0.936
70	95	8.71	0.897	45	90	7.53	0.958
70	100	9.55	0.885	45	95	5.99	0.978
75	80	9.58	0.875	45	100	5.27	0.980
75	85	8.49	0.895	50	80	8.43	0.961
75	90	9.10	0.894	50	85	6.81	0.980
80	75	9.41	0.880	50	90	6.07	0.978
80	80	8.71	0.900	50	95	6.37	0.966
80	85	9.28	0.893	50	100	7.23	0.946
85	70	9.41	0.882	55	75	8.40	0.968
85	75	8.60	0.906	55	80	7.19	0.977
85	80	9.27	0.893	55	85	7.15	0.967
90	65	9.67	0.881	55	90	7.87	0.944
90	70	8.63	0.905	60	70	8.62	0.972
90	75	9.19	0.895	60	75	7.77	0.972
95	60	10.12	0.873	60	80	8.21	0.950
95	65	8.49	0.905	60	85	9.44	0.910
95	70	8.95	0.898	65	65	9.49	0.969
100	60	8.47	0.907	65	70	8.85	0.958
100	65	8.76	0.906	65	75	9.25	0.933
100	70	10.16	0.871	70	65	9.67	0.953

B.5 EVALUATION OF SC. 2 REALIZATIONS (TRANSPORT IN GROUNDWATER)

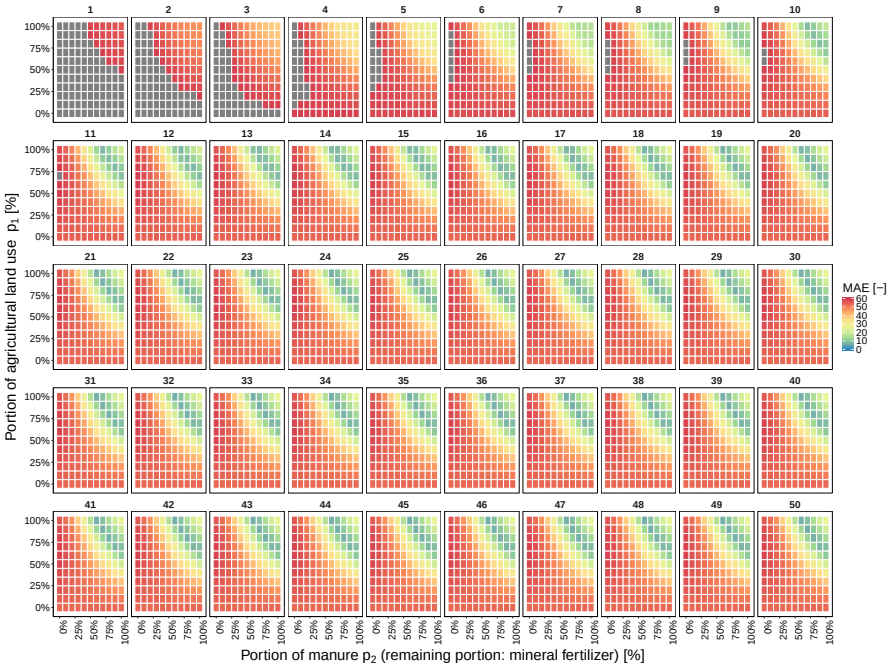

Figure S5: Mean absolute error (**MAE**) for the frequency distribution of simulated versus measured $\delta^{15}N$ in groundwater of the **perched aquifer**. Comparison of all considered realizations for **Sc. 2**. The number on top of each graph refers to the duration of nitrate transport in groundwater (in years).

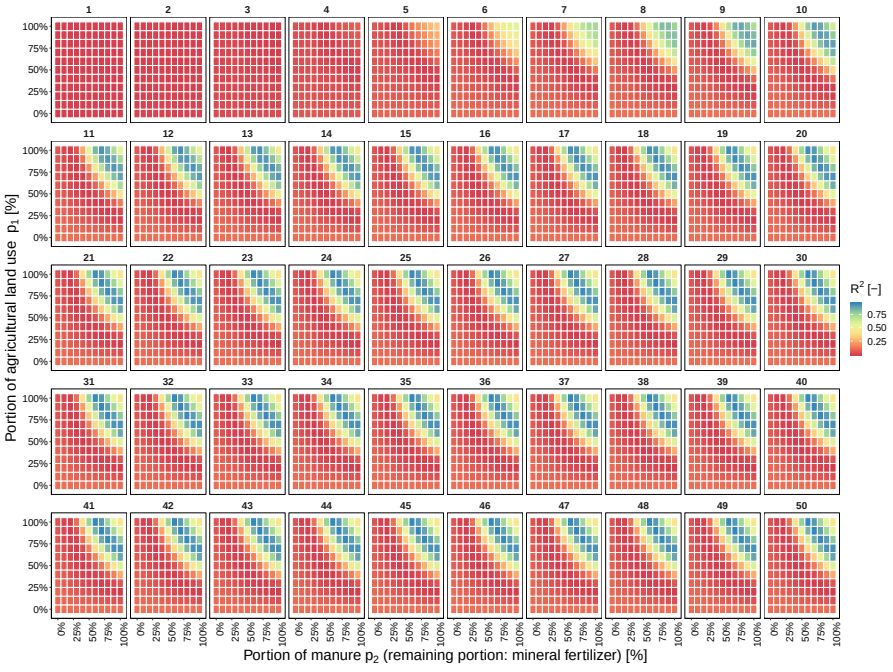

Figure S6: Coefficient of determination (**R^2**) for the frequency distribution of simulated versus measured $\delta^{15}N$ in groundwater of the **perched aquifer**. Comparison of all considered realizations for **Sc. 2**. The number on top of each graph refers to the duration of nitrate transport in groundwater (in years).

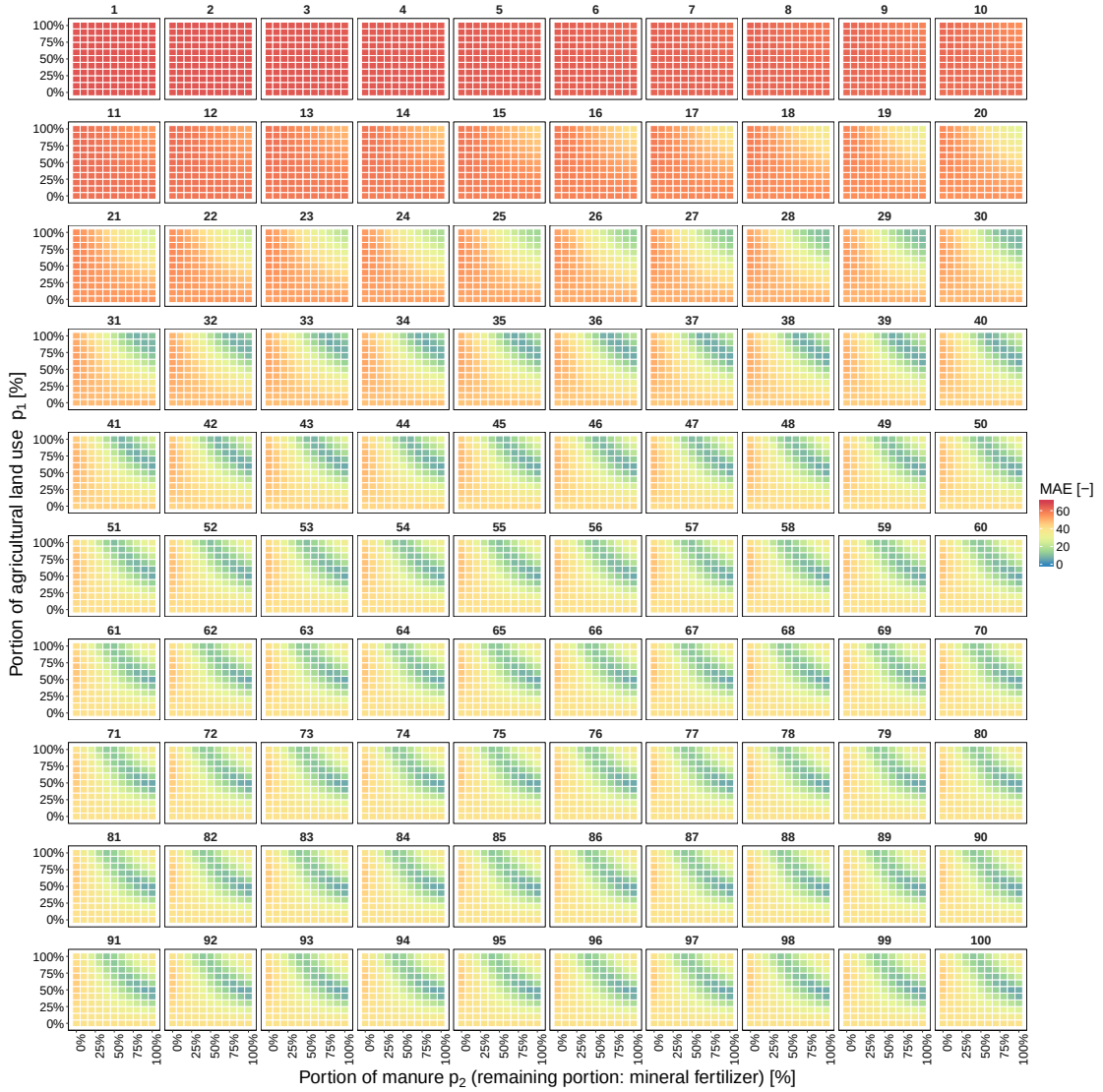

Figure S7: Mean absolute error (**MAE**) for the frequency distribution of simulated versus measured $\delta^{15}N$ in groundwater of the **main aquifer**. Comparison of all considered realizations for **Sc. 2**. The number on top of each graph refers to the duration of nitrate transport in groundwater (in years).

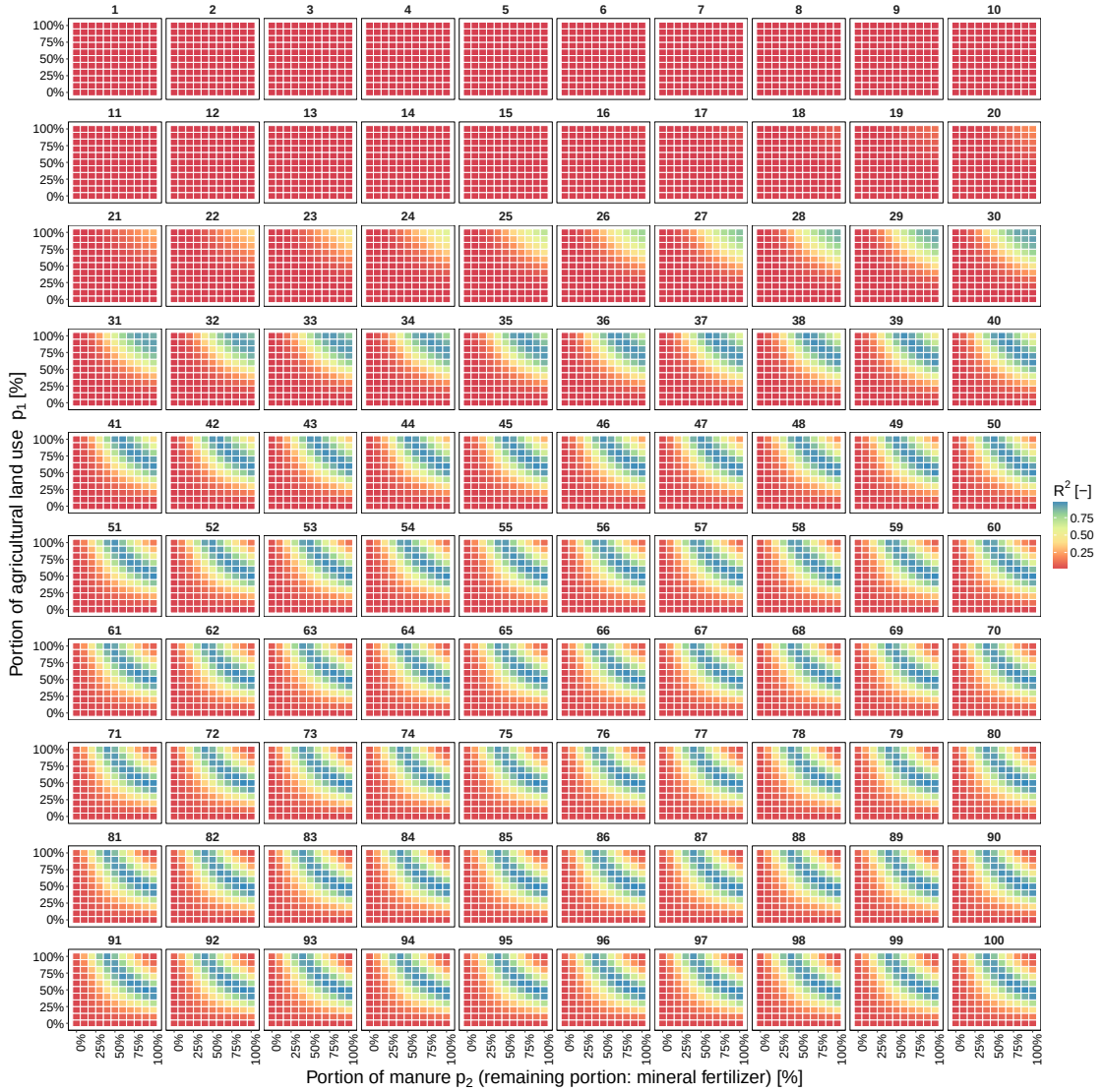

Figure S8: Coefficient of determination (**R²**) for the frequency distribution of simulated versus measured $\delta^{15}N$ in groundwater of the **main aquifer**. Comparison of all considered realizations for **Sc. 2**. The number on top of each graph refers to the duration of nitrate transport in groundwater (in years).

Table S7: MAE and R^2 for the frequency distribution of simulated versus measured $\delta^{15}N$ in groundwater of the perched and main aquifer. Selected realization of Sc. 2 within the best fit range (with MAE <9.9 for the perched aquifer and <10.7 for the main aquifer, i. e. below 5^{th} percentile MAE). Selected realizations, presenting lowest and highest MAE within the best fit range for each considered source composition (defined by p_1 and p_2). 'Time' refers to the duration of nitrate transport in groundwater (from the source to an observation point in the aquifer, downstream of the source). Green via yellow to red indicates decreasing goodness of fit.

Perched Aquifer					Main Aquifer				
Time [a]	p_1, portion agriculture [%]	p_2, portion manure [%]	MAE [-]	R^2 [-]	Time [a]	p_1, portion agriculture [%]	p_2, portion manure [%]	MAE [-]	R^2 [-]
50	70	90	7.40	0.928	99	40	100	7.55	0.956
14			9.47	0.886	62			10.57	0.906
13	70	100	8.19	0.911	96	50	80	8.75	0.959
11			9.01	0.884	69			10.65	0.93
50	80	80	6.69	0.947	98	50	90	6.01	0.986
12			9.40	0.887	50			10.59	0.92
12	80	90	7.85	0.924	65	50	100	5.97	0.977
22			9.32	0.902	43			10.35	0.912
43	90	70	6.53	0.952	100	60	70	9.13	0.971
12			9.23	0.897	66			10.61	0.951
11	90	80	8.41	0.913	78	60	80	7.93	0.963
27			9.91	0.886	47			10.63	0.934
47	100	60	6.37	0.950	49	60	90	6.74	0.976
13			9.44	0.896	83			10.7	0.886
12	100	70	7.47	0.930	42	60	100	6.24	0.967
24			8.94	0.905	55			10.41	0.888
					55	70	70	9.33	0.965
					46			10.65	0.944
					45	70	80	7.55	0.97
					58			10.57	0.9
					40	70	90	6.68	0.962
					49			10.4	0.888
					37	70	100	6.43	0.956
					43			10.56	0.88
					56	80	60	10.37	0.958
					50			10.7	0.956
					43	80	70	8.09	0.964
					53			10.5	0.912
					39	80	80	6.83	0.962
					46			10.63	0.886
					36	80	90	6.54	0.955
					40			9.81	0.895
					34	80	100	7.65	0.938
					29			10.64	0.838
					43	90	60	8.43	0.966
					52			10.59	0.923
					38	90	70	6.92	0.963
					45			10.44	0.897
					34	90	80	6.16	0.957
					30			10.66	0.848
					32	90	90	7.85	0.93
					36			10.22	0.889
					30	90	100	8.36	0.921
					28			10.52	0.86
					47	100	50	9.77	0.957
					42			10.64	0.943
					39	100	60	7.31	0.961
					46			10.46	0.901
					35	100	70	6.99	0.95
					40			10.07	0.89
					32	100	80	7.38	0.938
					36			10.28	0.892
					30	100	90	9.16	0.903
					32			9.98	0.899
					29	100	100	9.88	0.901
					30			10.09	0.897

B.6 EVALUATION OF SC. 3 REALIZATIONS (TRANSPORT AND MICROBIAL DENITRIFICATION IN GROUNDWATER WITH $\mu = 1\ a^{-1}$)

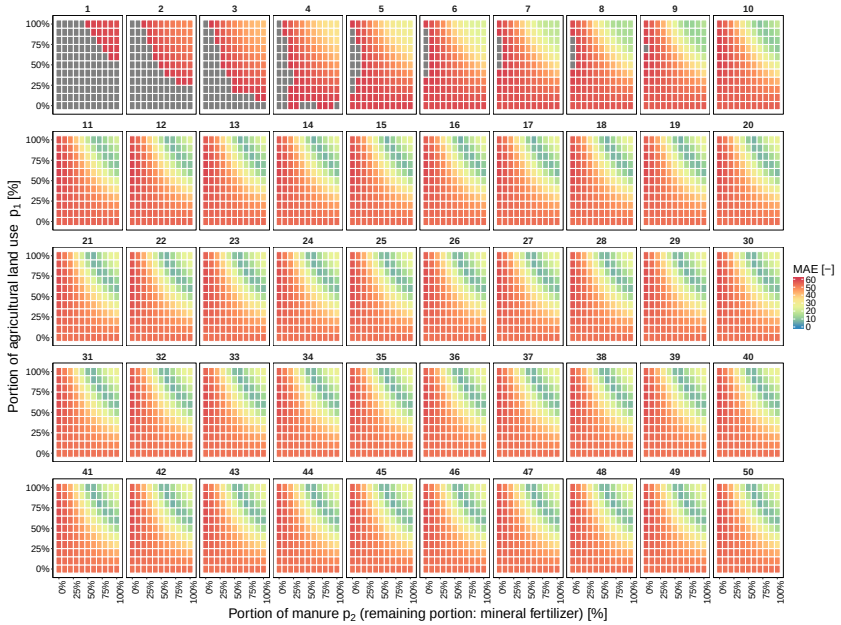

Figure S9: Mean absolute error (**MAE**) for the frequency distribution of simulated versus measured $\delta^{15}N$ in groundwater of the **perched aquifer**. Comparison of all considered realizations for Sc. 3, transport and microbial denitrification in groundwater with $\mu = 1\ a^{-1}$.

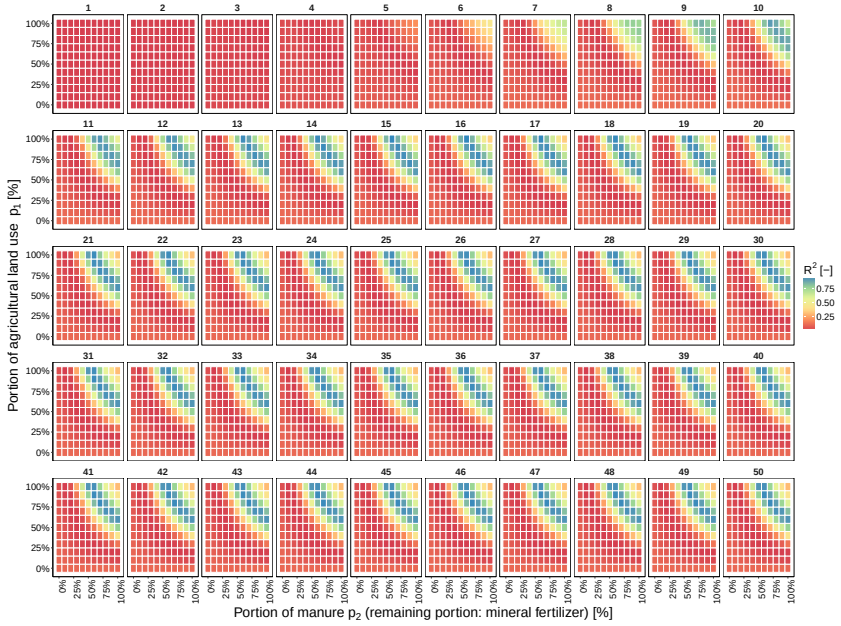

Figure S10: Coefficient of determination (**R^2**) for the frequency distribution of simulated versus measured $\delta^{15}N$ in groundwater of the **perched aquifer**. Comparison of all considered realizations for Sc. 3, transport and microbial denitrification in groundwater with $\mu = 1\ a^{-1}$.

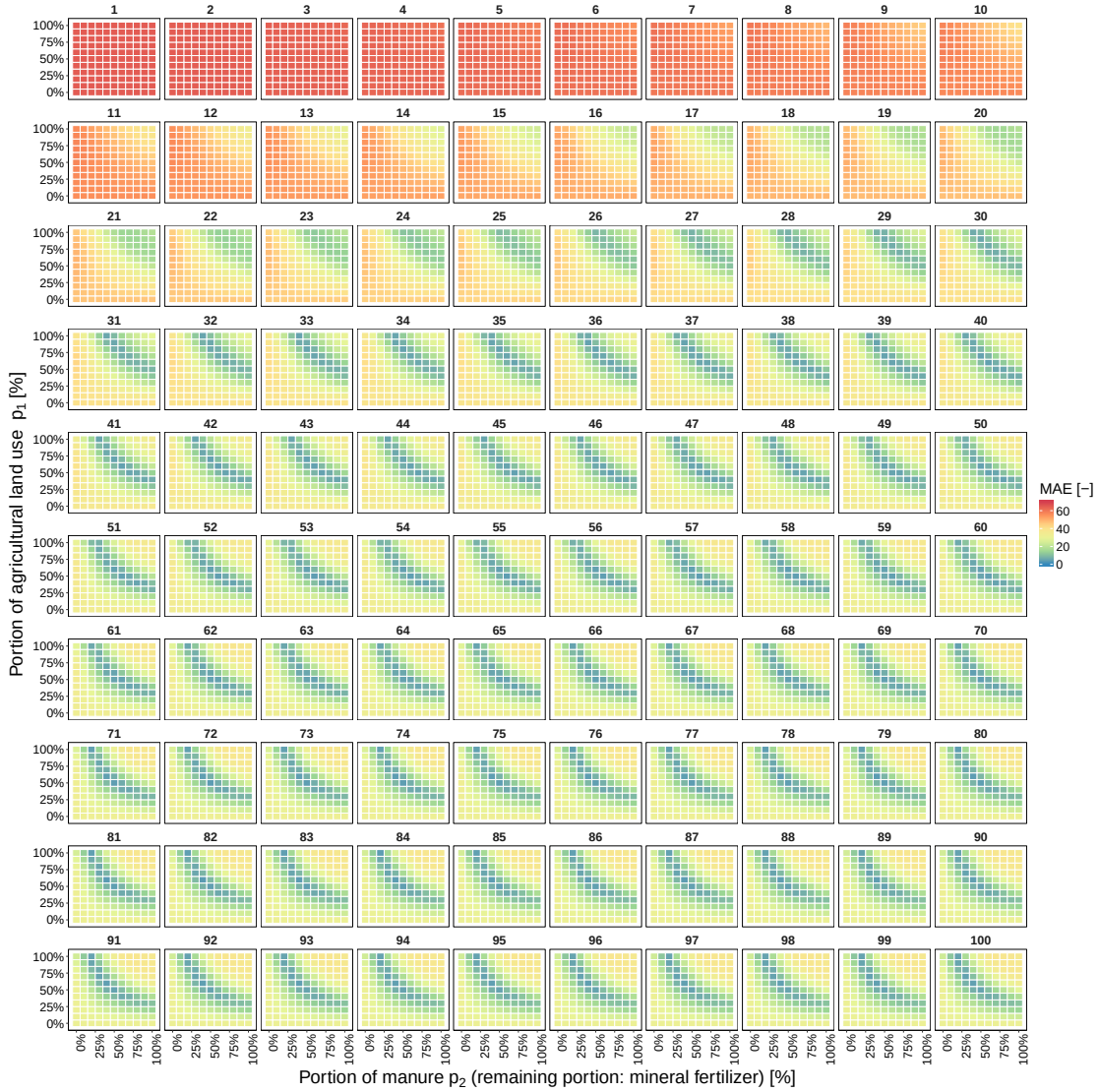

Figure S11: Mean absolute error (**MAE**) for the frequency distribution of simulated versus measured $\delta^{15}N$ in groundwater of the **main aquifer**. Comparison of all considered realizations for Sc. 3, transport and microbial denitrification in groundwater with $\mu = 1\ a^{-1}$.

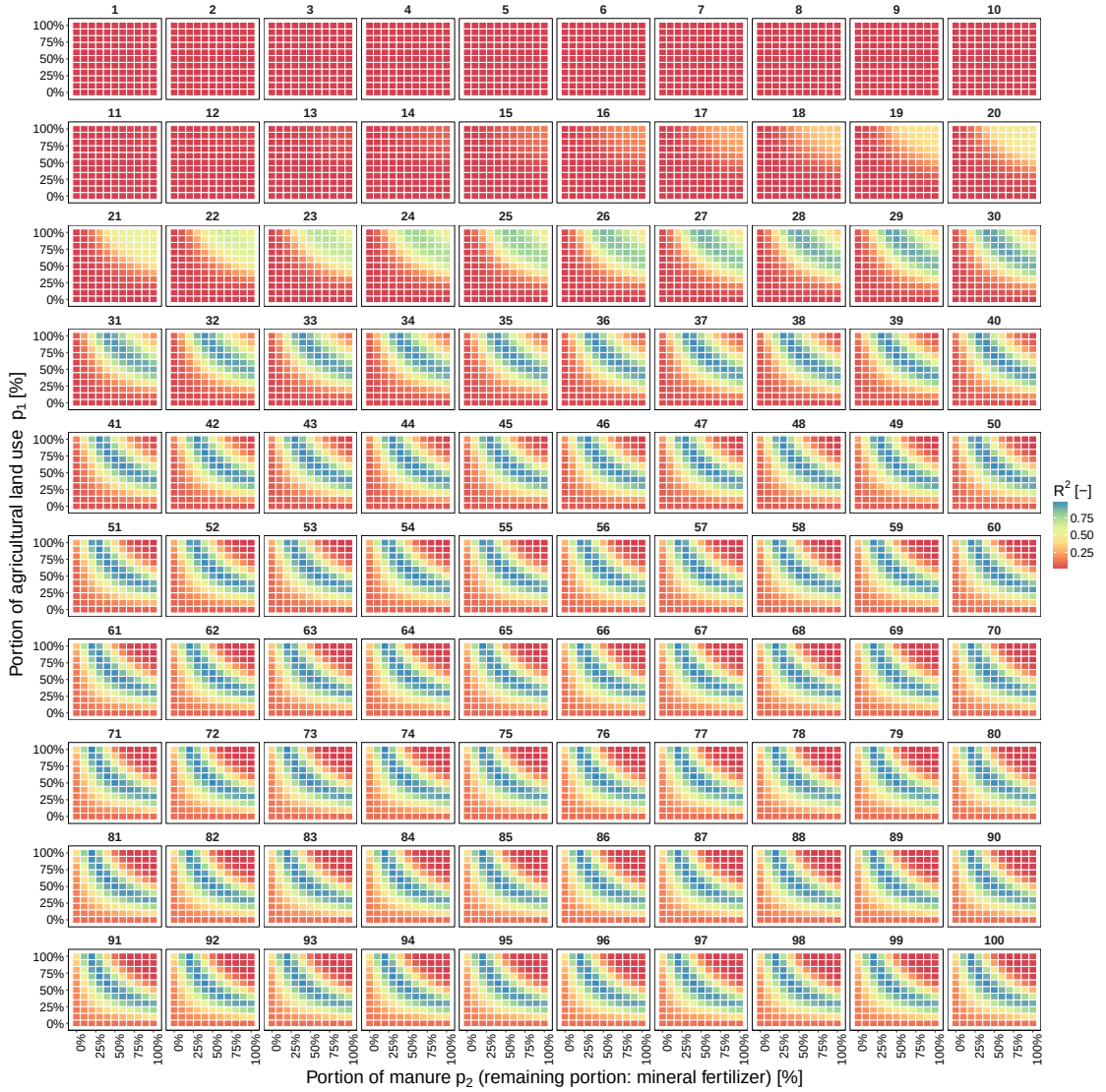

Figure S12: Coefficient of determination ($\mathbf{R^2}$) for the frequency distribution of simulated versus measured $\delta^{15}N$ in groundwater of the **main aquifer**. Comparison of all considered realizations for Sc. 3, transport and microbial denitrification in groundwater with $\mu = 1\ a^{-1}$.

B.7 EVALUATION OF SC. 3 REALIZATIONS (TRANSPORT AND MICROBIAL DENITRIFICATION IN GROUNDWATER WITH $\mu = 0.1\ a^{-1}$)

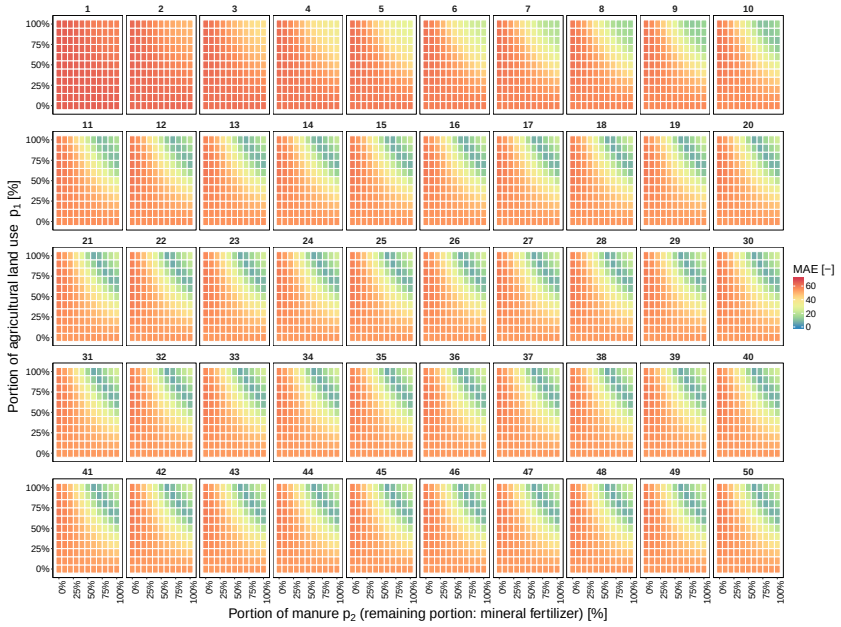

Figure S13: Mean absolute error (**MAE**) for the frequency distribution of simulated versus measured $\delta^{15}N$ in groundwater of the **perched aquifer**. Comparison of all considered realizations for Sc. 3, transport and microbial denitrification in groundwater with $\mu = 0.1\ a^{-1}$.

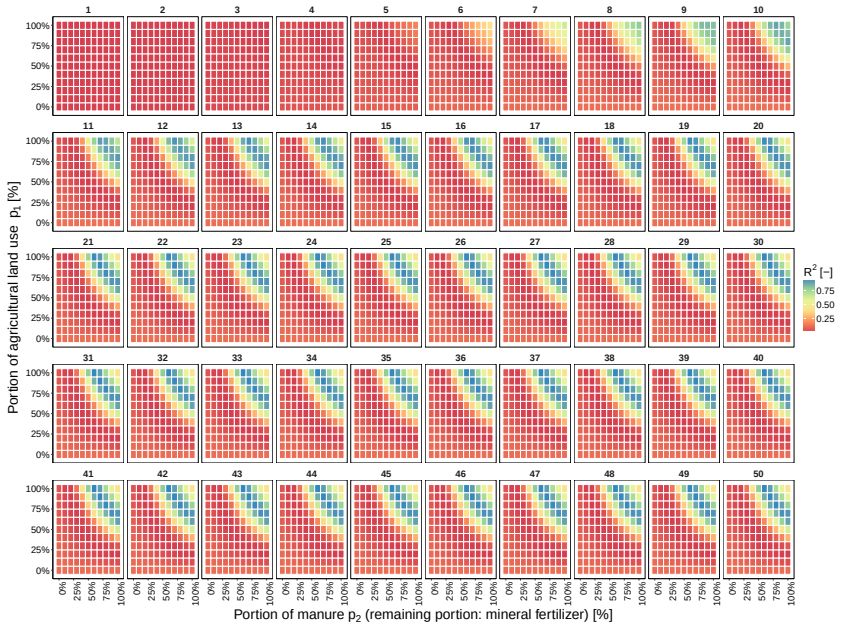

Figure S14: Coefficient of determination (**R^2**) for the frequency distribution of simulated versus measured $\delta^{15}N$ in groundwater of the **perched aquifer**. Comparison of all considered realizations for Sc. 3, transport and microbial denitrification in groundwater with $\mu = 0.1\ a^{-1}$.

Table S8: MAE and R^2 for the frequency distribution of simulated versus measured $\delta^{15}N$ in groundwater (perched & main aquifer). Selected realization of Sc. 3 (transport & microbial denitrification in groundwater with $\mu = 1\ a^{-1}$) within the best fit range (with MAE <9.9 for the perched aquifer and <10.7 for the main aquifer, i. e. below 5th percentile MAE). Selected realizations, presenting lowest and highest MAE within the best fit range for each considered source composition (defined by p_1 and p_2). 'Time' refers to the time of nitrate transport in groundwater (from the source to an observation point in the aquifer, downstream of the source). Green via yellow to red indicates decreasing goodness of fit.

Perched Aquifer					Main Aquifer				
Time [yr]	p_1, portion agriculture [%]	p_2, portion manure [%]	MAE [-]	R^2 [-]	Time [yr]	p_1, portion agriculture [%]	p_2, portion manure [%]	MAE [-]	R^2 [-]
21	60	100	7.90	0.917	56	30	100	7.12	0.933
15			8.89	0.900	59			7.46	0.937
30	70	80	7.48	0.922	79	40	60	6.17	0.947
17			9.26	0.890	65			7.46	0.921
15	70	90	7.51	0.929	65	40	70	5.23	0.963
12			9.10	0.883	92			7.44	0.945
12	70	100	9.18	0.904	50	40	80	5.01	0.959
43	80	70	6.49	0.939	66			7.47	0.936
15			9.06	0.900	43	40	90	5.71	0.949
14	80	80	7.19	0.930	53			7.49	0.933
48			9.30	0.892	39	40	100	6.77	0.935
36	90	60	6.65	0.938	36			7.49	0.913
16			9.14	0.902	98	50	40	7.24	0.921
13	90	70	6.91	0.936	92			7.44	0.920
33			9.30	0.894	72	50	50	3.83	0.980
11	90	80	9.14	0.909	55			7.44	0.935
44	100	50	8.35	0.911	53	50	60	4.07	0.977
23			9.24	0.900	76			7.41	0.933
16	100	60	6.31	0.947	45	50	70	4.73	0.970
49			7.90	0.926	38			7.37	0.931
11	100	70	8.61	0.912	38	50	80	5.50	0.958
10			9.11	0.899	34			7.32	0.921
					34	50	90	7.01	0.931
					33			7.41	0.921
					81	60	40	3.57	0.984
					58			7.24	0.946
					58	60	50	4.39	0.979
					73			7.50	0.937
					41	60	60	4.76	0.972
					49			7.17	0.938
					35	60	70	5.40	0.959
					32			7.32	0.923
					33	60	80	7.46	0.926
					32			7.46	0.924
					100	70	30	4.90	0.970
					72			7.45	0.953
					59	70	40	5.84	0.971
					74			7.39	0.942
					40	70	50	5.00	0.978
					48			7.20	0.944
					34	70	60	5.67	0.956
					39			7.40	0.933
					30	70	70	7.09	0.920
					29			7.45	0.906
					77	80	30	5.77	0.971
					58			7.37	0.968
					43	80	40	6.02	0.975
					50			7.48	0.949
					34	80	50	5.13	0.966
					31			7.43	0.931
					30	80	60	6.63	0.928
					32			7.30	0.930
					97	90	20	5.34	0.971
					75			7.48	0.952
					51	90	30	6.30	0.979
					62			7.47	0.946
					36	90	40	5.06	0.973
					42			7.28	0.944
					30	90	50	5.83	0.937
					28			7.40	0.901
					84	100	20	4.05	0.982
					56			7.48	0.956
					42	100	30	5.40	0.978
					50			7.20	0.946
					33	100	40	5.17	0.962

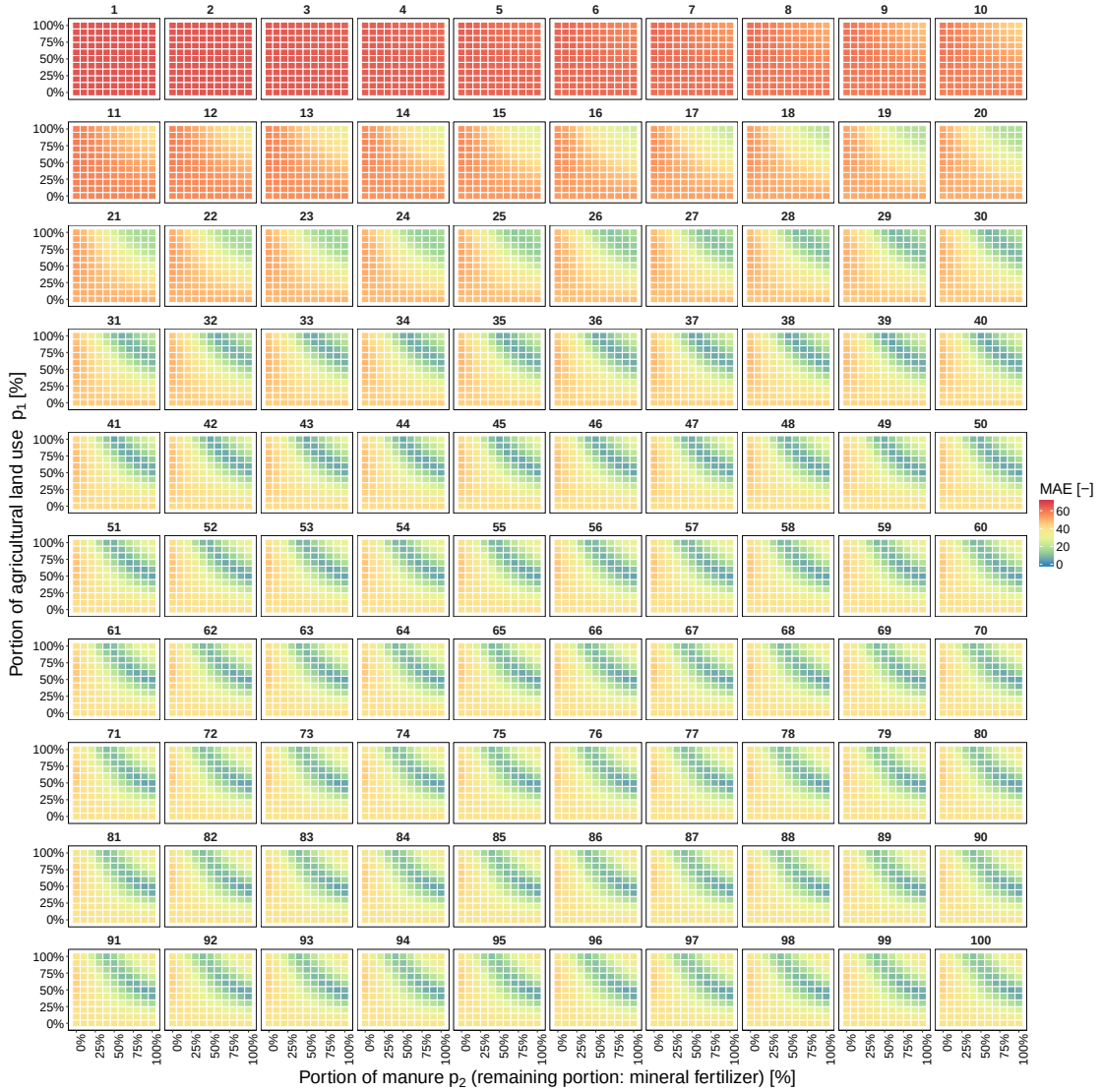

Figure S15: Mean absolute error (**MAE**) for the frequency distribution of simulated versus measured $\delta^{15}N$ in groundwater of the **main aquifer**. Comparison of all considered realizations for Sc. 3, transport and microbial denitrification in groundwater with $\mu = 0.1\ a^{-1}$.

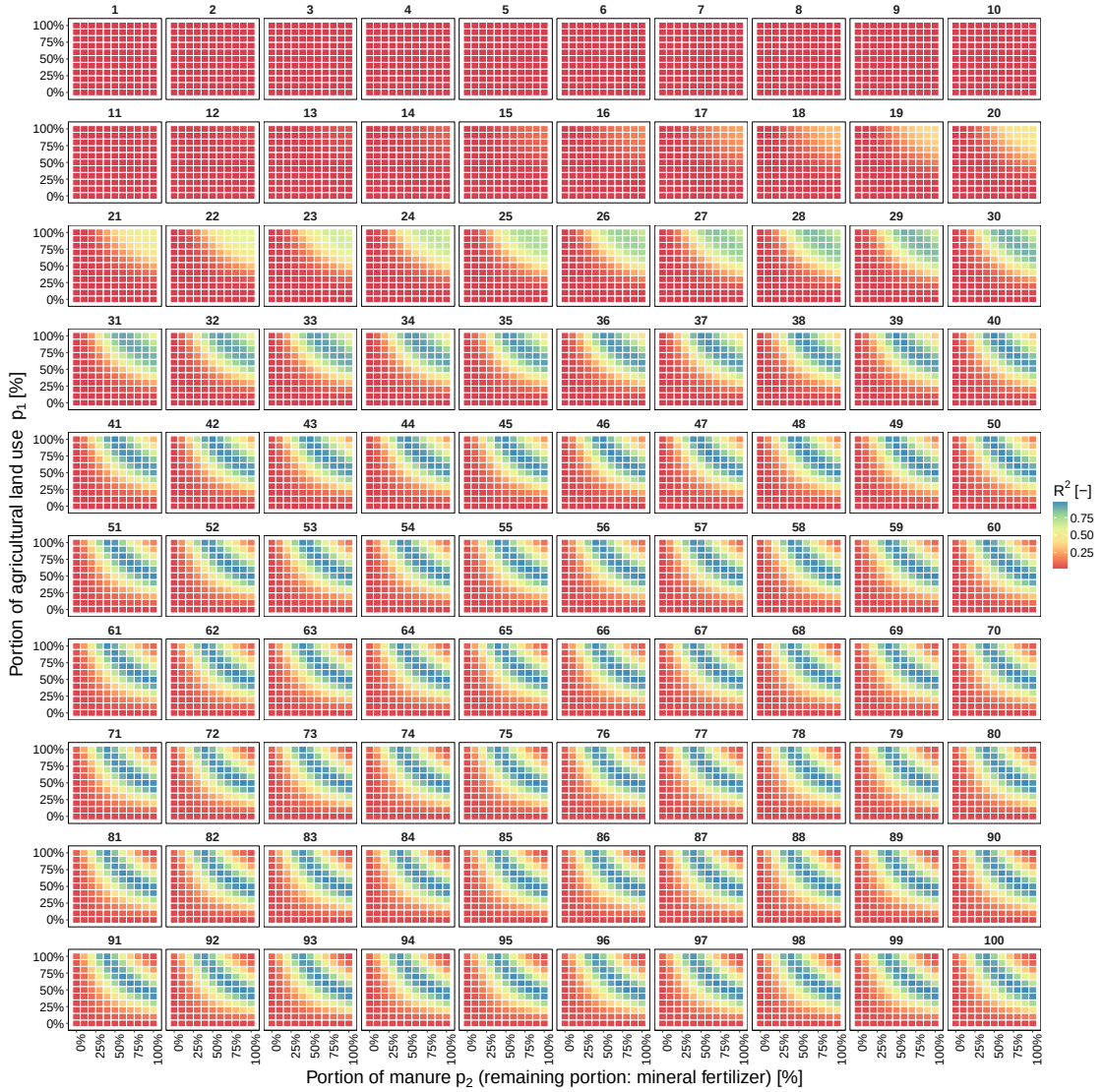

Figure S16: Coefficient of determination (**R^2**) for the frequency distribution of simulated versus measured $\delta^{15}N$ in groundwater of the **main aquifer**. Comparison of all considered realizations for Sc. 3, transport and microbial denitrification in groundwater with $\mu = 0.1\ a^{-1}$.

B.8 DIFFERENCES IN MAE AND R^2 BETWEEN SCENARIOS – PERCHED AQUIFER

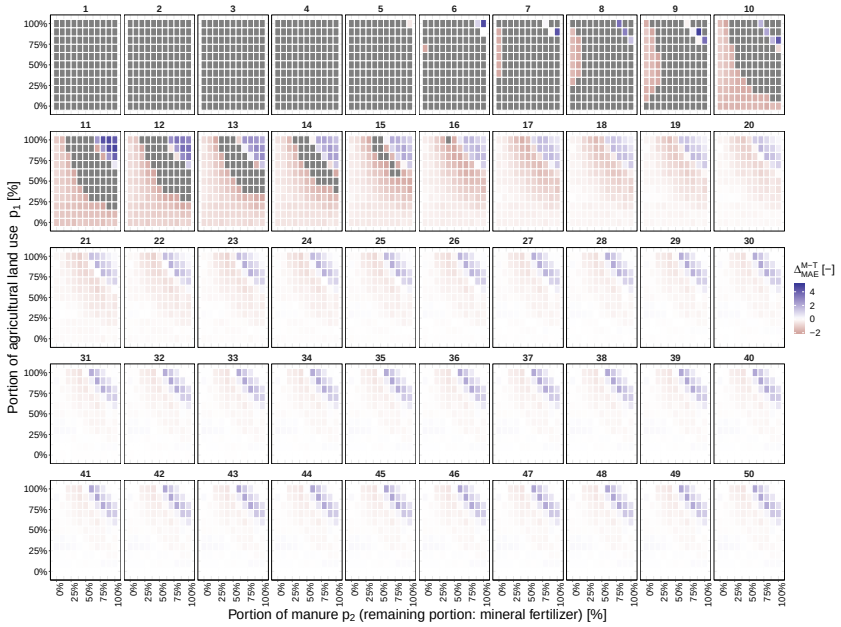

Figure S17: **Difference** in **MAE** between **Sc. 1 (mixing) and Sc. 2 (transport)**, Δ^{M-T}_{MAE}, in the perched aquifer. Values <−2 or >4 are displayed in grey.

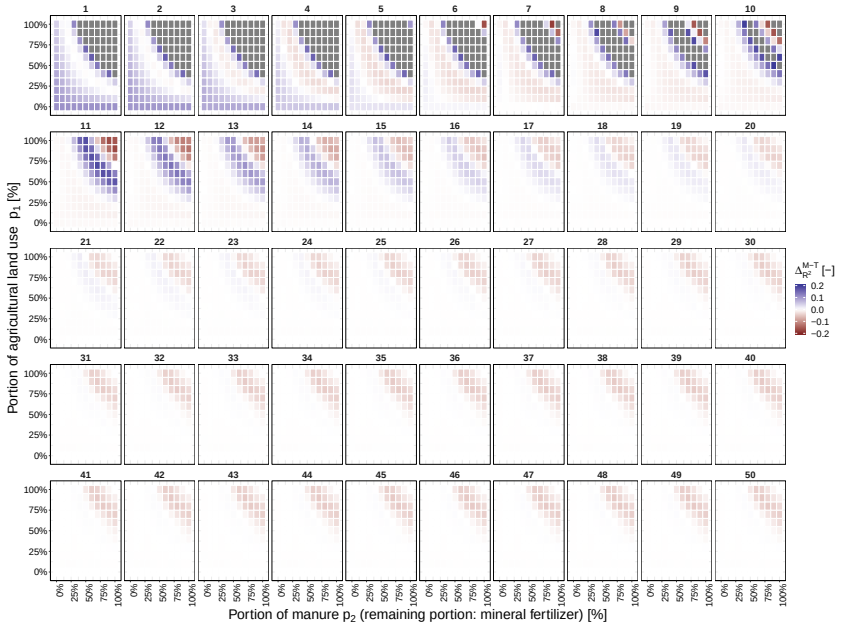

Figure S18: **Difference** in **R^2** between **Sc. 1 (mixing) and Sc. 2 (transport)**, $\Delta^{M-T}_{R^2}$, in the perched aquifer. Values <−0.1 or >0.1 are displayed in grey.

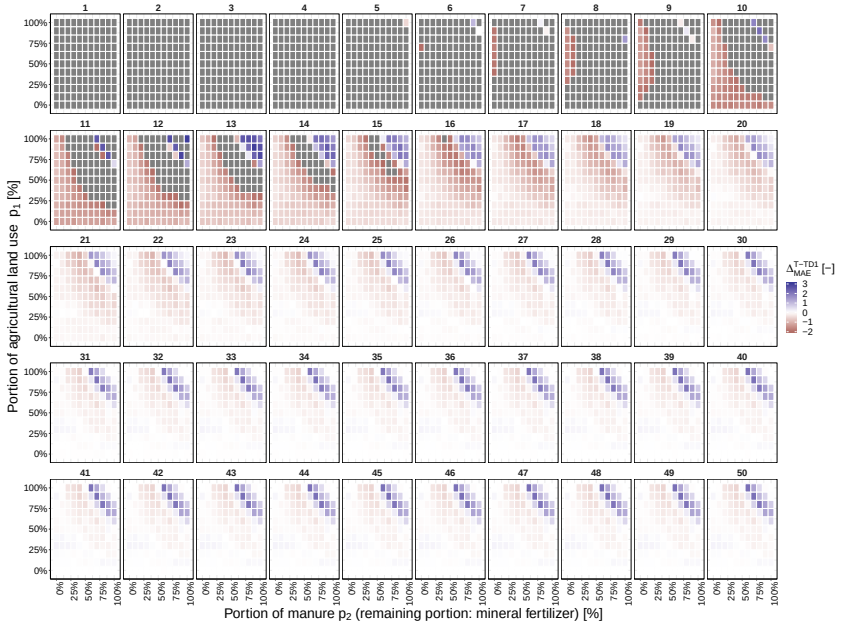

Figure S19: **Difference** in **MAE** between **Sc. 2 (transport) and Sc. 3 (transport and microbial denitrification μ_w = 1 a^{-1})** , Δ_{MAE}^{T-TD1}, in the perched aquifer. Values <−2 or >3 are displayed in grey.

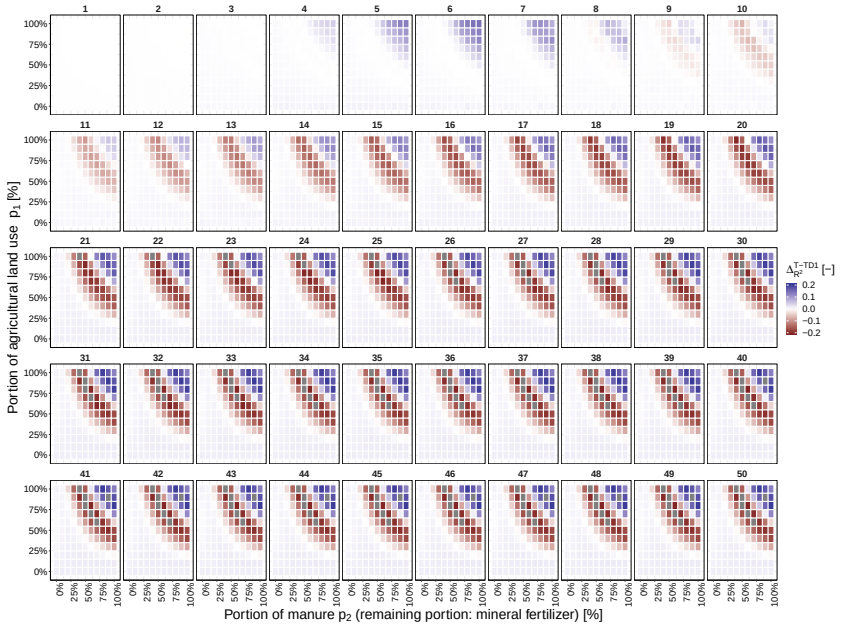

Figure S20: **Difference** in **R^2** between **Sc. 2 (transport) and Sc. 3 (transport and microbial denitrification μ_w = 1 a^{-1})** , $\Delta_{R^2}^{T-TD1}$, in the perched aquifer. Values <−0.2 or >0.2 are displayed in grey.

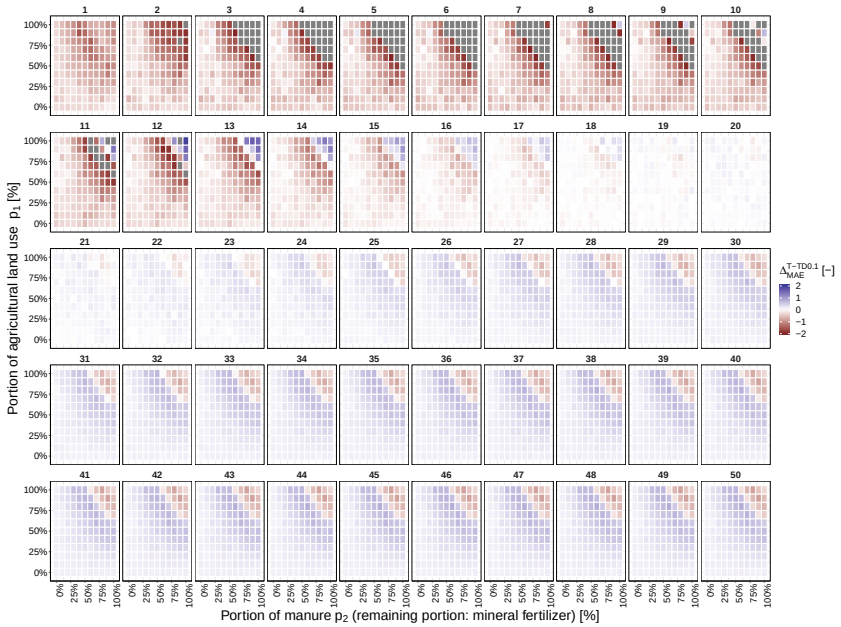

Figure S21: **Difference** in **MAE** between **Sc. 2 (transport) and Sc. 3 (transport and microbial denitrification μ_w = 0.1 a^{-1})** , $\Delta_{MAE}^{T-TD0.1}$, in the perched aquifer. Values <−2 or >2 are displayed in grey.

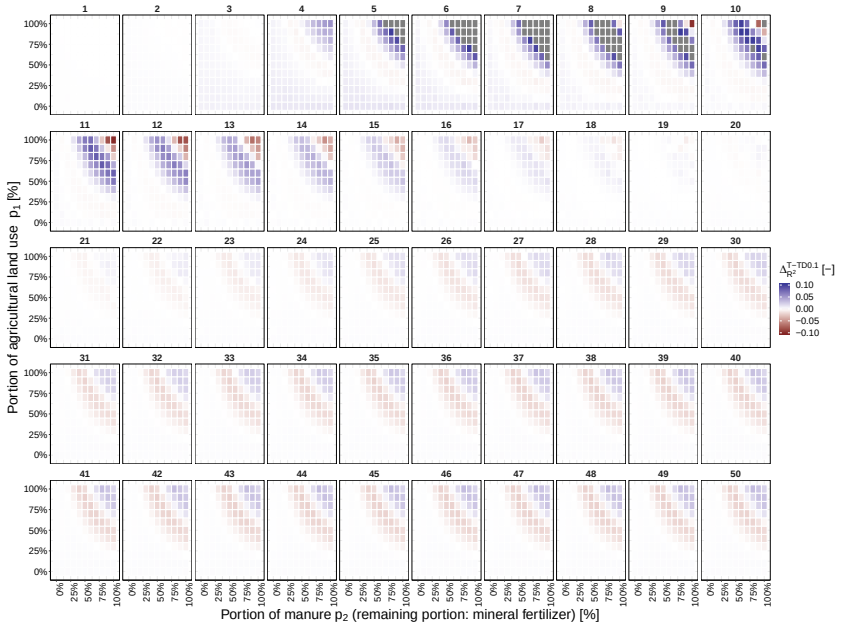

Figure S22: **Difference** in **R^2** between **Sc. 2 (transport) and Sc. 3 (transport and microbial denitrification μ_w = 0.1 a^{-1})** , $\Delta_{R^2}^{T-TD0.1}$, in the perched aquifer. Values <−0.2 or >0.2 are displayed in grey.

B.9 DIFFERENCES IN MAE AND R^2 BETWEEN SCENARIOS – MAIN AQUIFER

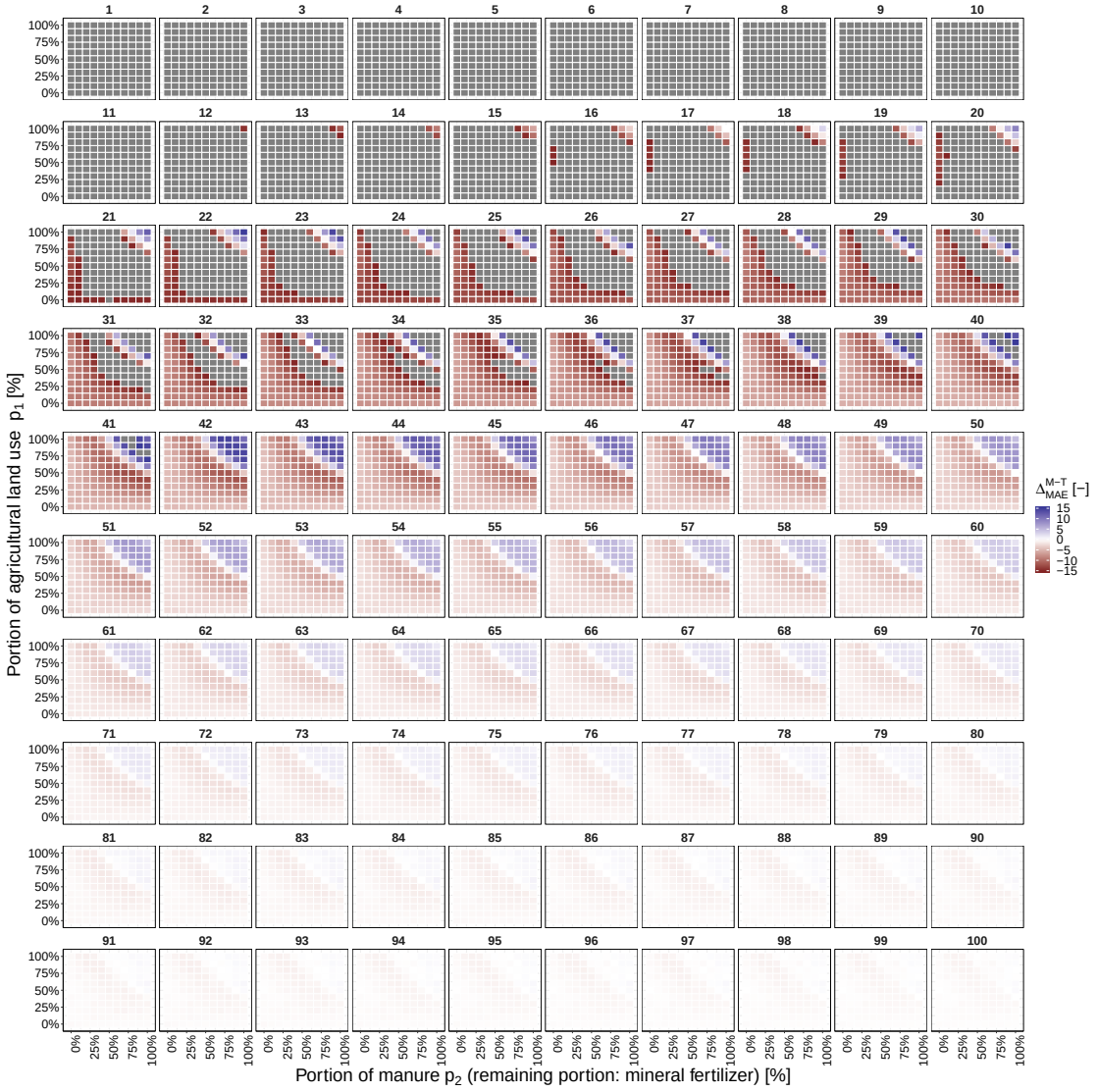

Figure S23: **Difference** in **MAE** between **Sc. 1 (mixing) and Sc. 2 (transport)**, Δ_{MAE}^{M-T}, in the main aquifer. Values <−15 or >15 are displayed in grey.

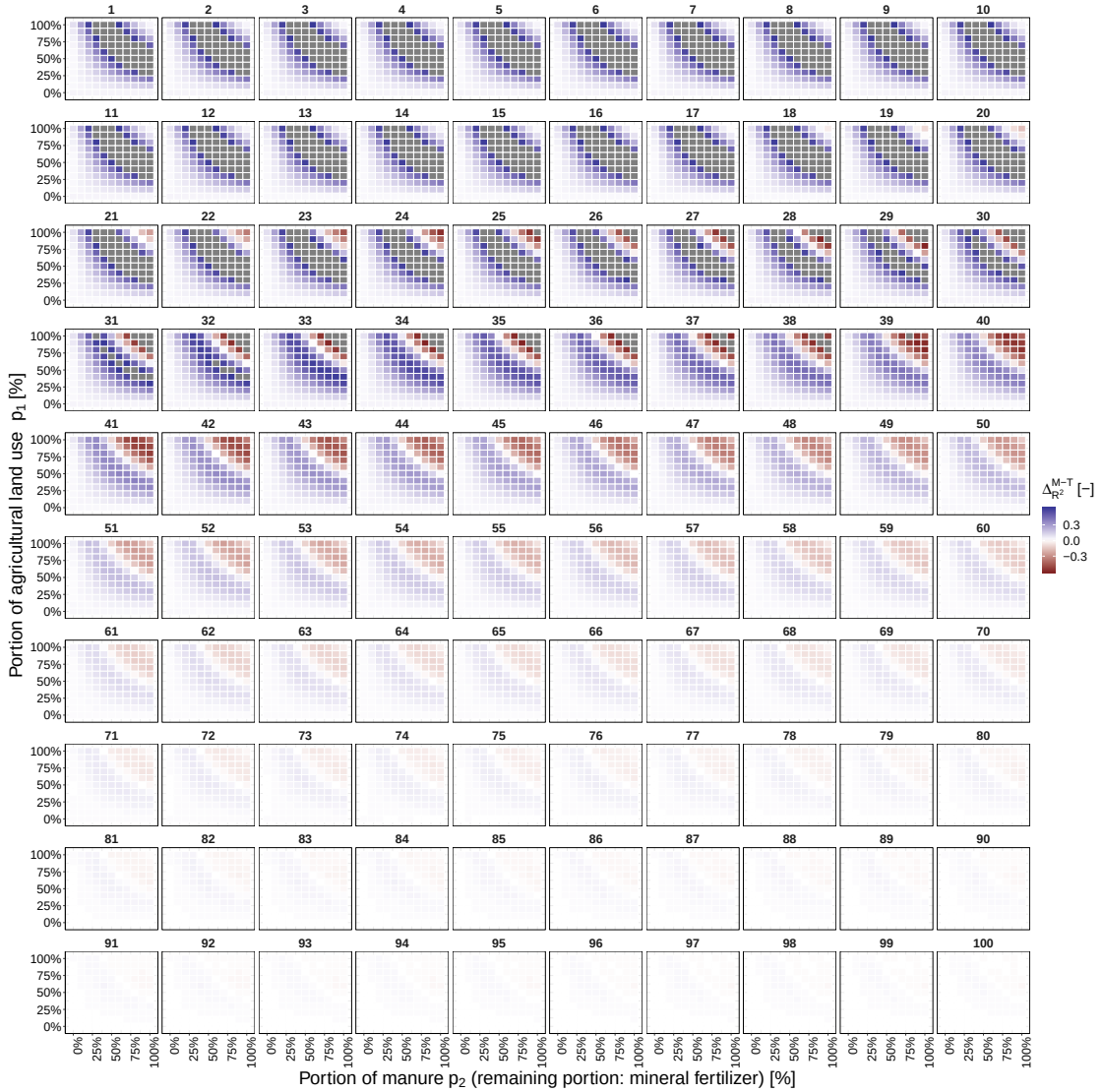

Figure S24: **Difference** in **R^2** between **Sc. 1 (mixing) and Sc. 2 (transport)**, $\Delta_{R^2}^{M-T}$, in the main aquifer. Values <−0.5 or >0.5 are displayed in grey.

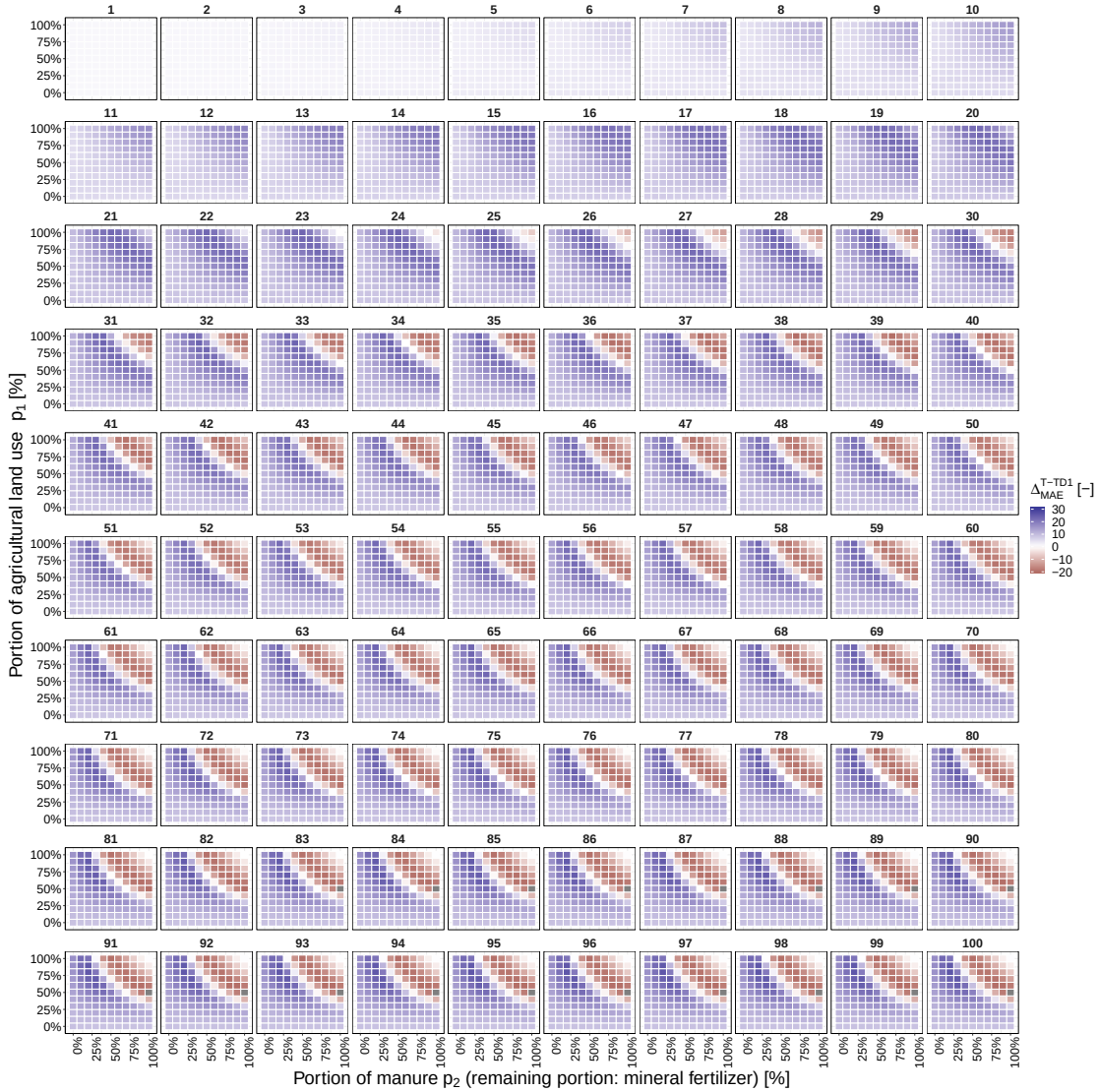

Figure S25: **Difference** in **MAE** between **Sc. 2 (transport) and Sc. 3 (transport and microbial denitrification μ_w = 1 a^{-1})** , Δ_{MAE}^{T-TD1}, in the main aquifer.

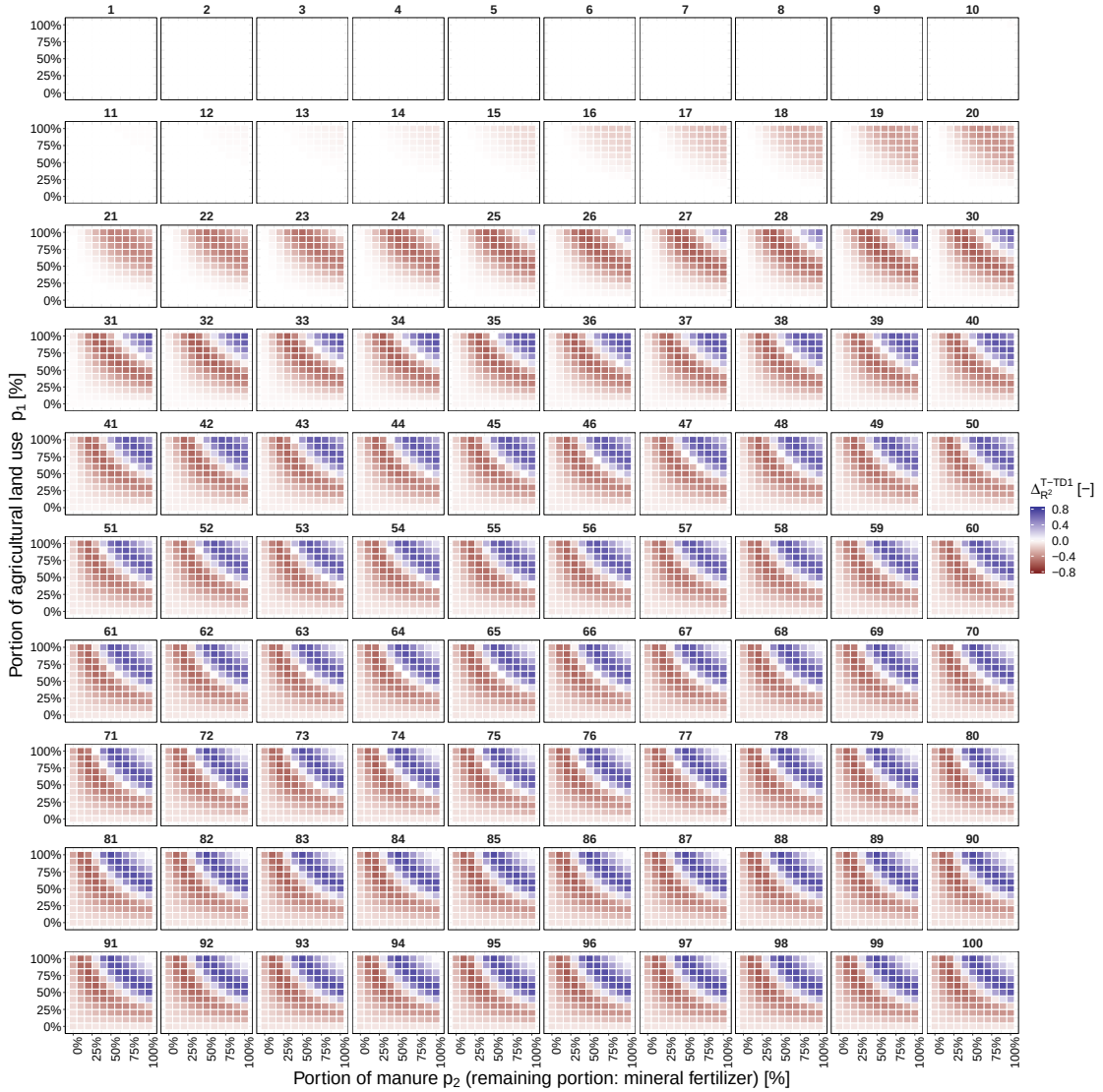

Figure S26: **Difference** in $\mathbf{R^2}$ between **Sc. 2 (transport) and Sc. 3 (transport and microbial denitrification μ_w = 1 a^{-1})** , $\Delta_{R^2}^{T-TD1}$, in the main aquifer.

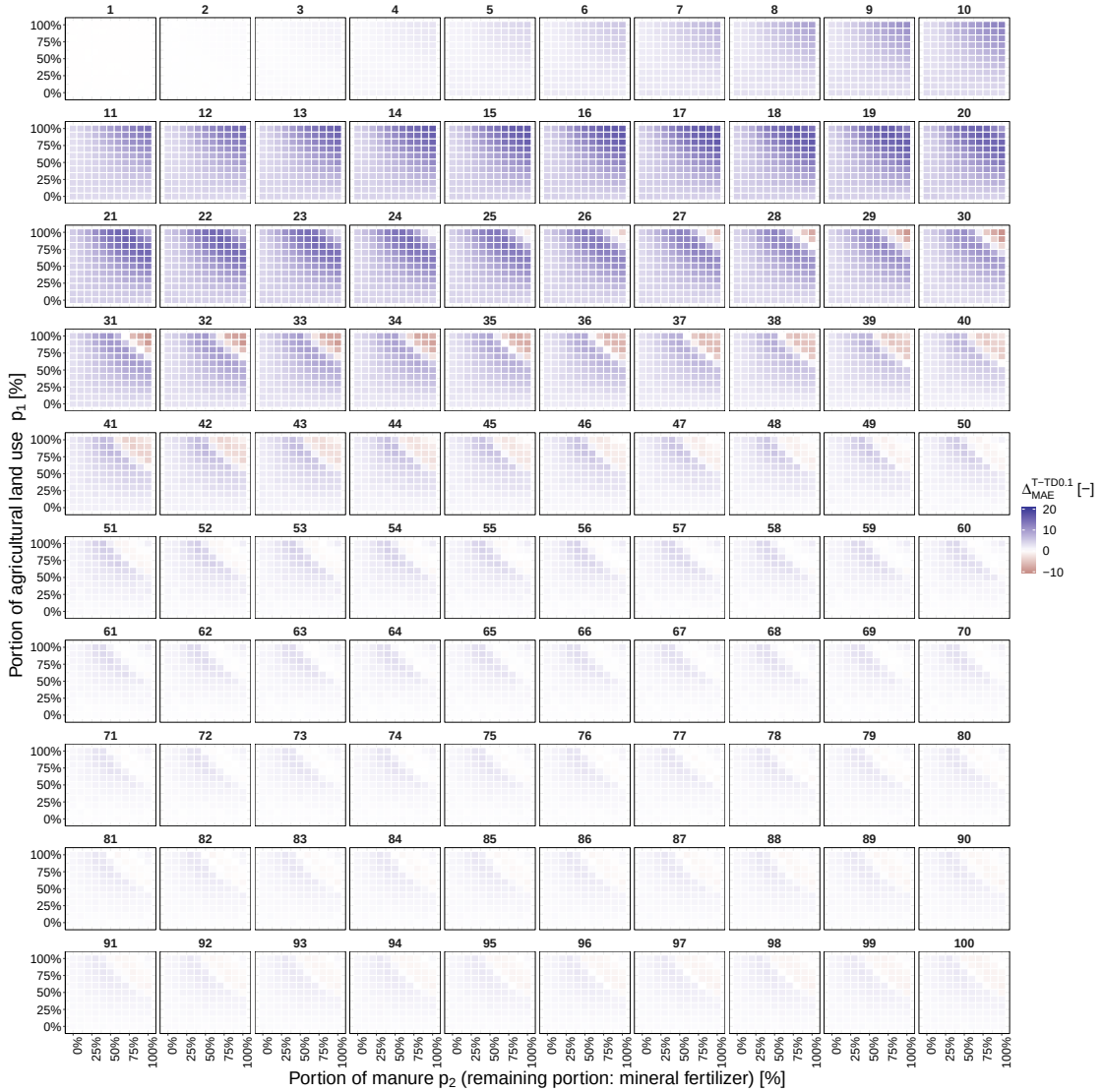

Figure S27: **Difference** in **MAE** between **Sc. 2 (transport) and Sc. 3 (transport and microbial denitrification μ_w = 0.1 a^{-1})** , $\Delta_{MAE}^{T-TD0.1}$, in the main aquifer.

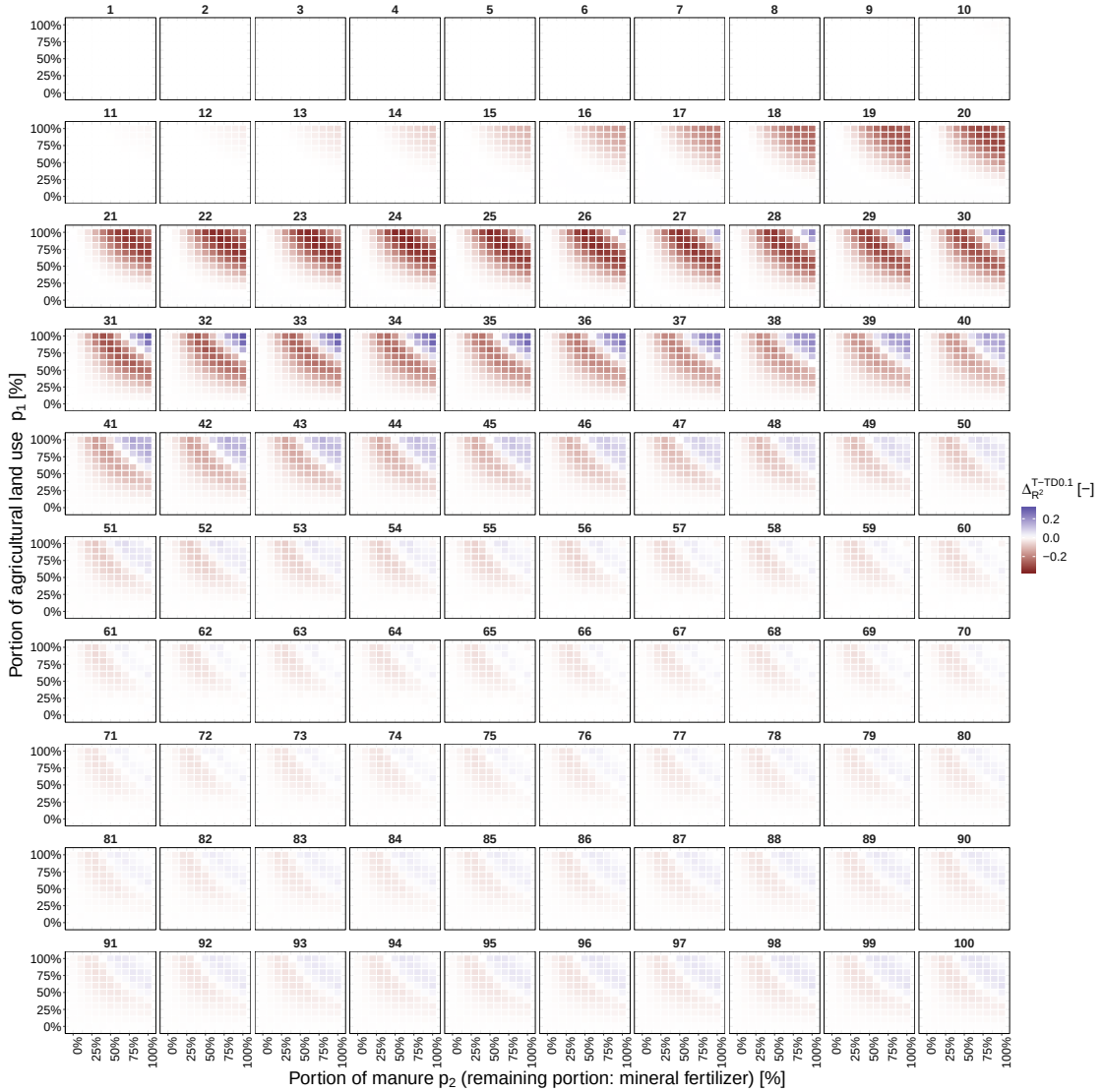

Figure S28: **Difference** in $\mathbf{R^2}$ between **Sc. 2 (transport) and Sc. 3 (transport and microbial denitrification μ_w = 0.1 $\mathbf{a^{-1}}$)** , $\Delta_{R^2}^{T-TD0.1}$, in the main aquifer.

B.10 DETERMINATION OF THE 5TH PERCENTILE FOR THE MAE DISTRIBUTION IN SC. 1 TO 3

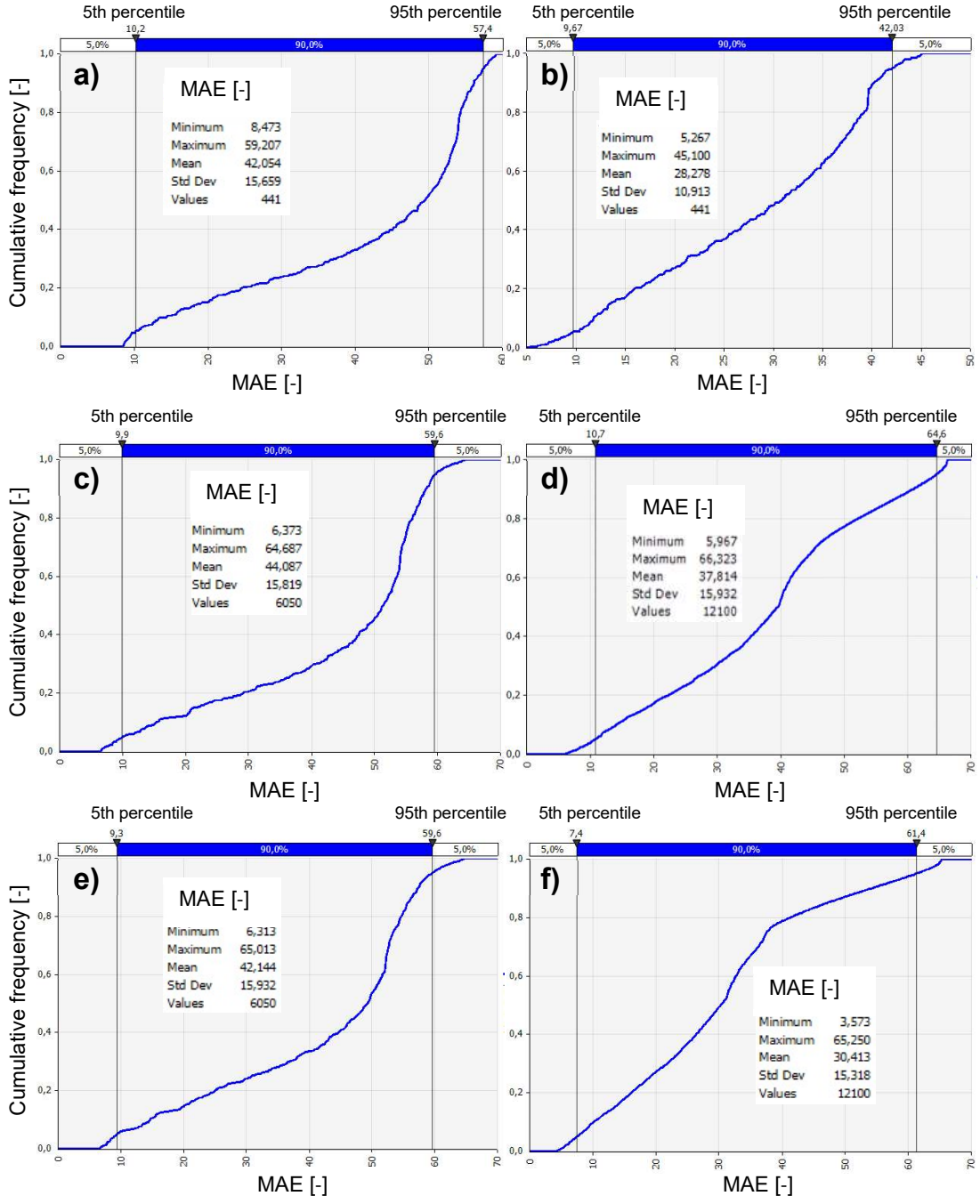

Figure S29: Cumulative frequency of mean error MAE for all considered realizations of Sc. 1 (a and b), Sc. 2 (c and d) and Sc. 3 with $\mu_w = 1\ a^{-1}$ (e and f), perched aquifer (a, c, e) and main aquifer (b, d, f).

B.11 HISTOGRAMS OF BEST FITTING SIMULATED $\delta^{15}N$ AND OBSERVED $\delta^{15}N$ DISTRIBUTIONS

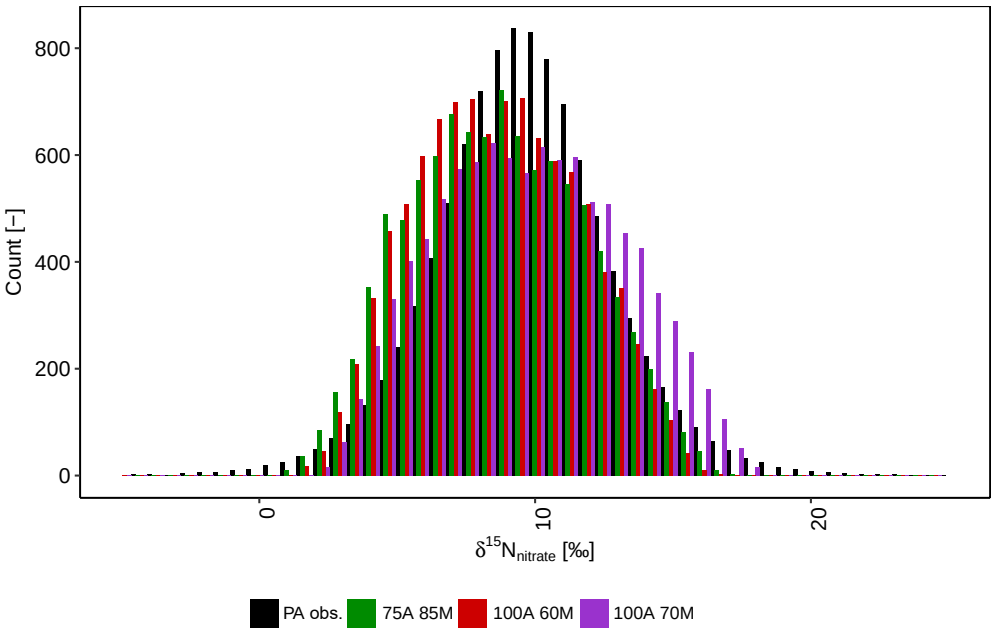

Figure S30: Histogram of best fitting simulated $\delta^{15}N$ (source mixing, Sc. 1) and observed (obs.) $\delta^{15}N$ for the PA. Numbers in the legend refer to percentage of agricultural land use (A) and manure (M).

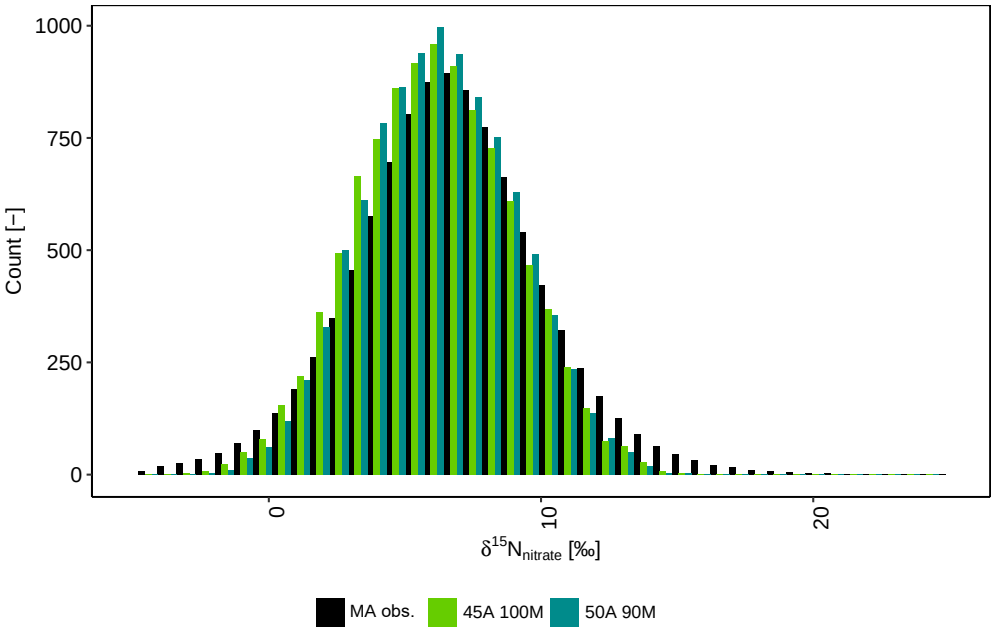

Figure S31: Histogram of best fitting simulated $\delta^{15}N$ (source mixing, Sc. 1) and observed (obs.) $\delta^{15}N$ for the MA. Numbers in the legend refer to percentage of agricultural land use (A) and manure (M).

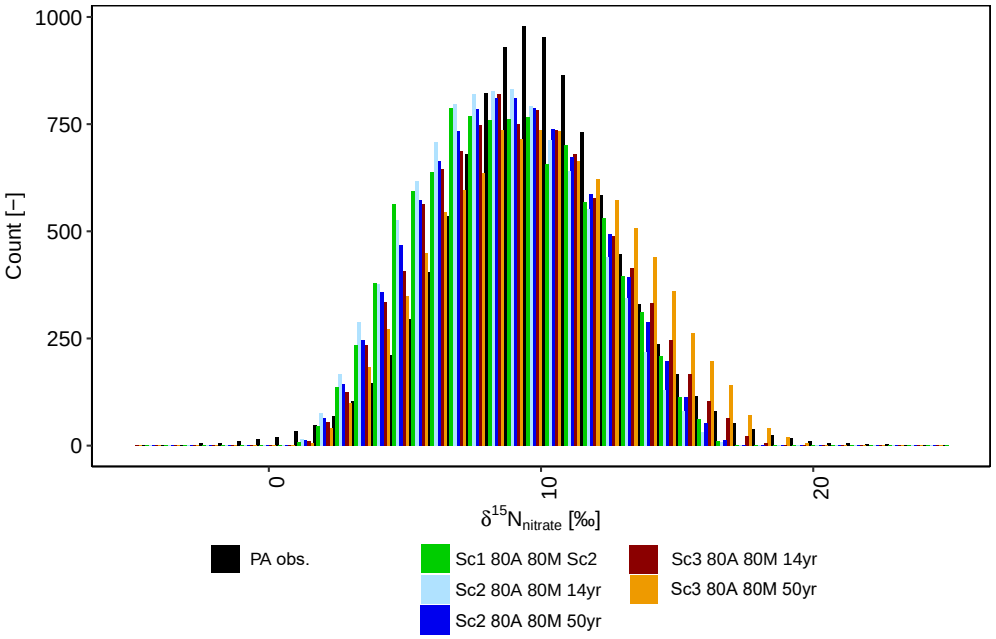

Figure S32: Histogram of observed and simulated $\delta^{15}N$, comparison of Sc. 1-3 for the PA. Percentage of agricultural land use (A) and manure (M), with transport duration in years (yr).

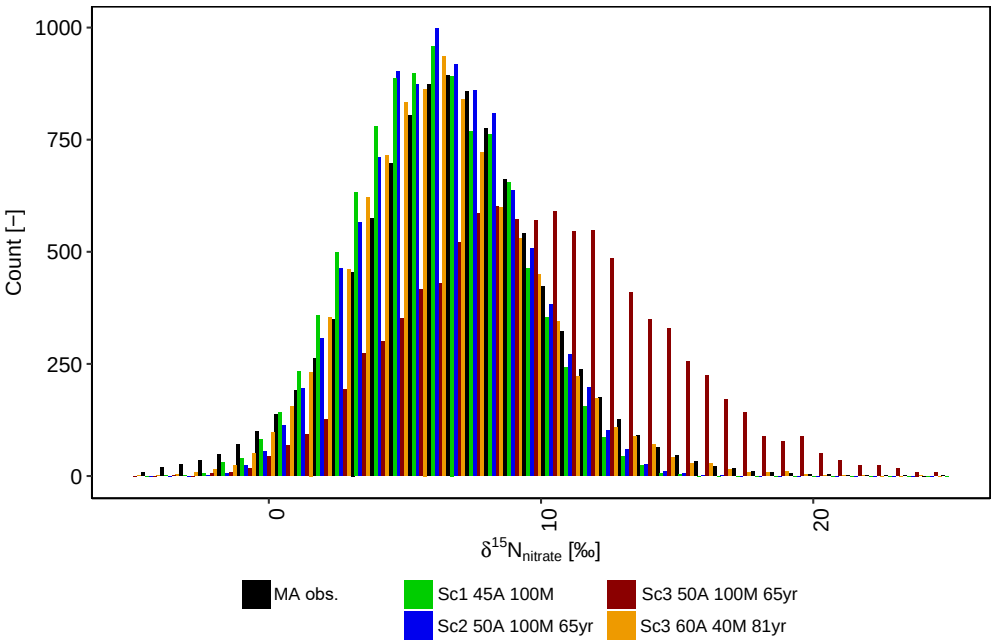

Figure S33: Histogram of observed and simulated $\delta^{15}N$, comparison of Sc. 1-3 for the MA. Percentage of agricultural land use (A) and manure (M), with transport duration in years (yr).

B.12 CONVERGENCE TESTING OF THE SAMPLE AVERAGE AND VARIANCE

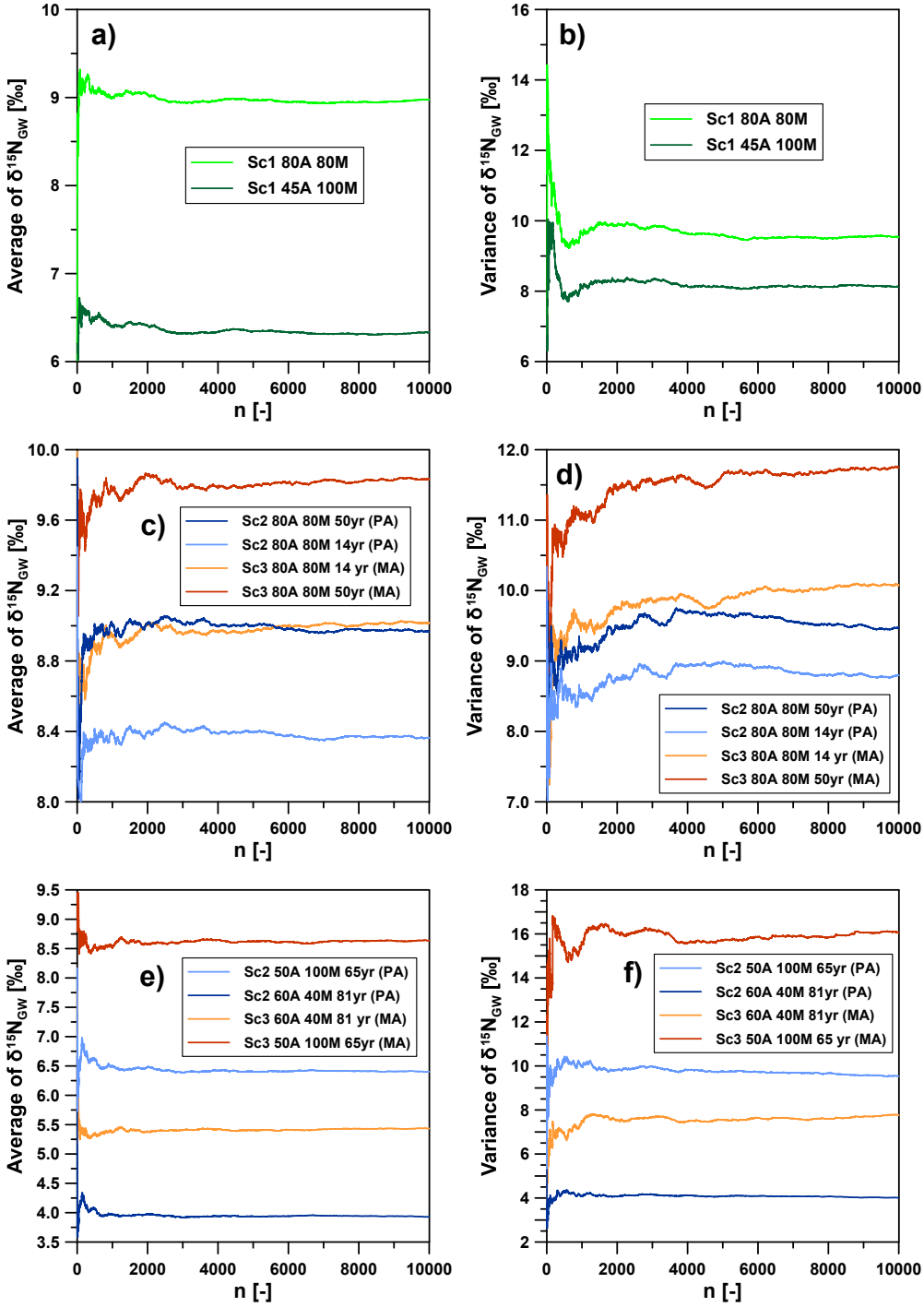

Figure S34: Convergence of the sample average (a, c, e) and variance (b, d, f) of simulated $\delta^{15}N$ (number of random samples n) for selected realizations of Sc. 1 (a and b), as well as Sc. 2 and 3 (b to f). Selected realizations correspond to those presented in Fig. 12.